Applications of gauge/gravity duality

Systems close to & far from equilibrium

Dissertation by Ann-Kathrin Straub

Applications of gauge/gravity duality

Systems close to & far from equilibrium

Dissertation
an der Fakultät für Physik
der Ludwig–Maximilians–Universität
München

vorgelegt von
Ann-Kathrin Straub

München, den 8. September 2017

DISSERTATION

submitted to the faculty of physics of the
Ludwig–Maximilians–Universität München

by Ann-Kathrin Straub

supervised by Prof. Dr. Johanna Karen Erdmenger

1st Referee: Prof. Dr. Johanna Karen Erdmenger
2nd Referee: Prof. Dr. Dieter Lüst
Date of submission: 08 September 2017
Date of oral examination: 19 October 2017

Zusammenfassung

Die vorliegende Dissertation widmet sich der Anwendung der Eich-Gravitations-Dualität im Bereich der Physik der kondensierten Materie und Systemen weit außerhalb ihres thermischen Gleichgewichts.

Die ursprüngliche Form und gleichzeitig das am besten verstandene Beispiel der Dualität ist die AdS/CFT Korrespondenz, die einen bemerkenswerten Zusammenhang zwischen einer Gravitationstheorie (AdS für Anti-de Sitter) und einer konformen Feldtheorie (CFT für conformal field theory) herstellt. Ihr Kernelement ist eine genaue Zuordnungsvorschrift zwischen Eigenschaften und Objekten der beiden beteiligten Theorien. Verallgemeinerungen der ursprünglichen Korrespondenz ermöglichen ihre Anwendung auf Fragestellungen verschiedener Forschungsfelder innerhalb der Physik, oft zusammengefasst unter dem Begriff Holographie. Insbesondere ist die Dualität ein bedeutsames Instrument um stark gekoppelte Systeme zu untersuchen. Der Fokus der vorliegenden Dissertation liegt auf der Anwendung der Eich-Gravitations-Dualität auf Hochtemperatursupraleiter und Systeme außerhalb ihres thermischen Gleichgewichts, charakterisiert durch einen stationären Wärmestrom.

Als erstes untersuchen wir holographische Hochtemperatursupraleiter. Wir analysieren ob und mit welcher Genauigkeit es möglich ist, die Ergebnisse eines jüngeren Experiments zur Temperaturabhängigkeit der Energie und Zerfallsbreite fermionischer Anregungen von realen Hochtemperatursupraleitern mit holographischen Methoden zu rekonstruieren. Eine wesentliche Charakteristik der experimentellen Daten ist der rapide Anstieg der Zerfallsbreite mit steigender Temperatur, gänzlich verschieden von konventionellen Supraleitern. Wir verwenden dafür zunächst das einfachst mögliche Modell eines holographischen Supraleiters. Das Ergebnis unserer Analyse ist, dass das experimentell beobachtete Verhalten mühelos auch im holographischen Modell auftritt. Darüber hinaus lässt sich mit einer Feineinstellung der Modellparameter eine erstaunlich genaue Beschreibung auf quantitativer Ebene erzielen.

Im nächsten Schritt konstruieren wir einen holographischen Supraleiter, dessen bereits bekannte normalleitende Phase in vielen Eigenschaften den experimentell beobachteten ‘seltsamen’ Metallen ähnelt. Diese weisen aufgrund starker Korrelation im Gegensatz zu Fermi-Flüssigkeiten unter anderem einen linearen Anstieg

des elektrischen Widerstands mit der Temperatur auf. Eine der Erweiterungen gegenüber dem im vorstehenden Absatz genannten Modell besteht darin, dass das System nicht mehr translationsinvariant ist. Wir untersuchen den Effekt der gebrochenen Translationsinvarianz auf die supraleitende Phase und im Besonderen auf die Temperaturabhängigkeit der Zerfallsbreite fermionischer Anregungen. Auch hier zeigt sich das gleiche qualitative Bild.

Als letztes wenden wir uns der Anwendung der AdS/CFT Korrespondenz auf Nichtgleichtgewichtssysteme zu. Im konkreten Fall betrachten wir die zeitliche Entwicklung eines Systems, das zunächst aus zwei unterschiedlich temperierten eindimensionalen Wärmebädern aufgebaut ist. Nachdem diese in Kontakt gebracht werden, bildet sich ein stationärer aber sich räumlich ausbreitender Wärmestrom aus. Wir berechnen die Verschränkungsentropie mithilfe der holographischen Methode und untersuchen ihren zeitlichen Verlauf. Je nach (relativer) Temperaturen der beiden Wärmebäder, beobachten wir verschiedene Charakteristika. Des Weiteren überprüfen wir die Gültigkeit von Ungleichungen für die Verschränkungsentropie in diesem System.

Diese Dissertation basiert auf der Arbeit, die die Autorin als Doktorandin unter der Betreuung von Prof. Dr. Johanna Erdmenger am Max-Planck-Institut für Physik in München im Zeitraum von Januar 2014 bis August 2017 durchgeführt hat. Die Ergebnisse wurden wie folgt publiziert:

[1] J. Erdmenger, D. Fernandez, M. Flory, E. Megias, A.-K. Straub and P. Witkowski, *Time evolution of entanglement for holographic steady state formation*, *JHEP* **10** (2017) 034, [`1705.04696`],

[2] N. Poovuttikul, K. Schalm, A.-K. Straub and J. Zaanen, *Fermionic excitations of a holographic superconductor*, *to appear* .

Abstract

In this thesis we study applications of gauge/gravity duality to condensed matter physics and systems far away from thermal equilibrium.

The original form of the duality is the AdS/CFT correspondence, which establishes an intriguing link between a gravity theory (AdS for Anti-de Sitter) and a conformal field theory (CFT). At its core is a one-to-one map between objects and properties of those two theories. Generalisations of the original correspondence allow to apply it to problems of other fields of research in physics. This more broadly defined duality is known as holography and is an important tool to study strongly coupled systems. The focus of this thesis are applications of gauge/gravity duality to high-temperature superconductors and systems out of thermal equilibrium, characterised by a steady heat current.

First, we study a holographic high-temperature superconductor. More specifically, we analyse if and to what extend it is possible to use holographic methods to describe the results of a recent experiment on high-temperature superconductors. The experiment measured the temperature dependence of the gap and pair-breaking term of fermionic excitations. An essential feature of the experimental data is the rapidly growing pair-breaking term as temperature increases. This behaviour is unfamiliar from conventional superconductors. We first employ the simplest holographic model of a superconductor. The result of our analysis is that the experimentally observed behaviour emerges naturally within the holographic model. Moreover, upon a fine tuning of the parameters one can reach a remarkably good agreement on a quantitative level.

As a next step we construct a holographic superconductor whose normal state is known to share a number of properties with strange metals in the laboratory, the most prominent being the linear increase of the electrical resistivity with temperature. One of the generalisations compared to the preceding superconductor model is that it is not translationally invariant. We investigate the effect of the broken translational invariance on the superconducting state and in particular the temperature dependence of the pair-breaking term. The qualitative picture is the same as before.

We then apply the AdS/CFT correspondence to a system far away from thermal equilibrium. We investigate the time dependence of two one-dimensional heat

baths at different temperatures, which are brought into contact. Attempting to reach thermal equilibrium, a steady state in a growing region centred around the initial contact surface emerges. We analyse the entanglement entropy by means of its geometrical holographic dual and find that, depending on the temperature configuration of the heat baths, its time evolution is distinctly characterised. Furthermore, we check the validity of entanglement inequalities in this time dependent setup.

This dissertation is based on work the author did during a PhD fellowship under the supervision of Prof. Dr. Johanna Erdmenger at the Max-Planck-Institut für Physik in Munich, Germany from January 2014 to August 2017. The relevant publications are:

[1] J. Erdmenger, D. Fernandez, M. Flory, E. Megias, A.-K. Straub and P. Witkowski, *Time evolution of entanglement for holographic steady state formation*, *JHEP* **10** (2017) 034, [1705.04696],

[2] N. Poovuttikul, K. Schalm, A.-K. Straub and J. Zaanen, *Fermionic excitations of a holographic superconductor*, *to appear* .

Contents

CHAPTER 1

Introduction

An intriguing new link between gravity and quantum field theory turns out to connect a number of puzzles of different branches of physics by mapping their dynamics to each other. In other words, this new link puts together already existing techniques and concepts in a new way and thereby gives these concepts a previously untapped field of application. It provides a common language for physicists of different backgrounds.

The link, known as *AdS/CFT correspondence* [3–5], has its roots in string theory and states the equivalence of two very specific theories: $\mathcal{N} = 4$ Super-Yang-Mills theory in four dimensions with gauge group $SU(N)$, which is conformally invariant (CFT), and type IIB supergravity on $\mathrm{AdS}_5 \times S^5$ (AdS). Even though this conjectured correspondence has not been proven yet, there is a lot of evidence in favour of it. The crucial feature, responsible for the importance of the duality, is that it relates a strongly coupled quantum field theory and a weakly coupled classical gravity theory. While the former generally poses a significant challenge, dealing with the latter is conceptually well established. The AdS/CFT correspondence thus offers a unique insight into the interplay between the fundamental principles of physics.

Its profound relevance is not restricted to its admittedly fascinating implications for fundamental theoretical considerations. The duality, understood as a means to provide two equivalent descriptions of the very same physics, has proven to be a remarkably successful tool to study strongly coupled systems, to which the standard approach of perturbation theory is not applicable. These applications of gauge/gravity duality are based on the *holographic dictionary*, which gives a precise prescription on how to translate between the two theories. This dictionary is a one-to-one map between properties and objects of the two involved theories. Moreover, the structure of the original dictionary, which is restricted to the original AdS/CFT proposal, points the direction to extrapolate it in order to construct more general dualities, summarised by the term *gauge/gravity duality* or *holography*.

The origin of the latter term is that the AdS/CFT correspondence is the best understood explicit realisation of the *holographic principle*. The holographic principle is based on the observation that the entropy of a black hole scales with the area of its event horizon [6], indicating that all of the information is stored on the surface of the black hole. At the same time, since black holes are the most compact objects in a gravity theory, there cannot be a volume in space with more entropy than a black hole extended over the same volume. As a conclusion, the holographic principle [7,8], states that the physical information content of a $(d+1)$-dimensional gravity theory can be equivalently described by a theory without gravity in d dimensions. In analogy with the black hole and its event horizon, this d-dimensional theory can be thought to be the theory on the boundary of the $(d+1)$-dimensional spacetime. Specifically, in the AdS/CFT correspondence the four-dimensional conformal field theory is believed to contain the exact same physical information as the gravity theory in the five-dimensional Anti-de Sitter spacetime, which often is referred to as the *bulk*.

The immediate consequence of the holographic principle realised by gauge/gravity duality is that a strongly coupled quantum system can be elegantly described by geometrising its properties following the guidance of the holographic dictionary. The attempt of applying the duality to systems whose underlying microscopic theories are different from $\mathcal{N} = 4$ Super-Yang-Mills theory, has been rewarded many times with striking results. The most famous example is the ratio of shear viscosity and entropy density η/s, which was shown to take the universal value $\eta/s = \hbar/4\pi k_B$ for any field theory with an isotropic Einstein-gravity dual [9–12]. The experimentally measured value for the quark-gluon plasma is very close to this universal result [13]. In contrast, for weakly coupled systems, this ratio is in general large and behaves as $\eta/s \sim 1/\lambda^2$ [10] in units of $\hbar$ and k_B, where λ is the coupling constant. The discrepancy between the measured and theoretically predicted value at weak coupling, lead to the conclusion that the quark-gluon plasma is strongly coupled.

Aside from the application to phenomena of particle physics, gauge/gravity duality by now has entered at least two more fields of research: condensed matter physics and quantum information theory, and thereby connected them to black hole physics and string theory. Physics, as one of the natural sciences, started with the goal of identifying the fundamental building blocks of nature. The current answer to this question is that they are quantum fields which continuously fill all of space and whose quantum excitations lead to matter as we observe it. The question about the nature of those excitations, whether they are point particles as in the standard model or strings as in string theory, is not settled. However, all of the research done along the way opened up new questions from which new branches of research emerged. The beauty of holography is that it unites them, in a sense that it can be utilised to shed light on unresolved questions in different branches. Notably, this insight goes beyond the mere use of the gauge/gravity duality as a tool. Rather it appears to be a manifestation of the similarity of physics in the strongly coupled regime, irrespective of the specific problem's microscopic degrees of freedom.

The common feature of situations where gauge/gravity duality is applicable and has proven to be useful, is strong coupling and long range quantum entanglement. In those cases, effective degrees of freedom emerge and replace the ones of the microscopic theory. This often results in universal low-energy properties, irrespective of the different microscopic details. The universal holographic result for η/s can thus be regarded as representing a possible universality class of real physical systems with similar values for that ratio. A further example in the context of condensed matter physics is the linear increase of the electrical resistivity with temperature in *strange metals* [14]. Holographic models, understood as gravity theories with a field theory dual, serve as toy models to investigate universal properties of a whole class of systems.

This thesis investigates applications of gauge/gravity duality to two different kinds of systems. On the one hand, we study holographic superconductors. In addition to the canonical analysis of for example the electrical conductivity, we probe the holographic superconducting state with fermionic degrees of freedom. This allows us to directly compare our holographically obtained results with experimental observations on high-temperature superconductors and we find a strikingly good agreement. On the other hand, we utilise the duality to investigate properties of the entanglement entropy in far from equilibrium systems. The results of this thesis are thus an example of the diversity of problems where holographic methods lead to new insight.

The holographic approach to condensed matter physics is known as *AdS/CMT* *correspondence*, where 'CMT' stands for 'condensed matter theory'. This field of application started with the holographic realisation of a superconductor [15–17]. Similarly to a real superconductor, the holographic version is characterised by a critical temperature at which the system undergoes a phase transition and below which the direct current (DC) conductivity is infinite. This is all the more impressive as the holographic dual of the normal conducting state is believed to resemble the mysterious experimentally observed strange metals. One of the analogies is the emergent local quantum criticality in the *infrared* (IR), which refers to an emergent scale invariance restricted to time and energy while the system is still local in space [18, 19]. Holographically, the phase transition to superconductivity is caused by an instability of a scalar field in the bulk. More precisely, the setup is an *AdS-Reissner Nordström* (AdS-RN) geometry which contains an electrically charged black hole, a $U(1)$ gauge field and the charged scalar mentioned above. In the holographic dual of the normal conducting state, the scalar vanishes identically. However, it becomes unstable at a certain temperature of the dual field theory. This instability leads to a new ground state, where the scalar acquires a non-trivial profile and thereby spontaneously breaks the $U(1)$ gauge symmetry in the gravity theory. The heuristic picture is that in the process, the black hole is partially discharged. The 'missing charge' is then accommodated outside the event horizon by the scalar field. We explain this mechanism and establish the required entries of the holographic dictionary in chapter 3. The discovery of the holographic superconductor is of major importance for both, the condensed matter theory and the black hole physics perspective. On the one hand, it can be regarded as a generalisation of *BCS theory*, the theory describing conventional superconductors [20]. On the other hand, the stable scalar in the vicinity of a black hole is a so-called black hole 'hair' and contrasts the *no-hair theorem*. This observation led to a number of new solutions to Einstein's equations. In fact, the achievements of AdS/CMT mostly are due to the thermodynamic and dissipative nature of classical black holes. Providing new insights into both sides of the duality is a common and very appreciated property of gauge/gravity duality.

The possibility to apply gauge/gravity duality to systems far away from thermal equilibrium is a manifestation of one of its most important and useful properties [21–24]. As an example, lattice models used as tools to study strongly coupled theories rely on working with Euclidean time and are thus not capable of describing real time processes. In contrast, there are no conceptual problems with time dependence in theories of gravity. One of the striking results is that strongly coupled systems reach the hydrodynamic regime, where the system can be appropriately described by long wavelength fluctuations around thermal equilibrium, long before reaching thermal equilibrium [25–28]. This is of course particularly interesting in the context, that systems with a holographic dual are understood to be in a regime of long-range quantum entanglement. Studying out-of-equilibrium systems using holography can thus provide new insight into the interplay between the equilibration process and quantum physics. In this thesis we are especially interested in properties of steady states, which are typically the result of connecting two reservoirs and thus special examples of systems far away from equilibrium.

An interesting quantity related to the quantum properties of a system is entanglement entropy, which is a measure of quantum entanglement. As a non-local quantity it provides a perspective different from the one obtained by studying correlation functions. The AdS/CFT correspondence is not only a weak-strong coupling duality but also maps the quantumness of the field theory to a classical gravity theory. In a seminal work [29, 30] a holographic dual of the entanglement entropy in a quantum field theory was proposed. The by now proven [31] proposal gives it a geometric counterpart: It states that the entanglement entropy of a region A within a quantum field theory is proportional to the area of the minimal surface in the bulk, attached to the boundary of the region A. In this context it is useful to have the heuristic picture in mind, in which the quantum field theory 'lives' on the boundary of the higher dimensional bulk, governed by the dual gravity theory. In this thesis we utilise the entanglement entropy to study the time evolution of quantum information in a steady state setup.

We now give an overview of the achievements presented in this thesis.

First, we work with the minimal setup of a holographic superconductor presented in reference [16]. Our goal is to describe the results of a recent experiment on high-temperature superconductors [32] with holographic methods. This experiment accurately quantified for the first time the long observed strong temperature dependence of the pair-breaking term in those materials and found that it behaves vastly different from conventional superconductors. In this thesis we aim for a comparison with the experiment on a quantitative level which is to be highlighted in the context of the mostly qualitative comparisons between holographic results and observed properties of real physical systems. More specifically, we probe the superconducting state with fermionic degrees of freedom in a way which may be called a 'holographic photoemission experiment' [33]. To this end, a holographic probe fermion is coupled to the superconducting background, while backreaction of the fermionic field to this background is not considered. We choose to work with the version of the coupling established in reference [33], the results therein imply that this coupling allows the setup to have a holographic dual of the gap which is necessary to describe the experimental results. We reconstruct the superconducting backgrounds and solve for the dynamics of the fermionic field to obtain the spectral density function whose pole structure can be directly compared to the experiment. The author developed all of code required to address those tasks. In contrast to the pioneering work in [33], we focus on the case of finite temperature. In the next step the author explored the qualitative effect of the setup's various parameters on the spectral density's pole structure in order to eventually tune the parameters such that the result mimics the experimental one. We find that not every feature can be mapped to the holographic results, however the form of the strong temperature dependence of the pair-breaking term turns out to appear naturally in the holographic context and does not require any fine tuning of the parameters. Upon such a tuning, a remarkable quantitative accordance between holographic and experimental results can be realised. This is a major achievement of this thesis and manifestly substantiates the conjecture, that there is indeed an underlying connection between holographic superconductors and real high-temperature superconductors. In particular, this is important as almost all of the previous results in this direction are based on comparing the metallic phase only. Our results will be published in [2].

Motivated by the results about the fermionic excitations of the simplest possible holographic superconductor model we then aim to find similar results in a more 'realistic' model, based on the holographic strange metal investigated in [34]. In particular, translational symmetry is explicitly broken with the consequence that momentum can dissipate and the observed universality of the electrical resitivity's temperature dependence in real strange metals can be described. In this thesis we extend the model such that it undergoes a phase transition to superconductivity. We then study the effect of momentum dissipation on the properties of the superconducting phase. Our results are in accordance with work on similar holographic models [35, 36], which appeared before our analysis was completed. Probing the superconducting phase with fermionic degrees of freedom, we find the same qualitative picture as for the simpler model. This indicates that the similarity to real high-temperature superconductors in this aspect may indeed be a more general feature of their holographic counterparts. The contribution of the author to this result includes the development of all the required code and the analysis of the setup.

The second focus of this thesis is a far away from equilibirium system in which a steady heat current emerges as a consequence of bringing together two independently thermalised infinite heat baths at different temperatures. Our results are presented in [1]. The heat current is the result of the attempt of this assembled system to reach thermal equilibrium. However, since the two heat baths are treated as infinite reservoirs, the final state of the system is an infinitely extended steady heat current. A holographic dual of this final state in d dimensions was given in [37], whose results are in accordance with results in two dimensions from a field theory perspective [38–40]. Based on the holographic model of [37], we study the time evolution of the entanglement entropy in the case of one-dimensional heat baths, dual to a gravity theory in three spacetime dimensions. With a partly analytical, partly numerical method we find two distinct behaviours, depending on the initial temperature configuration. If the temperature difference is large, the change of the entanglement entropy asymptotes to a linear behaviour. For small temperatures of the same order of magnitude, the entanglement entropy changes with a powerlaw. We present an analytical derivation of those two limits. Moreover, we check the validity of entanglement inequalities. The author contributed to the development of the numerical machinery and set the ground for the semi-analytical approach.

The structure of the thesis is as follows. In chapter 2 we motivate and introduce the AdS/CFT correspondence, after briefly reviewing relevant concepts and techniques of string theory. Moreover, we establish the holographic dictionary and give an overview over the most important generalisations of the original conjecture. In chapter 3 we explain the important entries of the holographic dictionary for applications to condensed matter physics and put it in context with methods of condensed matter theory and current challenges within this field. The remaining chapters contain the author's original work. Chapter 4 investigates a holographic superconductor probed with fermionic degrees of freedom. The results are compared with experimental results on a quantitative level and very good agreement is found. We present our results on a more complicated and at the same time supposedly more realistic holographic model of a superconductor in chapter 5. In particular we probe the superconducting state with fermionic degrees of freedom using the same method as in the previous chapter. Chapter 6 is based on reference [1] and presents our results on the properties and time dependence of the holographic entanglement entropy in a system far away from thermal equilibrium.

We conclude in chapter 7, summarising the results and giving an outlook for possible future research building on the results obtained in this thesis. The appendices A-C provide background information and several technical details.

Throughout this thesis we set the speed of light, the reduced Planck constant and the Boltzmann constant to one, $c = \hbar = k_B = 1$. We always use the mostly plus metric convention, where only the time component of the metric has a minus sign.

CHAPTER 2

AdS/CFT

In this chapter we introduce the holographic duality in its original form and discuss some generalisations of it. In section 2.1 we present the relevant concepts of string theory. The AdS/CFT conjecture is then motivated and explained in section 2.2.

2.1 Preliminaries

2.1.1 String theory and branes

In string theory the fundamental objects are spatially extended strings, sweeping out a 1+1 dimensional worldsheet rather than the one dimensional wordline of point particles. The dynamics of free strings is described by the Nambu-Goto action which is classically equivalent to the Polyakov action [41, 41–45]

$$S = \frac{1}{2\pi\alpha'} \int_{\mathcal{M}} \mathrm{d}^2\sigma \sqrt{-h}\, \eta_{MN} h^{\alpha\beta} \partial_\alpha X^M \partial_\beta X^N \,, \tag{2.1}$$

where h is the metric of the (1+1)-dimensional worldsheet $\mathcal{M}$ and X^M are the coordinates of the string in the D-dimensional target space in which the string lives. In the case of free strings the target space is flat and η is the D-dimensional Minkowski metric. The prefactor is the string tension $T = 1/2\pi\alpha'$ where $\alpha' = \ell_s^2$ parametrises the string scale ℓ_s. The defining gauge symmetries of the Polyakov action are diffeomorphism and Weyl invariance of the worldsheet metric h, i.e. it is conformally invariant [42, 46]. The three independent components of h are completely fixed by these two symmetries.

There are two types of strings: open and closed strings. They differ by the boundary conditions they satsify. Closed strings satisfy periodic boundary conditions $X^M(\tau, \sigma + 2\pi) = X^M(\tau, \sigma)$, with $\sigma \in [0, 2\pi)$. The endpoints of open strings where $\sigma \in [0, \pi)$, are subject to either Neumann or Dirichlet boundary conditions. The former ensures the absence of momentum flow at the strings' endpoints: $\partial_\sigma X^M(\tau, 0) = \partial_\sigma X^M(\tau, \pi) = 0$. The latter fixes the positions of the endpoints by demanding $\delta X^M(\tau, 0) = \delta X^M(\tau, \pi) = 0$. If an open string satisfies the Dirichlet condition for the time component and p spatial components of the target space, its endpoints are restricted to a $(p+1)$-dimensional hypersurface called Dp-brane.

The quantum spectrum of the bosonic Polyakov spectrum contains a tachyon, a state with negative mass. The associated tachyonic instability can be cured by fermionic superpartners ψ^M of the bosonic coordinate fields X^M. A consistent supersymmetric string theory requires the target space to be $(D = 10)$-dimensional. Unlike the bosonic fields, the fermionic fields ψ^M do not satisfy unique boundary conditions. The choice between different sets of conditions results in a choice between different types of string theory. The relevant type for the original AdS/CFT conjecture is type IIB string theory [3].

In the low energy limit only massless modes of the two quantum spectra of closed and open strings, respectively, are relevant. The massless state in the closed string sector is a spin-2 state and can be decomposed into a traceless symmetric, an antisymmetric and a scalar part. Each part is understood to be a quantum fluctuation of a corresponding field in the target space: the target space metric G_{MN}, the Kalb-Ramond field B_{MN} and the dilaton Φ.

The massless excitation in the open string sector is a spin-1 state. This state is decomposed into p+1 components parallel and D-(p+1) components perpendicular to the Dp-brane. The former transform as a vector under diffeomorphisms on the Dp-brane, whereas the latter transform as a scalar. The vector part is identified with a $U(1)$ gauge field A_a, $a = 0, ..., p$, living on the Dp-brane. The scalar excitations can be regarded as transverse fluctuations of the Dp-brane itself, turning it into dynamical object within string theory [46].

This classification of the massless spectra in the open and closed string spectra allows us to write down a low-energy effective action for each sector. Low-energy refers to small α', i.e. small string length ℓ_s. They are extensions of the Polyakov action (2.1) and describe a probe string in a background formed by the fields identified above. For the bosonic part of the closed string sector this gives

$$S = \frac{1}{4\pi\alpha'} \int_{\mathcal{M}} \mathrm{d}^2\sigma \sqrt{-h} \Big[G_{MN} h^{\alpha\beta} \partial_\alpha X^M \partial_\beta X^N + i B_{MN} \epsilon^{\alpha\beta} \partial_\alpha X^M \partial_\beta X^N \\ + \alpha' \Phi R^{(2)} \Big] \, . \tag{2.2}$$

The Ricci scalar $R^{(2)}$ of the worldsheet metric h does not contain dynamical information, as h can be fixed by the conformal symmetry. Instead it evaluates to an integer related to the topology of the string worldsheet. The dilaton is related to the string coupling $g_s = e^{\Phi_0}$, where we split $\Phi = \Phi_0 + \tilde{\Phi}$, a constant and a dynamical part. In the case of a free string, the target space reduces to Minkowski space, B vanishes, the dilaton Φ is constant and (2.2) reduces to (2.1).

The dynamics of a probe string in an open string background is determined by a low-energy effective action given by

$$S = \frac{1}{4\pi\alpha'} \int_{\mathcal{M}} \mathrm{d}^2\sigma \sqrt{-h}\, \eta_{MN} h^{\alpha\beta} \partial_\alpha X^M \partial_\beta X^N + \int_{\partial\mathcal{M}} \mathrm{d}\tau A_a \dot{X}^a \, , \tag{2.3}$$

where $a = 0, ..., p$ labels the direction on the Dp-brane. The second integral runs over the spatial boundary, the endpoints of the string, because it is those endpoints which are connected to the Dp-brane where the abelian gauge field A lives.

We must now ensure that the conformal symmetry of the Polyakov action for the free string (2.1) is still present in the generalised versions (2.2) and (2.3). For this purpose the background fields can be regarded as dynamial couplings whose β-functions have to vanish in order to preserve the conformal symmetry. Those β functions can be obtained as equations of motion from an action for the background fields. In the case of the closed string sector this action results in the type IIB superstring action whose bosonic part reads

$$S^{(b)}_{IIB} = \frac{1}{(2\pi)^7 \ell_s^8} \int \mathrm{d}^{10}X \sqrt{-G} \left[e^{-2\Phi} \left(R + 4(\partial\Phi)^2 \right) - \frac{2}{(D-2-p)!} F^2_{p+2} \right] \tag{2.4}$$

where F_{p+2} is the field strength of the form field A_{p+1}, $F_{p+2} = \mathrm{d}A_{p+1}$. For the type IIB sector, p can only take the odd values $p = 1, 3, 5$. Moreover, the five form $\tilde{F}_5$ has to be self dual: $\tilde{F}_5 = *\tilde{F}_5$ [43]. The equations of motion following from the type IIB action are Einstein's equations for the Einstein frame metric $G_{(\mathrm{E})}$, which is related to the string frame metric $G \equiv G_{(\mathrm{S})}$ as $G_{(\mathrm{E})} = \mathrm{e}^{-\tilde{\Phi}/2} G_{(\mathrm{S})}$. Performing this redefinition results in an extra factor of g_s^2, due to separating the constant part of the dilaton in (2.4). The prefactor of the corresponding Einstein frame action is then $1/8\pi G_{\mathrm{N}} \equiv 1/2\kappa_{10}^2 \sim g_s^2/\ell_s^8$.

With the same logic we obtain for open string sector the Dirac-Born-Infeld (DBI) action whose bosonic part is given by

$$S_{\mathrm{DBI}}^{(b)} = -T_p \int \mathrm{d}^{p+1}\zeta e^{-\tilde{\Phi}} \sqrt{-\det\left(P\left[G_{ab}\right] + P\left[B_{ab}\right] + 2\pi\alpha' F_{ab}\right)}\,, \tag{2.5}$$

where $T_p = 1/g_s(2\pi)^p(\alpha')^{(p+1)/2}$ is the brane tension and $F = \mathrm{d}A$ the field strength. P denotes the pullback of G and B onto the Dp-brane: $P[G_{ab}] = G_{MN}\partial_a X^M \partial_b X^N$. The action (2.5) is of the same form as the Nambu-Goto action for the (1+1)-dimensional string and can be thought of describing a probe Dp-brane in a potentially curved target space. By the open-closed string duality [46,47], the Dp-brane is a source of closed string excitations as well and hence is a gravitating object. Taking this into account, the DBI action (2.5) represents only the lowest order in the string coupling g_s of string perturbation theory and hence is only valid for $g_s \ll 1$ [48].

In the remainder of this section we discuss one specific solution of each of type IIB superstring theory (2.4) and the DBI action (2.5). These solutions will form the gravity and field theory part, respectively, of the AdS/CFT conjecture.

2.1.2 Type IIB supergravity on $\mathbf{AdS}_5\times\mathbf{S}^5$

Extended p dimensional objects, p-branes, embedded in the D-dimensional target space are solitonic solutions to supergravity [48]. In particular, we are interested in flat $(p+1)$-dimensional magnetically charged solutions of the type IIB string theory (2.4). A typical solution of this kind involves an event horizon. For a $(D = 10)$-dimensional target space, such a solution is given by [48]

$$\begin{aligned} \mathrm{d}s^2 = &- \frac{f_+(\rho)}{\sqrt{f_-(\rho)}}\mathrm{d}t^2 + \sqrt{f_-(\rho)}\delta_{ij}\mathrm{d}x^i\mathrm{d}x^j + \frac{f_-(\rho)^{-\frac{1}{2}-\frac{5-p}{7-p}}}{f_+(\rho)}\mathrm{d}\rho^2 \\ &+ \rho^2 f_-(\rho)^{\frac{1}{2}-\frac{5-p}{7-p}}\mathrm{d}\Omega_{8-p}^2\,, \end{aligned} \tag{2.6}$$

with the emblackening factors $f_\pm$ and the dilaton given by

$$f_\pm(\rho) = 1 - \left(\frac{r_\pm}{\rho}\right)^{7-p}\,, \quad e^{-2\Phi(\rho)} = g_s^{-2} f_-(\rho)^{-(p-3)/2}\,. \tag{2.7}$$

The p-brane carries N units of the magnetic charge [48]

$$N = (4\pi)^{\frac{p-5}{3}}\Gamma\left[\frac{7-p}{2}\right]^{-1} g_s^{-1}\left(\alpha'\right)^{\frac{p-7}{2}}\left(r_+r_-\right)^{\frac{7-p}{2}} . \tag{2.8}$$

In the extremal limit $r_+ = r_-$ the metric (2.7) reduces to

$$\mathrm{d}s^2 = \frac{1}{\sqrt{H(r)}}\eta_{\mu\nu}\mathrm{d}x^\mu\mathrm{d}x^\nu + \sqrt{H(r)}\left(\mathrm{d}r^2 + \mathrm{d}\Omega\right) , \tag{2.9}$$

where we switched from the string frame in (2.4) and (2.7) to the Einstein frame. The new coordinate r is related to ρ by $r^{7-p} = \rho^{7-p} - L^{7-p}$, with $L = r_+$, such that

$$H(r) = 1 + \left(\frac{L}{r}\right)^{7-p} , \quad e^{\Phi(r)} = g_s H(r)^{\frac{3-p}{4}} . \tag{2.10}$$

The horizon is now located at $r = 0$. Note that in the extremal limit a regular solution is only possible for $p = 3$, where also the dilaton, and hence the string coupling g_s, are constant. The case of $p = 3$ is the relevant one for the original AdS/CFT conjecture.

There are two types of low energy excitations in this extremal p-brane space (2.9). Low energy refers to the energy measured by an observer at $r \to \infty$. This observer measures the energy E of an object at position r to be $E = \sqrt{-g_{tt}}E_r$ compared to the energy E_r measured by an observer at position r. Close to horizon $r \ll L$ and far away $r \gg L$ this relation becomes

$$\frac{E}{E_r} = \sqrt{-g_{tt}} = H(r)^{-1/4} \sim \begin{cases} 1 & \text{for } r \gg L\,, \\ \frac{r}{L} & \text{for } r \ll L\,. \end{cases} \tag{2.11}$$

This means that low energy excitations can either be long-wavelength excitations in the asymptotically flat region $r \gg L$, or excitations of arbitrary wavelength, and hence energy arbitrary E_r, close to the horizon $r \ll L$. Close to the horizon, the geometry given in (2.9) reduces to the $\mathrm{AdS}_5 \times S^5$ geometry

$$\mathrm{d}s^2 = \frac{r^2}{L^2}\eta_{\mu\nu}\mathrm{d}x^a\mathrm{d}x^b + \frac{L^2}{r^2}\mathrm{d}r^2 + L^2\mathrm{d}\Omega_5\,, \tag{2.12}$$

where the first two terms constitute the Anti-de Sitter part and the last term the five-dimensional sphere. The isometry group of (2.12) is $SO(4,2) \times SO(6)$. The excitations in the near-horizon and asymptotic flat region decouple from each other [48]. In the low energy limit $\alpha' \to 0$, where only low energy excitations are allowed, this decoupling can be schematically expressed as

$$S_{\text{IIB}} \to S_{\text{IIB on AdS}_5\times S^5} + S_{\text{free IIB}}\,. \tag{2.13}$$

It is important to stress that throughout this subsection we assumed the supergravity limit of (2.4) to hold. This limit is justified only when the inverse curvature of the brane is smaller than the string length scale $\ell_s \ll L$. Moreover, the string coupling has to be small $g_s < 1$ in order to suppress string loop corrections. Comparing the prefactor of (2.4) in the Einstein frame with the definition of Newton's constant $G_{\text{N}} \sim \ell_P^8$ in terms of the Planck length ℓ_P, the smallness of the string coupling implies $\ell_P < \ell_{\text{s}}$. In combination with equation (2.8) the supergravity limit can be expressed by [48]

$$N > N g_s \gg 1\,. \tag{2.14}$$

2.1.3 $\mathcal{N}$=4 Super-Yang-Mills theory

The DBI action (2.5) describes the Dp-brane as an object on which open strings end and on which a Maxwell gauge field lives. Instead of just a single Dp-brane one can also consider a stack of N coincident branes. Open strings can now end in N^2 different ways on them. This extends the $U(1)$ symmetry of a single brane to a non-abelian $U(N) \simeq U(1) \times SU(N)$ symmetry. In the low-energy limit $\alpha' \to 0$ the DBI action in flat space can be expanded in α' and to leading order is given by [44]

$$S_{\text{DBI}} = -\frac{(2\pi\alpha')^2}{2} T_3 \int \mathrm{d}^4\zeta\, \mathrm{Tr}\left(\frac{1}{4}F^2 + ...\right)\,, \tag{2.15}$$

where the '...' refers to terms independent of the gauge field A. Moreover, the $U(1)$ modes decouple from the $SU(N)$ modes [48]. The standard prefactor of a Yang-Mills theory $1/4g_{\text{YM}}^2$, according to this action, is related to g_s through

$$4\pi g_s = g_{\text{YM}}^2\,. \tag{2.16}$$

D3-branes are 1/2 BPS states and preserve half of the 32 supercharges [49]. This manifests itself as maximal supersymmetry $\mathcal{N} = 4$ of the Super-Yang-Mills (SYM) theory on the brane. As mentioned before, the DBI action (2.5) describes a dynamical brane in potentially curved background. Only the probe limit, in which string loop corrections are suppressed, allows us to decribe the dynamics of the stack of N Dp-branes with equation (2.15). The effective expansion parameter in this case is Ng_s and this limit translates into the condition [48]

$$Ng_s \ll 1\,. \tag{2.17}$$

To summarise, in the low energy limit the DBI action (2.5) for a stack of N coincident Dp-branes reduces to $\mathcal{N}=4$ SYM theory plus free type IIB gravity

$$S_{\text{DBI}} \to S_{\mathcal{N}=4\text{ SYM}} + S_{\text{free IIB}}\,. \tag{2.18}$$

$\mathcal{N}=4$ SYM theory with gauge group $SU(N)$ is the gauge theory part of the AdS/CFT conjecture. Let us therefore have a closer look at its most important properties. Supersymmetry is a spacetime symmetry which extends the bosonic Poincaré algebra by fermionic supercharges Q^i, $i=1,...,\mathcal{N}$ that change the spin of states by 1/2. The maximal spin of a theory without gravity is spin 1 and hence $\mathcal{N}=4$ is the maximal supersymmetry which is encoded in a $SU(4)\simeq SO(6)$ global symmetry of the theory. Its field content is grouped in just one supermultiplet. As the gauge field A transforms in the adjoint representation of the gauge symmetry and all members of the supermultiplet have to transform alike, the theory does not contain fields transforming in the fundamental representation. In addition to the maximal supersymmetry, the theory is also conformally invariant. The β-function of the only coupling present in $\mathcal{N}=4$ SYM theory vanishes to all orders in perturbation theory and does not get non-perturbative corrections either [50]. The global superconformal symmetry is represented by the supergroup $SU(2,2|4)$ whose maximal bosonic subgroup is $SO(4,2)\times SU(4)$.

In the context of the AdS/CFT conjecture we will be interested in the limit of large number of colours $N\to\infty$. Introducing the *'t Hooft coupling*

$$\lambda = g_{\text{YM}}^2 N\,, \tag{2.19}$$

renders this limit well defined in perturbation theory. The large N limit can now be realised by taking $N\to\infty$ while at the same time keeping λ fixed. This is the so-called *'t Hooft limit* [51]. Feynman diagrams can be classified according to their scaling behaviour with N. An expansion in $1/N$ results in a topological expansion of diagrams where planar diagrams are the leading contribution. The ‘t Hooft limit is therefore a semi-classical limit [51]. Strong coupling then corresponds to large values for the ‘t Hooft coupling λ. In this case perturbation theory breaks down.

2.2 AdS/CFT conjecture

2.2.1 Maldacena's original argument

We discussed extremal 3-branes in the supergravity limit $Ng_s \gg 1$ (2.14), from the perspective of the closed string sector, and a stack of N coincident D3-branes in the string loop perturbation limit $Ng_s \ll 1$ (2.17). In the low energy limit they reduce to type IIB supergravity on $\mathrm{AdS}_5 \times S^5$ plus free type IIB gravity (2.13) in flat space and $\mathcal{N}$=4 SYM theory plus type IIB gravity in flat space (2.18), respectively.

It was stated in [47] that Dp-branes in the opposite limit, i.e. $Ng_s \gg 1$, may be described by extremal p-branes. Based on that, Maldacena concluded that the D3-branes and extremal 3-branes, and hence $\mathcal{N} = 4$ SYM theory and type IIB supergravity on $\mathrm{AdS}_5 \times S^5$, are ultimately two different descriptions of the same thing but in two different limits of Ng_s [3]. Or put differently, that the two theories are (continuously) converted into each other going from $Ng_s \ll 1$ to $Ng_s \gg 1$. The relation between the parameters of the two theories according to equations (2.8) and (2.19) can be combined into

$$4\pi g_s = g_{\mathrm{YM}} = \frac{\lambda}{N}\,, \quad L^4 = 4\pi g_s N \alpha'^2 = \lambda \alpha'^2\,. \tag{2.20}$$

Given this relation, the analogue of the supergravity limit $N > Ng_s \gg 1$ implies for $\mathcal{N} = 4$ SYM

$$N \to \infty \quad \text{and} \quad \lambda \to \infty\,. \tag{2.21}$$

Maldacena then conjectured that $\mathcal{N} = 4$ SYM in this limit is equivalent to the low energy supergravity on $\mathrm{AdS}_5 \times S^5$, where

$$g_s \to 0 \quad \text{and} \quad \alpha' \to 0\,. \tag{2.22}$$

This conjecture goes under the name of AdS/CFT conjecture. 'AdS' represents the gravity part of the equivalence and 'CFT' represents the conformal field theory part. Equations (2.21) and (2.22) constitute the so-called *Maldacena limit* which is the *weak form* of the conjecture. There are two stronger formulations. The *strong form* still requires the 't Hooft limit $N \to \infty$ but allows the 't Hooft coupling λ to take any value. In this case the string coupling $g_s = \lambda/N$ is small and perturbation theory in g_s corresponds to the perturbative epansion in $1/N$ on the field theory side. Looking at the second relation in (2.20) it becomes clear that finite λ allows $\alpha' = \ell_s^2$ to be finite as well. This relaxes the low energy bound on the supergravity side of the equivalence. The *strongest form* of the conjecture states the equivalence of $\mathcal{N} = 4$ SYM theory and type IIB string theory on $\text{AdS}_5 \times S^5$ for any value for N and λ and hence any value for g_s and α' . However, to date it is not possible to explicitly formulate a consistent quantum theory of gravity that allows strong string coupling. Given the profound knowledge about weakly coupled quantum field theories which would be dual to a strong string coupling limit, one might hope that the AdS/CFT conjecture can give insight to this problem. For the rest of this thesis only the weak form is relevant in which case the equivalence relates the strongly coupled conformal field theory to the weakly coupled classical gravity theory.

A key observation about the conjecture concerns the symmetries of the two theories: the superconformal group $SU(2,2|4)$ representing the global symmetry of $\mathcal{N} = 4$ SYM theory is the same as the gauge group of the gravity theory. The matching of the symmetries is most accessible of we look at the maximal bosonic subgroup $SO(4,2) \times SO(6)$ which is precisely the isometry group of $\text{AdS}_5 \times S^5$.

A proof of the conjecture can only be presented with the help of a fully quantum theory of strings, which to this date is not available. It is however a widely accepted consensus that it is true as there is a lot of evidence in favour of the conjecture. Some quantities and object were explicitly calculated on both sides and were found to be the same. One example are correlations functions of 1/2 BPS operators [48]. They are protected by non-renormalisation theorems and can thus be computed in the weakly coupled limit of $\mathcal{N}$=4 SYM theory. Another example is the spectrum of chiral operators which does not depend on the coupling either. Other tests such as the c-theorem are of qualitative nature [52, 53].

2.2.2 Field-operator map

The power of the AdS/CFT correspondence lies in the practical nature of its consequences. The equivalence of the two theories allows to establish a one-to-one map between their respective constituents and properties. This is called the holographic dictionary and in the course of the first two chapters of the thesis we will add more and more entries to that dictionary.

The map relates the generating functional of the conformal field theory given by

$$\begin{aligned} Z_{\mathrm{CFT}}\left[J_\Delta\right] &= \int \mathcal{D}\phi \exp\left(iS_{\mathrm{CFT}} + i\int \mathrm{d}^d x J_\Delta \mathcal{O}_\Delta\right) \\ &= \left\langle \exp\left(i\int \mathrm{d}^d x J_\Delta \mathcal{O}_\Delta\right)\right\rangle_{\mathrm{CFT}} , \end{aligned} \tag{2.23}$$

where J_Δ is the source of the operator $\mathcal{O}_\Delta$ of dimension Δ, to the generating functional on the gravity side of the duality. Making use of the non-dynamical boundary at $r \to \infty$ in (2.12) it is possible to formulate the gravity theory's partition function as a Dirichlet problem [54], where the fields ϕ asymptote to ϕ_0 at the boundary

$$Z_{\mathrm{gravity}}\left[\phi_0\right] = \int_{`\phi\to\phi_0`} \mathcal{D}\phi \exp\left(iS_{\mathrm{gravity}}\left[\phi\right]\right) . \tag{2.24}$$

This relation, known as *GKPW formula*, first formulated by Gubser, Klebanov, Polyakov [4] and Witten [5], equates those two generating functionals

$$Z_{\mathrm{gravity}}\left[\phi_0\right] = \left\langle \exp\left(i\int \mathrm{d}^d x\, \phi_0\, \mathcal{O}_\Delta\right)\right\rangle_{\mathrm{CFT}} . \tag{2.25}$$

The crucial element is that the sources J_Δ of the conformal field theory operators $\mathcal{O}_\Delta$ are equivalent the 'boundary values' ϕ_0 of the gravity theory fields ϕ. The GKPW formula thus establishes a field-operator map between operators $\mathcal{O}$ and their gravity duals ϕ. Note that in the large N limit, the gravity theory is classical and the generating functional (2.24) reduces to its saddle point where only the on-shell (os) solution contributes

$$Z_{\mathrm{gravity}}\left[\phi_0\right] = \exp\left(i\, S^{\mathrm{os}}_{\mathrm{gravity}}\left[\phi\right]\right) . \tag{2.26}$$

The GKPW formula suggests the intuitive picture that the field theory lives on the conformally flat boundary of the AdS space and that the 'boundary values' of the gravity theory fields really are the sources of the appropriate conformal field theory operator. In this picture the inner of the AdS space is often referred to as bulk. A matching of gravity fields and conformal field theory operators has to obey the condition that they should reside in the same representation of the supergroup $SU(2,2|4)$ [49].

To illustrate the field-operator map at work, let us look at the canonical example of a probe scalar field in the bulk, which can be thought of as the gravity dual of a single trace operator. It is described by the following action

$$S[\phi] = \int \mathrm{d}^{d+1}x \sqrt{-g} \left(\frac{1}{2} (\nabla\phi)^2 + \frac{m^2}{2}\phi^2 \right) \quad \Rightarrow \quad \nabla^2\phi - m^2\phi = 0\,. \tag{2.27}$$

The equation has two solutions characterised by their asymptotic behaviour at the AdS boundary

$$\phi = \phi_0 r^{\Delta_+ - d} + \ldots + \phi_1 r^{\Delta_+} + \ldots \tag{2.28}$$

where Δ_+ is the larger root of $\Delta(\Delta - d) = m^2L^2$. We can now clarify the meaning of the 'boundary value' in the context of the GKPW formula: It is the leading mode of the expansion at the boundary. The two modes sometimes also are referred to as *non-normalisable* (leading) and *normalisable* (subleading) mode. Performing a scale transformation $(x^\mu, r) \to (\lambda x^\mu, \lambda^{-1} r)$ under which the AdS metric (2.12) is invariant. The scalar field must be invariant as well and therefore $\phi_{0,1}$ must scale as

$$\phi_0 \to \lambda^{d-\Delta_+}\phi_0\,, \quad \phi_1 \to \lambda^{\Delta_+}\phi_1\,. \tag{2.29}$$

ϕ_0 plays the role of the source of the operator $\mathcal{O}$ dual to ϕ. According to the conformal field theory side of the GKPW formula this implies that under such a scale transformation the operator must behave as $\mathcal{O} \to \lambda^{\Delta_+}$, thus Δ_+ is the dimension of the operator $\mathcal{O}$. We can use the GKPW formula (2.25) to compute its one-point function

$$\langle \mathcal{O} \rangle = \frac{1}{Z_{\mathrm{QFT}}} \frac{\delta Z_{\mathrm{QFT}}}{\delta\phi_0} = \lim_{r\to\infty} i \frac{\delta S_{\mathrm{gravity}}}{\delta\phi_0} \propto \phi_1\,. \tag{2.30}$$

Note that we left out a subtlety concerning the divergences that arises in the above procedure. We will address this topic in the next section. The above example demonstrates that the sourced operator is proportional to the normalisable mode and its dimension is directly related to the mass of the bulk field [55, 56]. This mass-dimension relation provides another interesting information about the probe scalar. A closer inspection of the above equation reveals that the scalar mass can be negative without becoming unstable. The stability bound allows all masses which obey

$$m^2L^2 \geq -\frac{d^2}{4}\,. \tag{2.31}$$

This is called the *Breitenlohner-Freedman* (BF cound) [57, 58].

There are two further important examples of dual field-operator pairs. The first is the conformal field theory's stress energy tensor T. It couples to perturbations of the flat metric and hence the dual gravity field is the bulk metric itself. The second is a global $U(1)$ conserved current $\mathcal{J}$. It is dual to a Maxwell field A in the bulk. This is characteristic of the gauge/gravity duality: global symmetries of the conformal field theory are dual to gauged symmetries on the gravity side. The reason is that the bulk gauge symmetry also demands invariance under 'large' gauge transformations which reduce to global symmetries on the boundary of the geometry [48]. We thus can extend the holographic dictionary by two more entries

$$g_{\mu\nu} \leftrightarrow \langle T_{\mu\nu}\rangle \ , \quad A_\mu \leftrightarrow \langle \mathcal{J}_\mu \rangle \ , \tag{2.32}$$

where μ and ν label the directions of the conformal field theory and can thus be regarded as the AdS boundary indices.

2.3 Holography

2.3.1 Holographic principle

The holographic principle has its origin in Bekenstein's observation that the entropy of a black hole scales with the area A of its horizon [6]

$$S_{\mathrm{BH}} = \frac{A}{4G_{\mathrm{N}}}\,, \tag{2.33}$$

where G_{N} is Newton's constant. The black hole is the most compact object and hence this directly implies that the maximal entropy of any spatial volume V can, in a theory with gravity, only scale with the area A enclosing the volume. This is counterintuitive from a thermodynamical or even quantum field theory point of view, where entropy is proportional to the volume V. Two decades later the idea of the holographic principle was born [7]. It states that the information of a $(d+1)$-dimensional quantum gravity theory can be stored on the d-dimensional surface and completely be captured by a theory without gravity. The holographic principle has its name from the metaphorically similar hologram where the third dimension of an object is reconstructed via interference and coherence properties of light. After Susskind specified the idea of the holographic principle by giving it a possible realisation within string theory [8], the AdS/CFT conjecture is its first explicit realisation [3].

It seems that from a gravity perspective a non-gravitating quantum field theory at one fewer dimension is the minimal framework to describe its information content. From a quantum field theory perspective, the additional geometrical dimension has an interpretation on its own. The radial coordinate r in (2.12) represents an energy scale, where $r \to \infty$ is the *ultraviolet* (UV) limit of the gauge theory and $r \to 0$ the *infrared* (IR) fixed point. The origin of this interpretation is the observation that UV divergencies can be identified with divergencies at the AdS boundary [55]. Moreover, the renormalisation group (RG) flow of the quantum field theory is naturally represented by Einstein's equations on the gravity side. This can be viewed as a further entry in the holographic dictionary: RG flows of quantum field theories have a geometric interpretation in terms of the radial coordinate of their dual gravity theories. There are various examples of this interpretation such as the holographic c theorem [52,53], which states the existence of a real and positive function decreasing monotonically along the RG flow.

It is then natural to expect that there is a geometric version of the quantum field theory renormalisation procedure. The gravity dual of the UV-cutoff ϵ is the inverse radial coordinate near the boundary $\epsilon = 1/r$. Thus instead of evaluating expressions related to the field-operator map (2.25) and (2.30) directly on the AdS boundary, they have to be evaluated on a slice located just inside the boundary at $r = 1/\epsilon$. Adding appropriate counterterms to the gravity action removes the dependence on the cutoff ϵ, similarly to the quantum field theory renormalisation, and one can send $\epsilon \to 0$ [59]. This procedure is known as holographic renormalisation. Reference [55] provides a comprehensive introduction to this topic.

2.3.2 Other types of gauge/gravity dualities

The AdS/CFT conjecture as discussed above is the result of the identification of two interpretations of N coincident D3 branes in type IIB string theory in a ten-dimensional spacetime. It results in an equivalence between a (3+1)-dimensional quantum field theory and a (4+1)-dimensional classical gravity theory. There are further holographic dualities also motivated directly from string theory. Let us mention the two canonical examples. The first example is the duality between ABJM theory in 2+1 dimensions, taking the role of the quantum field theory side, and eleven dimensional supergravity on $\mathrm{AdS}_4 \times S^7/\mathbb{Z}_k$ [60]. The second example maps $\mathcal{N} = (4,4)$ superconformal field theory in 1+1 dimensions to type IIB supergravity in $\mathrm{AdS}_3 \times S^3 \times M^4$, see e.g. [48]. Just like for the original AdS/CFT correspondence the dualities involve a quantum field theory at one fewer dimension than the involved AdS space.

All of the dualities contain supersymmetry. Of course this arises naturally from a supersymmetric string theory. But its presence is also important on a technical level as it constrains the theories involved and in particular is responsible for many observables to be independent of the coupling strength.

2.3.3 Holographic models

Maldacena's original conjecture has its origin in string theory. Both, supergravity on $\mathrm{AdS}_5 \times S^5$ and $\mathcal{N} = 4$ SYM are well defined limits of consistent string theories. We recognised the weak form of the conjecture as a weak-strong coupling duality and a classical-quantum duality. It is well known that strongly coupled systems are difficult to handle theoretically as the otherwise powerful perturbation theory is not applicable in those cases. AdS/CFT seems to be a promising candidate for a method to study strongly coupled systems. However, the two theories involved in the AdS/CFT proposal are quite special due to their high degree of symmetry.

Nonetheless, it turns out that more general models, referred to as gauge/gravity duality, can describe less symmetric strongly coupled systems. The duality is thus a powerful tool to investigate phenomena due to strong coupling. It can be successfully applied to universality classes of systems, whose properties are governed by common principles or symmetries rather than the individual microscopic details. The most prominent example is the ratio of shear viscosity and entropy density which is generically bounded from below by $\eta/s \geq 1/4\pi$ for theories with a holographic dual [9–12]. A value very close to this bound was found for the quark-gluon plasma which is assumed to be strongly coupled [13]. Up to date, no other method is capable of generating a value for η/s anywhere near this bound. Backed up with this remarkable success, it is tempting to try to reduce the original conjecture to a minimal set of features: classical Einstein-Hilbert gravity on an asymptotic AdS space and a quantum field theory with a conformal symmetry in the UV at strong coupling. The corresponding action of such a setup is given by

$$S = \frac{1}{2\kappa^2}\int \mathrm{d}^{d+1}x\sqrt{-g}\,\left[R - 2\Lambda\right]\,, \tag{2.34}$$

where $\Lambda = -d(d-1)/2L^2$ is the negative cosmological constant of AdS space and κ is the $(d+1)$-dimensional gravitational constant.

Based on this approach it is possible to for example extend the field content of the dual quantum field theory or even give up conformal symmetry in the IR, see chapter 3. There are two different classes of those more general holographic models: the *top-down-* and the *bottom-up-models*. Top-down models are dualities between two theories that are consistent truncations of string or M-theory. They are obtained in the same way as the original conjecture but with different brane constructions. In contrast, bottom-up models start off with classical gravity on AdS space (2.34) supplemented by a set of fields which mimic properties of the dual quantum field theory one is interested in. The field content of bottom-up models is often motivated by consistent truncations of string or M-theory. However, the fixing of the coupling constants that generically accompanies such truncations is ignored. Bottom-up models treat the coupling constants as free and independent of each other. A prominent example for a bottom-up model is the holographic superconductor [16]. This model co-founded the field of *AdS/CMT*, where the holographic duality is applied to condensed matter theory (CMT).

2.3.4 Extensions of the original conjecture

Let us give a few explicit examples of extensions of the original AdS/CFT conjecture. All of them have been widely used to construct holographic models. But they also break conformal invariance in the IR. We can thus expect only qualitative insight into the properties of strongly coupled systems. The list is far from complete. More information on this topic can be found in the references [49] and [14]. The most important one is to give the quantum field theory a *finite temperature*. A thermal field theory is related to a theory at zero temperature by a Wick rotation $t \to i\tau$ along with the compactification of the Euclidean time coordinate τ on a circle with radius $\beta = 1/T$. The partition function of a thermal field theory is given by

$$Z_{\text{thermal}} = \int \mathcal{D}\phi \exp\left(-S_{\text{QFT}}\right) = \exp\left(-S^{\text{os}}_{\text{gravity}}\right) , \tag{2.35}$$

where we used the GKPW formula (2.26) in the last step. For the grand potential Ω this implies

$$\Omega = -\frac{1}{\beta} \log Z_{\text{thermal}} = \frac{1}{\beta} S^{\text{os}}_{\text{gravity}} . \tag{2.36}$$

The gravity dual of a thermal field theory is a geometry with a black brane, a geometry with a planar horizon [61][1]. The simplest realisation is the $(d+1)$-dimensional AdS-Schwarzschild solution

$$\mathrm{d}s^2 = \frac{r^2}{L^2}\left(-f(r)\mathrm{d}t^2 + \mathrm{d}\underline{x}^2\right) + \frac{L^2}{r^2 f(r)}\mathrm{d}r^2 \quad \text{with} \quad f(r) = 1 - \left(\frac{r_{\text{h}}}{r}\right)^d , \tag{2.37}$$

where f is the emblackening factor given in terms of the horizon radius r_{h}. The temperature of the thermal field theory is then equal to the Hawking temperature of the black brane. The latter is related to the surface gravity of the black hole horizon and can be derived from equation (2.37) by Wick rotating to Euclidean time τ and compactifying it close to the horizon with radius 2π in order to avoid a conical singularity. Identifiying the compactification radius with the field theory

[1] In this thesis only black branes are relevant. However, for the sake of convenience, we will inaccurately refer to them as black holes, which technically are characterised by a spherical horizon geometry.

analogue β gives the Hawking temperature

$$T = \frac{1}{4\pi}\sqrt{-g'_{tt}(r_\mathrm{h})g^{rr\prime}(r_\mathrm{h})}\,, \tag{2.38}$$

for any diagonal metric with an emblackening factor. In the case of the $(d+1)$-dimensional AdS-Schwarzschild metric the black hole temperature is $T = d\,r_\mathrm{h}/4\pi$. The AdS/CFT correspondence equates the Hawking temperature with the temperature of the dual thermal field theory.

Closely related to the temperature entry in the holographic dictionary is the identification of the black hole's Bekenstein-Hawking entropy (2.33) on the gravity side of the duality with the *thermal entropy* S_TFT of the thermal field theory side

$$S_\mathrm{TFT} \equiv S_\mathrm{BH} = \frac{2\pi}{\kappa^2_{d+1}}\left(\frac{r_\mathrm{h}}{L}\right)^{d-1}\sqrt{\Pi_{i=1,\ldots,d-1}g_{ii}}V_{d-1}\,. \tag{2.39}$$

For the last step we used $\kappa_d = 8\pi G_{\mathrm{N},d}$ and introduced $V_{d-1} = \int \mathrm{d}^{d-1}x$, which corresponds to the spatial volume of the dual field theory. The squareroot factor contains the potentially non-trivial metric components g_{ii} evaluated at the horizon. In the case of the AdS-Schwarzschild metric (2.37) they are $g_{ii} = 1$.

For many applications of the gauge/gravity duality to condensed matter systems it is inevitable to have a holographic realisation of compressible matter. More precisely, a holographic dual for a *finite charge density* is required, which can be varied, i.e. compressed smoothly. The charge density operator is the zeroth component of a charge current (2.32). As global symmetries of the field theory correspond to gauged symmetries of the gravity side, the holographic realisation of a charge current and hence of a finite charge density is a $U(1)$ gauge field in the bulk [14, 49]. We discuss this entry of the holographic dictionary in more detail in the next chapter 3.2.

We argued above that all the fields in $\mathcal{N} = 4$ SYM transform in the adjoint representation. Conclusively the AdS/CFT conjucture does not involve any *fundamental degrees of freedom* like the Standard Model quarks or leptons. Reference [62] presented their holographic realisation by adding N_f probe Dp-branes leading to a $U(N_f)$ flavour symmetry.

A conceptually rather different application of holography concerns the measurement of quantum information or quantum entanglement. Entanglement entropy is generically a quantity difficult to access with conventional methods as it is by definition related to long range quantum entanglement and cannot by captured by a perturbative approach on microscopic scales. The holographic dual of the entanglement entropy between a region A, with boundary ∂A, and its complement A_c is given by the area of the minimal surface in the bulk attached to ∂A at the AdS boundary divided by $4G_{\mathrm{N}}$, analogously to (2.33) [29, 63]. This entry of the holographic dictionary manifests the close relationship of quantum physics and geometry established by the AdS/CFT correspondence. The concept of holographic entanglement entropy is discussed in more detail in chapter 6.

CHAPTER 3

Holography and condensed matter physics

In this chapter we introduce the application of the AdS/CFT correspondence to condensed matter physics, known as AdS/CMT, where CMT stands for condensed matter theory. In the past years, AdS/CMT offered an entirely new perspective on open problems in condensed matter theory [14, 49, 54, 64, 65]. It translates its traditional language to the language of high energy physics. The success of the AdS/CMT duality is an astonishing example of the profound insight that seemingly unrelated fields of physics can be described by the same concepts. In section 3.1 we review basic elements of condensed matter theory formulated in the traditional language and thereby laying the ground for the holographic picture in the remaining sections of this chapter 3.2-3.5.

3.1 Basic elements of condensed matter theory

3.1.1 Fermi liquid theory

Landau's Fermi liquid theory was established more than five decades ago and is an important part of what may be called the standard model of condensed matter theory. It is capable of describing a wide range of observed metallic states. The model of interacting fermions captures almost all metals and superconductors. Yet it can be viewed as an example of a compressible state of quantum matter, where compressible refers to the property, that the density can be varied continuously. Quantum matter refers to a state of matter with long-range quantum entanglement. The source of its quantum nature are its constituents themselves. Fermions are doomed to obey the Pauli exclusion principle and the wave function of the whole system has to be antisymmetric under the exchange of any two fermions. The principles of quantum physics are thus naturally relevant on a macroscopic scale.

Let us introduce Laundau's fermi liquid theory as its concepts will reappear when we take the holographic perspective on condensed matter theory. Consider N free fermions in a box with volume V. Their dispersion relation is given by $E = k^2/2m$ in terms of the fermion mass m and the absolute value of the momentum $k = |\underline{k}|$. In order to construct the ground state at zero temperature, we have to fill the energy eigenstates starting at low energies until all of the N fermions are placed. Taking the two options for the spin orientation into account the required momentum space volume is determined by

$$N = 2\int_{V_k} \mathrm{d}^d k \frac{V}{(2\pi)^d}\,. \tag{3.1}$$

The dispersion relation only depends on the absolute value k of the momentum and thus V_k is a d-dimensional sphere with radius

$$k_\mathrm{F} = 2^{(d-1)/d}\sqrt{\pi} n^{1/d} \Gamma\left(1+\frac{d}{2}\right)^{1/d}\,, \tag{3.2}$$

where $n = N/V$ is the particle density. The ground state of the free electron system is therefore a sphere of radius k_F in momentum space inside of which all the states are filled while all states outside the sphere are empty. The boundary of the sphere is called Fermi surface. The energy associated to k_F according to the dispersion relation is the Fermi energy E_F.

If we were to add an extra fermion to the system we would have to invest at least the Fermi energy, since all the states with less energy are already occupied. The energy necessary to add a fermion to a system is called the chemical potential μ which in this case is equal to the Fermi energy. The chemical potential is a thermodynamic variable of the grand canonical ensemble, a system with a fixed number of particles. Alternatively ,we could also remove a fermion just inside the Fermi surface. Those lowest energy excitations are called *particle* and *hole*, respectively. As they are assumed to be close to the Fermi surface, i.e. $k - k_F \ll k_F$ their dispersion relation can be obtained by linearising around the Fermi momentum

$$\epsilon(k) = E(k) - E_F = E(k) - \mu = \frac{k_{\mathrm{F}}}{m}(k - k_{\mathrm{F}}) + \mathcal{O}\big((k - k_{\mathrm{F}})^2\big). \tag{3.3}$$

In general the volumes and particle numbers are assumed to be large, therefore the excitations can cost arbitrarily few energy measured from the chemical potential, the excitations are gapless.

What happens if we allow the fermions to interact? Laundau's fermi liquid theory postulates that the system behaves qualitatively similar as the non-interacting gas [66]. This implies that the ground state of the system is still given by a Fermi surface and that the dispersion relation for particle excitations (3.3) is still valid for quasiparticle excitations with an effective mass m_*. It can be shown that the generic local interactions in the vicinity of a Fermi surface necessarily result in quasiparticles which makes the second statement self-consistent. Quasiparticles are excitations which live long enough the reveal their particle-like properties, i.e. whose decay rate $\Gamma \ll \epsilon$. They show up as poles in the retarded Green's function

$$G^R \sim \frac{1}{\omega - v_F(k - k_{\mathrm{F}}F) + \Sigma(\omega, k)}, \tag{3.4}$$

where $v_F = k_F/m_*$ and Σ is the self energy

$$\Sigma \sim i\omega^2. \tag{3.5}$$

Note that in this notation ω is measured with from the chemical potential μ.

The success of the Fermi liquid theory reliess on the fact that it can be shown to be a stable fixed point of a generic theory of quasiparticles. It holds even for intrinsically strongly coupled systems as long as the interactions between the quasiparticles are weak. Strong interactions of the fundamental constituents manifest themselves in large effective masses m_*. They can be as high as 10^3 times the electron mass. Such high values for the effective mass indicate that the Fermi surface is on the verge of being destroyed by quantum fluctuations [14].

At finite temperature we expect the sharp spectrum to smoothen out, as thermal fluctuations can excite some fermions to a state above k_F such that some of the states below k_F are empty. The probability for states of energy E to be occupied at finite temperature is given by the Fermi-Dirac statistics

$$f(E) = \left(1 + e^{\frac{E-\mu}{T}}\right)^{-1} . \tag{3.6}$$

The logic of the Fermi liquid theory still applies and makes predictions for the low energy behaviour of a system. Two examples that will become important later in this chapter, concern the electrical resistivity ρ and the specific heat c [66]:

$$\rho - \rho_0 \sim T^2 \quad \text{and} \quad c \sim T . \tag{3.7}$$

There are however a number of examples in which the observed low energy properties do not match the predictions from Fermi liquid theory, the so-called non-Fermi liquids. A prominent example are strange metals. At the same time those are also assumed to be the best candidate to be approached with holographic methods. We will discuss strange metals and their superconducting counterpart, the high temperature superconductors, in more detail at the end of this section 3.1.3.

Photoemission spectroscopy is the canonical experiment to study the Fermi surface of a material. It is based on the photoelectric effect: the material is hit with a beam of high energy photons which kick out electrons. The energy and momentum that is missing in the detected electrons as compared to the initial photons allow to draw conclusions about the properties of the electronic structure of the material. Photoemission experiments essentially measure the spectral density function

$$\mathcal{A}(\omega, \underline{k}) = \frac{1}{\pi} \mathrm{Im}\, G_{\mathrm{R}} . \tag{3.8}$$

3.1.2 BCS superconductivity

The electrical resistivity of metals is determined by the scattering of the conducting electrons with phonons, the collective excitations in a lattice and impurities of the material as well as the interaction between the electrons themselves. With decreasing temperature it is natural to expect that the electrical resistivity decreases as the phonons freeze out. However, it should remain finite at zero temperature due to the scattering with the impurities of the material. In the beginning of the twentieth century the phenomenon of superconductivity was discovered. The electrical resistivity of mercury suddenly became immeasureably small below a certain temperature, the critical temperature. Decades later Bardeen, Cooper, Robert Schrieffler were the first to present a microscopic theory of superconductivity, the

BCS theory [20, 67].

In BCS theory, superconductivity is the result of each two electrons forming Cooper pairs. These boson-like states in turn form a coherent ground state, allowing the electrons to move collectively and thereby transporting charge with no electrical resistivity. The crucial ingredient for the electrons to condense into a Cooper pair is an attractive interaction that overcomes their Coulomb repulsion. The attractive potential can be arbitrarily weak for the BCS theory to apply and the origin of the attraction is not relevant either. However, in most materials the interaction is mediated by the lattice. In this case the intuitive picture is given by the following: As an electron moves through the lattice of positively charged ions, the lattice is deformed because of the Coulomb attraction between electron and ion. The electron thus leaves behind lattice ions that temporarily form a region in which the positive charge dominates before they relax back into their normal position. This in turn generates an attractive potential for another electron. The two electrons enter a correlation with each other. It is crucial that this mechanism is retarded in time. While the ions relax back into their equilibrium position the first electron can travel, creating a sufficient distance to the second electron and allowing this attractive interaction to overcome the Coulomb repulsion between them [68].

At zero temperature, when the superconductor is in a macroscopic quantum state consisting of a condensate of the Cooper pairs, the correlation of the electrons due to the Pauli exclusion principle is turned into a correlation of all Cooper pairs constructed from these electrons. Therefore in order to break up one Cooper pair the energies of all other Cooper pairs has to be changed. As a result the single-particle excitations in a superconductor cost a finite amount of energy in contrast to normal metals, where the excitation of an electron can be realised with an arbitrary small portion of energy. The minimal excitation energy is called the gap Δ of the spectrum. Based on the presence of a sufficiently weak attractive interaction between the electrons, BCS theory allows to derive a quantitative prediction for this most characteristic property of superconductors at zero temperature. It is given by

$$\Delta(0) = 1.764\, k_b T_c\,. \tag{3.9}$$

Experimentally values between 1.5 and 2.5 are found [68]. The stronger the attractive interaction between the electrons, the higher is the value, until at some point

BCS theory breaks down. We can see that within BCS theory the gap Δ also sets the critical temperature. In fact the size of the gap, and hence the strength of the interaction, sets all relevant thermodynamic properties of the BCS superconductor. Besides the critical temperature the knowledge of the temperature dependence of the gap allows to derive the heat capacity, the free energy and the enthalpy. It is also related to the Debye frequency which represents the maximal frequency with which the atoms in the lattice can oscillate. This renders the gap the only relevant scale of the system.

With increasing temperature, as the thermal fluctuations get stronger, they eventually become large enough to break up the Cooper pairs. In turn, with fewer Cooper pairs around, the minimal excitation energy decreases and the gap in the spectrum closes. At the critical temperature all the pairs and the gap are gone. Just before the critical temperature is reached, the gap shows mean-field behaviour

$$\Delta(T) \sim (1 - T/T_c)^{1/2} \, . \tag{3.10}$$

In the superconducting state the notion of a Fermi surface is no longer applicable. The dispersion relation, showing up in the denominator of the fermion correlator, is then given by [14]

$$\omega = v_F \, (k - k_{\mathrm{F}}^*)^2 + \Delta - i\Gamma \, , \tag{3.11}$$

where the gap Δ and the pair-breaking term Γ are functions of temperature. The latter can be regarded as the counterpart of the self energy Σ (3.4) for superconductors. It is related to the inverse lifetime of the Cooper-pairs. For BCS superconductors it is generically very small [32]

$$\Gamma \ll \Delta \tag{3.12}$$

and almost temperature independent. We will see in the next chapter that the pair-breaking term shows a very different behaviour in high-temperature superconductors compared to BCS superconductors. The momentum k_{F}^* is the remnant of the Fermi momentum and now indicates the surface in momentum space with minimal excitation energy. More precisely, if $k = k_{\mathrm{F}}^*$ the minimal energy required to excite an electron is given by the gap Δ [68].

It seems plausible that for stronger and stronger correlations of the constituents, the superconducting state can be uphold at ever higher temperatures. Materials with a critical temperatures higher than about 30K are referred to as high-temperature superconductors. There are a number of techniques within condensed matter theory that address the phenomenon of high temperature superconductivity. However, these techniques lack a predictive and quantitative description of their experimentally observed phenomena. We will discuss this in more detail in the next subsection.

3.1.3 Challenges in CMT

Fermi liquid theory, introduced in subsection 3.1.1, describes a wide range of experimentally studied metallic states. There are, however, also materials which behave drastically different in their thermodynamic properties. These are referred to as *non-Fermi liquids.* A natural question to ask is which of their aspects are responsible for this deviation. Photoemission experiments, which indirectly measure the behaviour of the retarded Green's function, show that their spectral densities still exhibit a peak, albeit much broader than the Fermi liquid quasiparticle peak at the Fermi momentum. This indicates that the quasiparticle assumption no longer applies, resulting in a breakdown of the Fermi liquid theory. It is a longstanding challenge to understand the physics of phases without quasiparticles. It is believed that non-Fermi liquids belong to the class of quantum matter, where long-range and collective quantum entanglement governs the system's properties on a macroscopic scale. There are two main classes of non-Fermi liquids. Heavy fermion systems and the metallic or non-superconducting phase of high-temperature superconductors.

At very small temperatures, heavy fermion systems can be described by a Fermi liquid with high effective fermion mass m^*. As temperature is increased this description rapidly falls apart and the systems exhibits emerging collective properties which is characteristic of a local quantum critical state [14]. A local quantum critical state is characterised by an emerging scaling symmetry of energy and temperature while it is local in space. We will see in the next few sections that local quantum criticality is a generic phenomenon of holographic metals.

One of the most distinctive properties of the metallic phase of high-temperature superconductors, often referred to as strange metals, is that the electrical resistivity scales linearly in temperature over a wide range of temperature [69].

$$\rho \propto T\,. \tag{3.13}$$

This 'linear T resistivity' is remarkably simple, given the various kinds of electron scatterings at different temperature scales in those complex materials. Morover the residual resistivity ρ_0 (3.7) at zero temperature vanishes. It is those simple scaling behaviours which hint to quantum criticality where macroscopic scaling takes over. Studying the spectral density of strange metals one finds the following behaviour of the self energy

$$\Sigma(\omega) = a\,\log(\omega) + i\,b\,\omega\,, \tag{3.14}$$

where a and b are real coefficients. This behaviour was given the name *marginal Fermi liquid* behaviour.

At the same time, high-temperature superconductors cannot be described by conventional BCS theory, which is also based on the quasiparticle picture. Its most characteristic property, the high critical temperature is still lacking a theoretical explanation so far. In chapter 4 we will discuss a comparably recent experiment which quantified another characteristic feature, namely a strong temperature dependence of the pair-breaking term Γ [32].

Holographic metals have proven to share a number of the properties of non-Fermi liquid theories and high-temperature superconductors. The results of this thesis join the ranks of those insights. It is worth noting that the holographic perspective actually refers to the 'strangest' metals and optimally doped superconductors, the regime where the deviations from Laundau's Fermi liquid and BCS theory are maximal. It is hoped that holography can nonetheless reveal the underlying principles of non-Fermi liquid behaviour and high-temperature superconductivity on a more general level.

3.2 Finite density systems in holography

Let us now take the holographic perspective on condensed matter systems and address the question to what extend the problems raised above can be solved. An essential ingredient for applying gauge gravity duality to condensed matter systems is finite density. The simplest model to obtain such finite density or compressible matter phases is realised by Einstein-Maxwell theory [70]

$$S = \int \mathrm{d}^{d+1}x\sqrt{-g}\left[\frac{1}{2\kappa^2}\left(R-2\Lambda\right)-\frac{1}{4}F^2\right], \tag{3.15}$$

where we extended the minimal model (2.34) by a Maxwell field A, minimally coupeld to the gravity sector. It essentially introduces a chemical potential μ whose dual operator is a finite charge density ϱ in the field theory. The equations of motion of the above action (3.15) are solved by

$$\mathrm{d}s^2 = \frac{r^2}{L^2}\left(-f(r)\mathrm{d}t^2+\delta_{ij}\mathrm{d}x^i\mathrm{d}x^j\right)+\frac{L^2}{r^2f(r)}\mathrm{d}r^2\,, \quad A = A_t\mathrm{d}t\,, \tag{3.16}$$

with

$$f(r) = 1-\left(1+\frac{\mu^2}{r_\mathrm{h}^2\gamma^2}\right)\left(\frac{r_\mathrm{h}}{r}\right)^d+\frac{\mu^2}{r_\mathrm{h}^2\gamma^2}\left(\frac{r_\mathrm{h}}{r}\right)^{2(d-1)}, \tag{3.17}$$

$$A_t(r) = \mu\left(1-\left(\frac{r_\mathrm{h}}{r}\right)^{d-2}\right), \tag{3.18}$$

where $\gamma^2 = dL^2/(d-1)\kappa^2$. The solution describes a charged black hole of charge $Q^2 = \mu^2/r_\mathrm{h}^2\gamma^2$ and horizon radius r_h which gives the dual boundary theory a finite temperature. The spacetime asymptotes to AdS_{d+1} as $r\to\infty$ and is called *AdS-Reissner Nordström* (AdS-RN) spacetime. The chemical potential

$$\mu = \lim_{r\to\infty} A_t \tag{3.19}$$

acts as a bulk electrostatic potential which transports the information about the charged horizon to the boundary field theory and sources an electric current at the boundary. As only the time-component of A is switched on, only the charge density operator $\varrho = \mathcal{J}^0$ is non-zero

$$\varrho \equiv \langle\varrho\rangle = \lim_{r\to\infty}\frac{\delta S^{\mathrm{os}}}{\delta A_t^{\mathrm{b}}} = \lim_{r\to\infty}\left(\frac{r}{L}\right)^{d-3}A_t' = \frac{(d-2)r_\mathrm{h}^{d-2}}{L^{d-3}}\mu\,. \tag{3.20}$$

Moreover by equation (2.38) the temperature is given by

$$T = \frac{1}{4\pi r_\mathrm{h}}\left(d-\frac{(d-2)\mu^2}{\gamma^2r_\mathrm{h}^2}\right). \tag{3.21}$$

Note that we have now two scales in our theory: the temperature T and chemical potential μ. The conformal symmetry of the dual field theory is thus explicitly broken. However, as the bulk space still assymptotes to AdS space at the boundary, the UV fixed point is still conformal. In the bulk, where the field theory is thought to be on its way to the IR fixed point, the two scales demand to be treated as just one. Every dimensionful quantity can now be expressed in units of either the temperature or the chemical potential. In the literature both possibilities are present. In this thesis we will canonically choose to express dimensionful quantities in units of the chemical potential. Low or high temperature then really means $T/\mu \ll$ or $\gg 1$, respectively.

For $\mu^2/r_{\rm h}^2 = \gamma^2 d/(d-2)$, the AdS-RN black hole has the special property of reaching zero Hawking temperature at a finite value of the horizon radius $r_{\rm h}$. This is in contrast to for example the ordinary Schwarzschild solution (2.37), where zero temperature is associated with zero horizon radius. In this limit the black hole is called extremal and $f'(r_*) = 0$, where the extremal horizon radius is denoted by r_*. The extremal black hole has the unusual property, that its Bekenstein-Hawking entropy (2.33) is nonzero at zero temperature

$$s_* = \frac{1}{4G}\left(\frac{r_*}{L}\right)^{d-1} . \tag{3.22}$$

The holographic dictionary tells us to identify the Bekenstein-Hawking entropy with the entropy of the dual field theory. Consequently the extremal RN black hole is dual to a field theory with finite ground state entropy. A property which is alien to any real world situations.

The geometry near the horizon of extremal black hole is an $\mathrm{AdS}_2 \times \mathbb{R}^{d-1}$ space

$$\mathrm{d}s^2_{T=0} = \frac{L_2^2}{\zeta^2}\left(-\mathrm{d}t^2 + \mathrm{d}\zeta^2\right) + \frac{L_2^2}{r_*^2}\delta_{ij}\mathrm{d}x^i\mathrm{d}x^j . \tag{3.23}$$

where we introduced the radius $L_2 = L/\sqrt{d(d-1)}$ of the emergent AdS_2 space and the radial coordinate $\zeta = (z - z_*)$ with $z = L/r$. ζ measures the distance away from the extremal horizon z_*. The geometry near the horizon corresponds to the IR regime of the field theory. It is invariant under the rescaling

$$t \to \lambda\, t\,, \quad x_i \to x_i\,, \quad \zeta \to \lambda\,\zeta\,. \tag{3.24}$$

This particular scaling symmetry indicates local quantum criticality of the dual field theory, where a scaling symmetry emerges only in the time direction but not in the spatial directions which constrains the criticality to be local in momentum space[1]. This property that was experimentally detected for empirical strange metals as well. Thus to some extend the holographic AdS-RN metal is a strange metal because of its properties in the IR, but in many ways it is not. We will see in the next section that apart from the undesired behaviour of the entropy density at zero temperature, the universal behaviour of the DC resistivity (3.13) is not reproduced by the minimal Einstein-Maxwell model (3.15). Neither is the scaling of the conductivity at large frequency [71]. A wide range of different holographic models have been created and studied to address these shortcomings of the simple Einstein-Maxwell theory [72–75]. Often they asymptote to the same boundary behaviour, i.e. have the same UV completion, but differ in the IR, where most of the properties of interest manifest themselves. Note that the underlying physics of the gravity theory is different from the microscopic physics of any of the systems we are trying to model. In a sense we simply express the processes in a different language. The fact that this approach is successful, suggests that the dynamics of the effective, not necessarily microscopic, degrees of freedom can be mapped onto each other.

3.3 Holographic transport coefficients

The thermodynamic equilibrium of a system can be described with just a few thermodynamic variables, such as the temperature and pressure. However in particular in the context of condensed matter physics the truly interesting properties of a system can be revealed only by perturbing the system and observing its reaction. The information about this reaction or response is encoded in so-called transport coefficients. Different transport coefficients characterise the system's response to different perturbations. In the history of AdS/CFT an important coefficient is the shear viscosity η mentioned before, as it is part of the celebrated η/s result. It measures the resistance of a material to an externally applied shear force. Another important coefficient is the *electrical* or *optical conductivity* σ. It characterises the electric current as the response to an externally applied electric field. If the electric field is constant in time the systems responds with the direct current (DC) conductivity σ_{DC}.

[1]This emergent scale invariance can be related to the Lifshitz scaling $t \to \lambda^z t$, $x_i \to \lambda x_i$ by the redefinition $\lambda \to \lambda^{1/z}$ with $z \to \infty$. The parameter z is the dynamical critical exponent.

3.3.1 Method

Transport coefficients are computed from Kubo formulae which are based on linear response theory. Imagine a small external perturbation J_j which couples to some operator $\mathcal{O}_i$ of a theory with Hamiltonian H_0. In presence of the perturbation the Hamiltonian is modified to

$$H(t) = H_0(t) + H_{\mathrm{ext}}(t) = H_0(t) + \int \mathrm{d}^{(d-1)}x\, \mathcal{O}_i(x) J_j(x)\,. \tag{3.25}$$

Naturally the expectation value of this operator changes

$$\langle \mathcal{O}_i(x) \rangle_J = \langle \mathcal{O}(x) \rangle_0 + i \int \mathrm{d}t'\, \Theta(t-t') \left\langle [H_{\mathrm{ext}}(t), \mathcal{O}_i(x)] \right\rangle \tag{3.26}$$

$$= \langle \mathcal{O}_i(x) \rangle_0 - i \int \mathrm{d}^d\, \Theta(t-t') \left\langle [\mathcal{O}_i(x), \mathcal{O}_j(x')] \right\rangle J_j(x')\,, \tag{3.27}$$

where in the last step the expansion of the time evolution operator to linear order in H_{ext} was used. Defining the retarded Green's function $G^{\mathrm{R}}_{ij}(x,x') = i\,\Theta(t-t') \left\langle [\mathcal{O}_i(x), \mathcal{O}_j(x')] \right\rangle$, we can now write down the Kubo formula in momentum space

$$\delta \left\langle \mathcal{O}_i(k) \right\rangle = -G^{\mathrm{R}}_{ij}(k)\, J_j(k)\,. \tag{3.28}$$

For the locality in momentum space to valid, we need translational invariance of the original theory H_0. Note that the retarded Green's function vanishes before the perturbation is switched on at $t' < t$ and is computed with the unperturbed Hamiltonian H_0. In words, the Kubo formula gives a linear relation between the response $\delta \left\langle \mathcal{O}(k) \right\rangle$ and the small external perturbation J. The correlator $-iG^{\mathrm{R}}$ is identified with the transport coefficient. A canonical example is Ohm's law. The small external source A_i induces an electric current $\delta \left\langle \mathcal{J}_i(k) \right\rangle$. As A_i is proportional to the electric field $E_i = -\partial_t A_i \sim i\omega A_i$ the Kubo formula (3.28) gives

$$\delta \left\langle \mathcal{J}_i(k) \right\rangle = -\frac{1}{i\omega}\, G^{\mathrm{R}}_{ij}(k)\, E_j(k) \equiv \sigma_{ij}(k) E_j(k)\,, \tag{3.29}$$

where we assumed that in absence of the external electric field there is no electric current $\mathcal{J}$.

Coming back to the holographic duality, the question we have to address is: How can an external perturbation as discussed above be implemented in the a truly microscopic field theory and what is its gravity dual? The answer is that we do not need to actually implement it in this way. The reason is the fluctuation dissipation theorem [76] which states that the response of G^{R} of a system to a small external perturbation is given by the retarded Green's function of a spontaneous microscopic fluctuation around the equilibrium state. This in turn is a standard exercise within quantum field theory. The GKPW formula (2.25) is thus essential for the holographic dual of this procedure. For the causal correlator it states

$$\begin{aligned} G^{\mathrm{R}}_{ij}(x,x') = &- i \left\langle T\mathcal{O}_i(x)\mathcal{O}_j(x')\right\rangle = -i\,\frac{\delta^2 Z_{\mathrm{QFT}}\left[J\right]}{\delta J_j(x')\delta J_i(x)} \\ &= i\,\frac{\delta^2 S^{\mathrm{os}}_{\mathrm{gravity}}\left[\phi\right]}{\delta J_j(x')\delta J_i(x)}\bigg|_{\phi(r\to\infty)=J} . \end{aligned} \tag{3.30}$$

T denotes the time ordering operation. Thus to compute a retarded correlator, and hence transport coefficient, of a given quantum field theory with holographic dual in the language of gravity we first need to perturb the field ϕ, whose boundary value represents J. For the leading order of the response $\delta\left\langle\mathcal{O}\right\rangle$ the gravity action has to be expanded to second order in those perturbations $\delta\phi$, which results in linear equations of motion for $\delta\phi$.

As an example let us look again at the electrical conductivity of the finite density model introduced in 3.2. Note that every conceptual step in the following discussion applies to any other transport coefficient as well. In the case of the conductivity the Maxwell field A takes the role of ϕ and we start by[2]

$$A_x \to A_x + a_x\,. \tag{3.31}$$

where a_x satisfies the following equation of motion in momentum space

$$\left(r^2 f a_x'\right)' + \frac{\omega^2}{f} a_x = 2\kappa^2 L^4 \left(A_t'\right)^2 a_x\,. \tag{3.32}$$

This equation is valid only for a perturbation constant in space. Close to the black hole horizon r_{h} the equations demand a_x to behave as

$$a_x \sim \mathrm{e}^{-i\omega t}\left(a_{\mathrm{R}}\left(r-r_{\mathrm{h}}\right)^{-i\omega/4\pi T} + a_{\mathrm{A}}\left(r-r_{\mathrm{h}}\right)^{+i\omega/4\pi T}\right) h(r)\,, \tag{3.33}$$

where T is the equilibrium temperature. Defining $\tilde{r} = \log(r-r_{\mathrm{h}})/4\pi T$ this can be

[2]The correct way to implement the perturbations is to introduce fluctuations for all the fields of the gravity theory and all of their respective components of perturbations. In the present case, with the background as given in 3.2, however, the equation of motion of a_x can be shown to be independent of any other fluctuation.

rewritten as

$$a_x \sim a_{\mathrm{R}} \mathrm{e}^{-i\omega(t+\tilde{r})} + a_{\mathrm{A}} \mathrm{e}^{-i\omega(t-\tilde{r})} \,. \tag{3.34}$$

In this notation it is clear that a_{R} parametrises a wave that moves towards the black brane horizon and a_{A} one that moves away form it. The latter represents an acausal process because classically nothing can leave the black hole. A finite a_{A} imposes a boundary condition at the past horizon. In contrast, the former describes a causal process and a finite a_{R} imposes a boundary condition at the future even horizon. Choosing $a_{\mathrm{A}} = 0$ is the so-called ingoing boundary condition that is gives rise to the retarded Green's function of the boundary theory via (3.30).

The equation of motion (3.32) is a second order differential equation. To uniquely fix the solution, two boundary conditions have to be imposed. The first is the ingoing boundary condition. The second is given by the boundary value (non-normalisable mode) a_x^{b} of a_x which is dual to the small external perturbation J in the field theory. Equation (3.32) can be solved numerically only. The resulting on-shell action is of the form

$$S^{\mathrm{os}}_{\mathrm{gravity}} = \int \mathrm{d}\omega \, a_x^{\mathrm{b}}(-\omega) \mathcal{F}(\omega, r) a_x^{\mathrm{b}}(\omega) \Big|_{r_{\mathrm{h}}}^{\infty} \,, \tag{3.35}$$

where $\mathcal{F}$ is a differential operator in the radial coordinate r. It was shown in [77] via a Schwinger-Keldysh approach that the retarded Green's function is given by

$$G^{\mathrm{R}}(\omega) = -2 \lim_{r \to \infty} \mathcal{F}(\omega, r) \,. \tag{3.36}$$

It is important to stress that the result in (3.36) is highly nontrivial. We just computed a real time correlator in a thermal field theory which is naturally formulated in terms of the Wick rotated time coordinate. Real time computations thus require to deal with complex Euclidean time. To date AdS/CFT is the only framework that allows to study real time properties of strongly correlated systems at all. This is one of the main reasons for the importance of AdS/CFT on a practical level.

Equation (3.36) can be rephrased into a more practical prescription of how to compute the transport coefficient of interest

$$S^{\mathrm{os}}_{\mathrm{gravity}} = \int \mathrm{d}\omega \, \mathrm{c} \, a_x^{\mathrm{b}}(-\omega) a_x^{\mathrm{s}}(\omega) \Big|_{r_{\mathrm{h}}}^{\infty} \quad \Rightarrow \quad G^{\mathrm{R}}(\omega) = -2c \frac{a_x^{\mathrm{s}}(\omega)}{a_x^{\mathrm{b}}(\omega)} \,, \tag{3.37}$$

where a_x^{s} is the normalisable mode or subleading term of the boundary expansion of a_x and c is some constant. The systematic generalisation to the case of several coupled fluctuations and hence a whole set of coupled operators and sources on the field theory side is explained in detail in [78].

3.3.2 Electrical conductivity in holography

From a gravity theory perspective the electrical conductivity is given by

$$\sigma(\omega) = -\frac{1}{i\omega} G^{\mathrm{R}}_{\mathcal{J}\mathcal{J}}(\omega) = 2c \frac{a_x^{\mathrm{s}}(\omega)}{i\omega\, a_x^{\mathrm{b}}(\omega)} \,. \tag{3.38}$$

The Kramers-Kronig relations relate the imaginary and real part of the conductivity[3]. In particular, a pole in the imaginary part $\mathrm{Im}\,\sigma \sim \omega^{-1}$ implies a δ-peak in the real part $\mathrm{Re}\,\sigma \sim \delta(\omega)$ giving rise to an infinitely high DC conductivity. There are two scenarios in which this happens. The first is the absence of momentum dissipation. In this case, once there is an electrical current, understood as a stream of moving charged particles, the current will persist, because there is no mechanism to stop it. This results in perfect, i.e. infinite, DC conductivity. The phenomenological Drude model provides a more quantitative explanation. The average velocity v at which a charged particle moving through a material satisfies

$$m \frac{\mathrm{d}v}{\mathrm{d}t} = -m \frac{v}{\tau} + e\, E \,, \tag{3.39}$$

in terms of the particle's mass m and its charge e. The average time τ between collisions parametrises the momentum dissipation. With the current density given by $\mathcal{J} = env$, the electrical conductivity (3.29) behaves as

$$\sigma(\omega) = \nu \frac{\tau}{1 - i\omega\tau} \quad \text{with} \quad \nu = \frac{e^2 n}{m} \,. \tag{3.40}$$

In chapter 5 we will find exactly this behaviour in a holographic context. As dissipation is switched off by $\tau \to \infty$, the conductivity acquires a pole $\sigma \sim -1/i\omega$.

Holographically the origin of the pole is the effective mass term of the Maxwell field fluctuation (3.32) generated by the background field A_t: In the zero frequency

[3]The Kramers-Kronig relations are given by the following: $\mathrm{Re}\,\sigma(\omega) = \frac{\mathcal{P}}{\pi} \int \mathrm{d}\omega' \frac{\mathrm{Im}\,\sigma(\omega')}{\omega' - \omega}$ and $\mathrm{Im}\,\sigma(\omega) = -\frac{\mathcal{P}}{\pi} \int \mathrm{d}\omega' \frac{\mathrm{Re}\,\sigma(\omega')}{\omega' - \omega}$, where $\mathcal{P}$ is the principal value.

limit the subleading term, on dimensional grounds, behaves as

$$a_x^{\mathrm{s}} \sim r^2 f a_x' \big|_{r\to\infty} \sim 2\kappa^2 L^4 r^4 \left(A_t'\right)^2 a_x^{\mathrm{b}} \big|_{r\to\infty} , \tag{3.41}$$

and thus $a_x^{\mathrm{s}} \sim \mathcal{O}(\omega^0)$ which by equation (3.29) leads to a pole in the imaginary part of the conductivity proportional to the effective mass term[4].

Infinite DC conductivity is also a characteristic of superconductors which we introduce in the next section.

In appendix A we present a different approach to compute the DC conductivity with holographic methods. It is based on the so-called Einstein relation which allows to express σ_{DC} entirely in terms of quantities characterising the thermodynamic equilibrium.

3.4 Holographic superconductivity

The discovery of holographic superconductor can really be seen as the start of AdS/CMT, the application of holography to condensed matter problems. The holographic superconductor was first suggested by Gubser [15] and then implemented as a holographic bottom-up model by Hartnoll, Herzog and Horowitz [16, 17]. Let us review this original minimal setup [64, 79].

We start by extending the minimal bottom-up model (2.34) once more to

$$S = \int \mathrm{d}^{d+1}x\sqrt{-g}\left[\frac{1}{2\kappa^2}\left(R - 2\Lambda\right) - \frac{1}{4}F^2 - \left|D\chi\right|^2 \pm m^2\left|\chi\right|^2\right] , \tag{3.42}$$

where we added a minimally coupled complex charged scalar field χ to the Einstein-Maxwell theory (3.15). The covariant derivative is $D_\mu = \partial_\mu - ieA_\mu$. It is still consistent to only switch on the time component of the Maxwell field but the metric ansatz has to be generalised to

$$\mathrm{d}s^2 = \frac{r^2}{L^2}\left(-f(r)\mathrm{d}t^2 + g(r)\delta_{ij}\mathrm{d}x^i\mathrm{d}x^j\right) + \frac{L^2}{r^2 f(r)}\mathrm{d}r^2 , \quad A = A_t(r)\mathrm{d}t . \tag{3.43}$$

The equations of motion from the action (3.42) are solved by the AdS-RN solution

[4]The parameter κ parametrises the backreaction of the matter fields to the geometry. $\kappa = 0$ corresponds to ignoring their effect on the then fixed background (3.16). This explicitly breaks diffeomorphism invariance of the bulk and thereby also its field theory dual the translation invariance. Consistently, the $1/i\omega$ pole of the conductivity is removed (3.41).

when $\chi \equiv 0$. However, as the temperature is lowered a second branch of solutions develops, the holographic dual of a superconducting state. To understand this let us look at the equation of motion for χ independently

$$\chi'' + \left(\frac{4}{r} + \frac{f'}{f} + \frac{g'}{g}\right)\chi' - \left(\frac{L^2 m^2}{r^2 f} - \frac{L^4 e^2 A_t^2}{r^4 f^2}\right)\chi = 0\,. \tag{3.44}$$

Note that of course the metric fields f and g and the Maxwell field A_t are dynamical as well. However, the logic of the holographic superconductor forgoes without considering their dynamics. There are two effects which contribute to an arising instability of the scalar as temperature is decreased. Firstly, recall that a scalar in an AdS background is only stable above the BF bound (2.31). Thus a scalar mass M which satisfies that BF bound in the asymptotic AdS_4 with radius L geometry can still violate the BF bound of the emerging AdS_2 space with radius L_2 in the IR (3.23). This has the consequence that as temperature is lowered and the geometry resembles more and more the IR geometry (3.23) the scalar can become unstable[5]. The second effect is due to the coupling to the Maxwell field A_t which effectively reduces the mass of the scalar (3.44). A_t grows with decreasing temperature until eventually causes the effective mass to violate the BF bound. The instability results in a non-trivial profile of the scalar field $\chi(r) \neq 0$. To summarise, we find the following allowed range for the scalar mass

$$-\frac{9}{4} < L^2 m^2 < -\frac{3}{2} + \frac{3e^2 L^6}{4\kappa^2}\,, \tag{3.45}$$

where the upper bound is derived from the BF bound of AdS_2 space and the contribution of the Maxwell field evaluated at $T = 0$. Choosing $L^2 M^2 = -2$, in accordance with this range (3.45), the scalar's boundary behaviour according to (2.28) is given by

$$\chi = \frac{\chi_1}{r} + \frac{\chi_2}{r^2} + \mathcal{O}\left(r^{-3}\right)\,. \tag{3.46}$$

We do not want to source the non-trivial profile explicitly so we impose the boundary condition $\chi_0 = 0$, switching off the non-normalisable mode. Nonetheless below a certain temperature, χ_1 can be finite which leads to a spontaneous breaking of the $U(1)$ gauge symmetry. The dual field theory operator has the interpretation

[5] With this logic it seems possible that there is a scalar instability even for a neutral scalar $e = 0$. This indeed was found and discussed in [17].

of a condensate Δ

$$\Delta \equiv \chi_2 \,. \tag{3.47}$$

Comparing the field theory grand potential (2.36) of the two branches of solutions it can be shown, that the dual of the solution with the scalar condensate indeed is energetically preferred over the dual of the AdS-RN solution. The transition to the new ground state behaves like a second order phase transition which goes in line with the mean field behaviour of the scalar condensate[6]

$$\Delta \sim (1 - T/T_c)^{1/2} \tag{3.48}$$

close to the critical temperature T_c.

The development of the scalar profile can be thought of as a discharging process of the black hole due to pair production close to the horizon. The result goes as a 'hair' of the black hole. Note that this is not in contradiction with the *'no-hair'*-theorems, which state that black holes in flat space have to be uniquely characterised by a few charges, like their mass or electrical charge. In flat space, matter can only either fall into the black hole or radiate away to infinity. In AdS space however, the situation is different because the charged matter is trapped within the boundary but at the same time pushed away from the black hole by the electromagnetic force. As a result it is allowed to equilibrate in the vicinity of the horizon. This 'work around' the no-hair theorem lead to the discovery of many now black hole solutions.

It remains to show that the name giving feature of superconductor holds for this new type of solution: the infinite DC conductivity. Let us look at the equation of motion for the perturbation a_x of the Maxwell field, analogously to the last section (3.32)[7]

$$\left(r^2 f a_x'\right)' + \frac{\omega^2}{f} a_x = \left(2\kappa^2 L^4 \left(A_t'\right)^2 + 2e^2|\chi|^2\right) a_x + \frac{L^2 e^2 A_t |\chi|^2}{r^2 f} \delta g_{tx} \,. \tag{3.49}$$

Comparing this equation to the one in the previous section it is clear that the scalar field term contributes to the effective mass of a_x, in fact increases it. The

[6]The mean field behaviour is a consequence of the large-N limit [79].

[7]In contrast to the holographic setup in 3.3.2, it is now no longer possible to consistently switch on only the Maxwell field fluctuation. However, we use equation (3.49) at this point only on a conceptual level.

logic of (3.41) applies here despite the additional term proportional to the metric fluctuation δg_{tx}. We can conclude that the presence of the condensate indeed contributes to the infinite DC conductivity and hence represents a superconducting phase of the dual field theory.

In addition to the infinite conductivity, a superconductor is also characterised by a gap in the fermion spectrum (3.11). This gap reappears in the frequency dependent behaviour of the electrical conductivity: Aside from the δ-peak at $\omega = 0$, at low frequency the optical conductivity vanishes for frequencies smaller than the gap. This can be thought of shifting the superconducting degrees of freedom at low energy into the δ-peak. Holographic superconductors do not show a true gap in the optical conductivity. However, it is suppressed exponentially and the order of magnitude of the gap is set by the condensate Δ (3.47) [17], this may be called a pseudogap behaviour [14].

The situation where one part of the charge is still behind the horizon while the other part escaped and formed a condensate in the bulk corresponds to a state where part of the charge carriers is still in the normal phase while the other part forms a superconductor. Once again the microscopic physics of holographic superconductor may be different from BCS theory, where charged quasiparticles form Cooper pairs. The systems with a holographic dual are truly quantum and have no quasiparticles.

At closer inspection we just discussed spontaneous symmetry breaking of the $U(1)$ gauge symmetry in the bulk. However, according to the holographic dictionary, gauge symmetries of the gravity theory are dual to global symmetries of the quantum field theory [50]. The photon in holographic superconductors is thus not dynamical and the holographic superconductor really is a holographic superfluid. Luckily this is not relevant for many of the properties of a real superconductor [79, 80]. For example the Meissner-Ochsenfeld effect, where magnetic fields are expelled form the superconductor is captured by the holographic model as well [17].

3.5 Holographic probe fermions

3.5.1 Probe fermions in AdS/CFT

With the origin of the AdS/CFT correspondence in mind it seems natural that somehow the duality in principle also includes fermions. In the context of this thesis we consider 'probe' fermions only. By this we mean that the fermionic fields are understood not to backreact on neither the geometry nor any other bosonic matter field that may be part of the holographic model at hand. We mentioned in the course of the first section of this chapter that a fermionic system naturally has a quantum nature. Probe fermions in holography can thus be thought of as a quantum correction of the bulk theory which is dual to $1/N$ corrections of the boundary theory [14][8].

The first step is to naively write down the action for a charged probe fermion ψ in a finite density holographic background

$$S_{\text{bulk}} = \mathcal{N} \int \mathrm{d}^4x \sqrt{-g}\, i \left[\bar{\psi}\Gamma^{\mu} D_{\mu}\psi - m\,\bar{\psi}\psi\right] \,, \tag{3.50}$$

where the covariant derivative is given by

$$D_{\mu} = \partial_{\mu} + \frac{1}{4}\omega_{ab\mu}\Gamma^{ab} - i\,e\,A_{\mu}\,. \tag{3.51}$$

The spin connection $\omega_{ab\mu}$ accounts for the fact that the fermions are placed in a curved space. It describes the way in which the basis of the flat tangent space is oriented along a path in the curved spacetime. Roman indices a, b, ... indicate the flat tangent space, while greek indices μ, ν, ... label the indices of the real curved space. The gamma matrices Γ^{μ} in the action are related to the gamma matrices Γ^{a} in the flat tangent space via the vielbein e^{a}_{μ}, defined by $g_{\mu\nu} = e^{a}_{\mu}e^{b}_{\nu}\eta_{a,b}$, $\Gamma^{\mu} = e^{\mu}_{a}\Gamma^{a}$. The overall factor $\mathcal{N}$ is a normalisation factor which is fixed to be negative by the requirement of bulk unitarity [84].

The field-operator map in the case of fermions is more subtle than in the case of bosonic fields and operators discussed in 2.2.2. Unsurprisingly a bulk spinor field is dual to a spinor operator in the boundary theory. The GKPW formula for a

[8]Taking holographic fermions beyond the probe limit is highly non-trivial and to date it is not entirely clear how to approach this matter in full generality. For work in this direction see for example [81–83].

spinor operator $\mathcal{O}$ is given by

$$\exp\left(iS^{\text{os}}_{\text{gravity}}\left[\chi_0,\bar{\chi}_0\right]\right) = \left\langle \exp\left(i\int \mathrm{d}^d x\,\left(\bar{\chi}_0\mathcal{O}+\bar{\mathcal{O}}\chi_0\right)\right)\right\rangle\,, \tag{3.52}$$

where ψ_0 is understood to be the boundary value of the fermionic field ψ. However, a spinor in d dimensions has $2^{[(d+1)/2]}$ complex components, where $[x]$ denotes the integer part, and thus the boundary spinor only has half of the components of the bulk spinor. This poses a question about what the field-operator map means in the case of fermions. In appendix B we explicitly show that one half of the components of the bulk spinor ψ is the conjugate momentum of the other half. Roughly speaking this means that only one half of the components are independent. On a technical level, this means that one can only impose boundary conditions for half of the components thereby automatically fixing the values of the other half at the asymptotic AdS boundary. Moreover, a bulk Dirac spinor field ψ is dual to a chiral spinor operator $\mathcal{O}$ for even boundary dimensions d and dual to a Dirac spinor operator $\mathcal{O}$ for d odd [84].

The dimension to bulk mass relation of the fermion operator similarly to the scalar field is given by [48]

$$\Delta_f = \frac{d}{2} + m\,L\,. \tag{3.53}$$

3.5.2 Holographic Fermi surface

Remarkably, the probe fermions allow to holographically analyse the 'electrical' structure of the holographic materials. This is sometimes referred to as the 'holographic photoemission experiment' and requires a holographic version of the spectral density function (3.8) defined in the beginning of this chapter. From here on we fix the number of boundary dimensions to $d = 3$.

The Dirac equation according to the action (3.50) is given by

$$0 = \left(\Gamma^\mu D_\mu - m\right)\psi\,. \tag{3.54}$$

Following reference [85] we choose the basis of the gamma matrices to be

$$\Gamma^a = \begin{pmatrix} 0 & \gamma^a \\ \gamma^a & 0 \end{pmatrix}\,,\quad \Gamma^{\underline{r}} = \begin{pmatrix} 1 & 0 \\ 0 & -1 \end{pmatrix}\,,\quad \psi = \begin{pmatrix} \psi_+ \\ \psi_- \end{pmatrix}\,. \tag{3.55}$$

where the $a = \underline{t}, \underline{x}, \underline{y}$. The underlined indices label the explicit directions in the flat tangent space and γ^a are the gamma matrices of the boundary field theory. The decomposition of the spinor ψ in the two two-component spinors ψ_+ and ψ_- follows from the discussion in the appendix (B.1). The spin connection in the equation of motion can be removed by rescaling the the two two-component spinors $\psi_\pm = (-g g^{rr})^{-1/4} \mathcal{F}_\pm$ which after a Fourier transformation $\mathcal{F}_\pm(x, r) = \int \mathrm{d}\omega \mathrm{d}\underline{k} \mathrm{e}^{-i\omega t + i\underline{k}\cdot\underline{x}} \mathcal{F}_\pm(\omega, \underline{k}, r)$ gives

$$0 = \sqrt{\frac{g_{ii}}{g_{rr}}} \left(\partial_r \mp m\sqrt{g_{rr}}\right) \mathcal{F}_\pm \pm i \left(-\sqrt{\frac{g_{ii}}{-g_{tt}}} \left(\omega + e\, A_t\right) \gamma^0 + \underline{k} \cdot \underline{\gamma} \right) \mathcal{F}_\mp \,. \tag{3.56}$$

In order to construct the spectral density function we need to compute the retarded Green's function. The first step is to determine the near boundary behaviour of the spinors. It is entirely determined by the first term in the equations of motion (3.56), as the coupling to the Maxwell field A_t is subleading

$$\mathcal{F}_+ = a\, r^m + b\, r^{-m-1} \,, \quad \mathcal{F}_- = c\, r^{m-1} + d\, r^{-m} \,, \tag{3.57}$$

where each two of the two-coefficients are directly related by

$$b = \frac{i k_\mu \gamma^\mu}{2m+1}\, d \,, \quad c = \frac{i k_\mu \gamma^\mu}{2m-1}\, a \,, \tag{3.58}$$

with $k_\mu = (-(\omega + \mu), \underline{k})$. It becomes clear that the four component spinor indeed only has two independent coefficients at the boundary in accordance with previously explained fact that the dual spinor on the field theory side has only half as much components as the bulk spinor. The source, by definition the leading term, and the one point function of the boundary operator $\mathcal{O}$ according to (2.30) and (3.52) are

$$\chi_0 = a = \lim_{r\to\infty} r^{-m} \mathcal{F}_+ \,, \quad \langle \mathcal{O} \rangle = d \sim \mathcal{F}_- \,. \tag{3.59}$$

The two point function G is defined by

$$d = i\, G_{\mathcal{O}\mathcal{O}^\dagger} \gamma^0 a \,. \tag{3.60}$$

The additional factor of γ^0 [85] corrects the two point function $G \sim \left\langle \{\mathcal{O}, \bar{\mathcal{O}}\} \right\rangle$ one gets from the holographic prescription to the one we are actually interested in $G \sim \left\langle \{\mathcal{O}, \mathcal{O}^\dagger\} \right\rangle$. To get the retarded Green's function one has to choose the appropriate boundary conditions at the horizon. This is explained in more detail in the next chapter by means of an explicit example. The Green's function in the setup discussed here turns out to be diagonal [85], where the two entries can be mapped onto each other by $k_x \to -k_x$[9]. Choosing the component, where the non-trivial structure of the Green's function is located at positive values for $k = k_x$, we can finally define the holographic spectral density as

$$\mathcal{A}(\omega, k) = \frac{1}{\pi} \mathrm{Im}\, G_{22}(\omega, k)\,. \tag{3.61}$$

The analysis of the spectral density function revealed something that may be called a 'holographic fermi surface' [85,86]. In fact, it seems that the probe fermion ansatz together with the knowledge about the holographic strange metal is capable of interpolating between what behaves as a Fermi liquid, albeit a non-Landau Fermi liquid, to a marginal Fermi liquid and finally to a true non-Fermi liquid. They manifest themselves as characteristic features of the spectral density function $\mathcal{A}$ depending on the parameter regime.

At large temperatures $T/\mu \gg 1$ the system is completely determined by the conformal symmetry. In this case the spectral density is given by

$$\mathcal{A}(\omega, k) \sim \sqrt{k^2 - \omega^2}^{2(2\Delta_f - d - 2)} \tag{3.62}$$

where Δ_f is the scaling dimension of the boundary fermion operator (3.53).

At small temperatures $T/\mu \ll 1$ one has to distinguish between large and small Δ_f corresponding to an irrelevant and relevant operator in the UV, respectively. Different scaling dimensions can be realised by different masses m of the fermionic field. For a charged fermion in the presence of a Maxwell field this classification has to be generalised to consider the limit of large or small values of the ratio m/e [14].

In reference [19] a matching method was developed which allows to obtain a semi analytical expression for the correlators at low frequencies $\omega/\mu \ll 1$. The idea is to compute the low energy Green's function in the IR and the UV and in the end numerically determine the unknown coefficients. This allows to trace the origin of the spectral density's Fermi liquid like behaviour and to for example read off scaling

[9]Note that without loss of generality one can set $k_y = 0$, as the problem is rotationally invariant.

exponents. For $m/e \gg 1$ the spectral density generically takes this form [19]

$$\mathcal{A}(\omega, k) \sim \omega^{2\nu_k}\,, \tag{3.63}$$

where the scaling exponent ν_k, according to equation (57) of [19] and adapted to the notation and conventions in this thesis, is given by

$$\nu_k = \sqrt{\frac{m^2L^2}{6} + \frac{k^2L^2}{6r_*^2} - \frac{e^2L^2}{3}}\,, \tag{3.64}$$

with r_* the extremal AdS RN horizon radius. This is called the pseudogap behaviour [14].

In the case of $m/e \ll 1$ the spectral density shows sharp peak at zero frequency but finite momentum $k/\mu \sim 1$, much like a Fermi liquid. Upon closer inspection, it turns out that this peak does not behave in the Landau Fermi liquid manner [14]. Expanding the general expression of the Green's function in the IR around k_F, where k_F denotes the location of the pole, gives

$$G_\mathrm{R}(\omega, k) \simeq \frac{Z}{\omega - v_\mathrm{F}(k - k_\mathrm{F}) - \Sigma(\omega, k)} + \ldots\,, \tag{3.65}$$

where the residue Z is a complex number. The frequency behaviour of the self-energy Σ is given by

$$\operatorname{Im}\Sigma(\omega, k) \sim \omega^{2\nu} \quad \text{with} \quad \nu \equiv \nu_{k_\mathrm{F}}\,. \tag{3.66}$$

Recall that the Laundau Fermi liquid is characterised by $\operatorname{Im}\Sigma \sim \omega^2$ (3.5). Depending on the value of ν, the system exhibits three different regimes. For $\nu > 1/2$ the life time of excitations, given by the inverse of the imaginary part of Σ is larger than their energy ω. In this regime the quasiparticle picture should be applicable and the system can be classified as a (non-Landau) Fermi liquid. For $\nu < 1/2$ the inverse lifetime to energy relation is reversed which prohibits a quasiparticle nature of the excitations. The peak in the spectral density can be interpreted as some structure in momentum space which allows for massless excitations. This regime is classified as the non-Fermi liquid regime.

In the case of $\nu = 1/2$ the above expansion (3.65) is not quite right as for this special value of the scaling exponent a cancellation of divergencies takes place resulting in a self energy of the form

$$\mathrm{Re}\,\Sigma \sim \omega \log \omega\,, \quad \mathrm{Im}\,\Sigma \sim \omega\,, \tag{3.67}$$

Remarkably this is precisely the behaviour observed experimentally for marginal Fermi liquids (3.14), appearing seemingly naturally in the holographic perspective. In the next chapter we present a thorough analysis of the spectral density function in the context of a holographic superconductor. We engineer the parameters of the setup such that the normal state corresponds to the holographic marginal fermi liquid.

Chapter 4

Fermionic excitations of a holographic superconductor

4.1 Introduction and summary

It is widely believed that the materials with a high-temperature superconducting phase are governed by strongly interacting quantum field theories. This is partly supported by the fact that, in their normal state, the temperature dependence of the transport coefficients differs from the prediction of Landau-Fermi liquid theory[1] (see e.g. [89] and references therein). At the same time, gauge/gravity duality and in particular AdS/CMT has revealed a close relationship [14, 54] between field theories describing 'metals' with a holographic dual and the normal state of high-temperature superconductors, usually referred to as strange metals. Thus one could expect that holography is capable of describing properties of high-temperature superconductors as well.

A recent experiment [32] on high-temperature superconductors offers an ideal playground to test how close the relation between holographic and real superconductors really is. It quantified for the first time the long observed strong temperature dependence of the pair-breaking term $\Gamma(T)$ in high-temperature superconductors in greater detail. Moreover, it relates this feature to their special properties, see also [90, 91]. This behaviour is vastly different from BCS superconductors. The two measured quantities, namely pair-breaking term Γ, related to the inverse life-

[1] From the renormalisation group flow point of view, all small perturbation around free fermions at finite density are irrelevant [87, 88]. This explaines why the Landau-Fermi liquid theory is capable of describing all conventional metals.

time of the Cooper-pairs in the case of conventional superconductors[2] , and the gap Δ in the excitation spectrum, are straightforwardly related to the spectral density function $\mathcal{A}$, whose gravity dual we established in 3.5. The idea we pursue in this chapter is to describe the experimental results of [32] for optimally doped high-temperature superconductors with holographic methods. More precisely, we attempt to compare the results on a quantitative level.

To this end we use the concept of probe fermions in a gravity setup representing a fermionic excitation of a ground state of the holographic metal 3.5, which may be referred to as a 'holographic photoemission experiment'. The fermionic excitation in the gauge/gravity duality setup has been intensively studied over the past few years. In what is referred to as bottom-up constructions [19,85,86,92], one utilises the freedom in the bulk action to engineer fermionic excitations similar to those found in families of non-Fermi liquids. Interestingly, [93] showed with a different approach called semi-holography that the fermion two-point functions obtained holographically can also be found in a simple QFT construction consisting of a singlet fermion coupled to a strongly interacting sector dual to the IR geometry. Such a construction works extremely well to capture holographic results at zero temperature, see also [94] for a more recent discussion.

In this chapter we work with the bottom-up approach, more precisely we put probe fermions following the pioneering work of [33] in a holographic superconductor background constructed with the minimal setup of [17]. The reason to work with this minimal setup is to minimise the risk of observing additional features originating from more complicated gravity constructions and to avoid larger numbers of model-parameters. In chapter 5 we generalise our analysis to a holographic superconductor model whose normal state is more similar to real strange metals as compared to the one studied in this chapter. Moreover, the choice to follow reference [33] for the probe fermion setup is due to the fact, that this setup was shown to possess a physically sensible holographic version of a gap Δ, which is essential for our analysis. In contrast to the original work [33] we work at finite temperature.

After briefly introducing the holographic background we work with in section 4.2, we describe the fermion setup in detail in section 4.3. In section 4.4 we explain the different steps of our analysis, discuss the model-parameters and establish the map between the holographically accessible quantities and the experimentally

[2]Even though there is at the moment no general theory of high-temperature superconductors, it is believed that generalisations of the ideas of BCS theory 3.1.2 are at work in those materials.

measured ones. Section 4.5 contains our results: we explore the effect of the model parameters on the temperature dependence of gap Δ and pair-breaking term Γ and find that the latter seemingly naturally behaves similar to what was observed in the experiment. Moreover, we show that tuning the parameters leads to a quantitive accordance between holographic and experimental results. A summary is given in section 4.6.

The author of this thesis wrote the code to reconstruct the backgrounds of [17], to compute the spectral density function and extract its pole structure which is the central object of this chapter. Moreover the author analysed the resulting pole structure with respect to the model parameters and identified the set of parameters which yield to good quantitative agreement with the experimental results.

4.2 Superconducting background

Setting out to quantitatively describing the experimental results in [32] with holographic methods, we decided to work with the minimal setup to realise a holographic superconductor introduced in the previous chapter 3.4. In short, one places a charged scalar field into an AdS-RN background. At sufficiently low temperatures this setup develops an instability which on the field theory side leads to a phase transition to superconductivity. The action we use in this chapter is given by

$$S = S_{\mathrm{sc}} + S_{\mathrm{bdy}}\,, \tag{4.1}$$

where S_{sc} is the action given in (3.42) and S_{bdy} contains the counter terms to renormalise the theory

$$S_{\mathrm{bdy}} = \int_{\partial \mathrm{aAdS}} \mathrm{d}^3 x \, \sqrt{-\gamma} \left(2K - \frac{4}{L} - \frac{|\chi|^2}{L} \right) . \tag{4.2}$$

Note that we now work in a convention where the factor $1/2\kappa^2$ multiplying the gravity terms in (3.42) is scaled out and the matter fields are redefined accordingly. This choice is also responsible for the extra factor of 2 of the gravity related boundary terms in (4.2) as compared to for example [59]. As mentioned before, when computing one-point functions and correlators using the GKPW formula (2.25), the functional derivatives have to be evaluated at a slice located at $r = 1/\epsilon$, just inside the boundary of the asymptotic AdS space. Including the boundary terms S_{bdy} to the functional derivative, also evaluated at $r = 1/\epsilon$, causes the divergencies to cancel. The equations of motion for this action are

$$
\begin{aligned}
0 =& A_t'' + \left(\frac{2}{r} + \frac{g'}{g}\right) A_t' - \frac{e^2\chi^2 A_t}{r^2 h}\,,\\
0 =& \chi'' + \left(\frac{4}{r} + \frac{g'}{g} + \frac{h'}{h}\right)\chi' - \left(\frac{L^2M^2}{r^2h} - \frac{e^2L^4A_t^2}{r^4h^2}\right)\chi\,,\\
0 =& g'' - \frac{g'^2}{4g} + \left(\frac{4}{r} + \frac{h'}{2h}\right) g' + \left(\frac{3}{r^2} - \frac{3}{r^2h} + \frac{e^2L^4A_t^2\chi^2}{4r^4h^2} + \frac{L^2M^2\chi^2}{4r^2h} + \frac{L^4A_t'^2}{4r^2h}\right.\\
&\left. + \frac{h'}{rh} + \frac{\chi'^2}{2}\right) g\,,\\
0 =& h'' + \left(\frac{5}{r} + \frac{g'}{2g}\right) h' + \left(\frac{3}{r^4} - \frac{g'^2}{4g^2} + \frac{\chi'^2}{2}\right) h - \frac{3}{r^2} + \frac{L^2M^2\chi^2}{2r^2} - \frac{e^2L^4A_t^2\chi^2}{r^4 f}\\
&- \frac{3L^4A_t^2}{4r^2}\,,\\
0 =& \frac{3}{r^2} - \frac{3}{r^2h} - \frac{e^2L^4A_t^3\chi^2}{2r^4h^2} + \frac{L^2M^2\chi^2}{2r^2 f} + \frac{L^4A_t'^2}{4r^2h} + \frac{2g'}{rg} + \frac{h'}{rh} + \frac{g'h'}{2gh} + \frac{g'^2}{4g}\,.
\end{aligned}
\tag{4.3}
$$

The complex scalar field in the radial gauge $A_r = 0$ can be chosen to be real.

In the subsequent sections we study probe fermions in the superconducting state of the above setup. At zero temperature this was done before in [33] on which this project is based. We do not give any details on how to numerically construct the superconducting state in this chapter as we discuss the procedure in the context of a different holographic superconductor in the next chapter. The superconducting background used in this chapter is discussed in detail in e.g. [17].

4.3 Fermion setup

4.3.1 Action

For the analysis of the fermions ψ we use the following action for the fermions

$$
\begin{aligned}
S_{\text{fermion}} = \int \mathrm{d}x^4 \sqrt{-g} \Big[& i\,\overline{\psi}\left(\Gamma^\mu D_\mu - m_f\right)\psi \\
& + \left(\eta_5^* \chi^* \psi^T C \Gamma^5 \psi + \eta_5 \chi \overline{\psi} C \Gamma^5 \overline{\psi}^T\right)\Big]\,,
\end{aligned}
\tag{4.4}
$$

with the covariant derivative

$$D_\mu = \partial_\mu + \frac{1}{4}\omega_{\mu ab}\Gamma^{ab} - ie_f A_\mu \,, \tag{4.5}$$

and m_f and e_f the fermion mass and charge, respectively. This is the action which was constructed and used in the pioneering work [33]. The particular form of the coupling of the charged scalar χ and the fermion parametrised by η_5, first of all, is allowed by $U(1)$ gauge invariance if one demands

$$e_b = 2\, e_f \,, \tag{4.6}$$

where the index b refers to the bosonic scalar χ. In principle there are a number of other terms which are allowed as well. We discuss some of them in the last section 4.6. However, it seems that at least in the limit $T \to 0$ only the one we included here (4.4) results in a dispersion relation conceptually similar to the one of the BCS superconductor (3.11). The same schematic form is also observed experimentally for high-temperature superconductors. As was pointed out in [33] the physical interpretation of this coupling is that it describes the pairing up of modes at the Fermi surface in resemblance of conventional superconductors.

The effect of the charge conjugation operation C on the spinor and the gamma matrices can be expressed as

$$\psi^c = C\Gamma^{\underline{t}}\psi^* \qquad \left(C\Gamma^{\underline{t}}\right)\Gamma^{\underline{\mu}}\left(C\Gamma^{\underline{t}}\right)^{-1} = \Gamma^{\underline{\mu}*}, \tag{4.7}$$

For convenience we use the same gamma matrix basis as [19, 33], namely

$$\Gamma^{\underline{t}} = \begin{pmatrix} i\sigma_1 & 0 \\ 0 & i\sigma_1 \end{pmatrix} \quad \Gamma^{\underline{x}} = \begin{pmatrix} -\sigma_2 & 0 \\ 0 & \sigma_2 \end{pmatrix} \quad \Gamma^{\underline{y}} = \begin{pmatrix} 0 & \sigma_2 \\ \sigma_2 & 0 \end{pmatrix} \quad \Gamma^{\underline{r}} = \begin{pmatrix} -\sigma_3 & 0 \\ 0 & -\sigma_3 \end{pmatrix}, \tag{4.8}$$

written in terms of the Pauli matrices σ_i. The chirality matrix is given by

$$\Gamma^5 = \begin{pmatrix} 0 & i\sigma^2 \\ -i\sigma^2 & 0 \end{pmatrix} . \tag{4.9}$$

This basis is designed to give a relatively simple set of equations of motion for the case where the momentum $\underline{k}$ is aligned with the x-axis. This choice is allowed because of the rotational symmetry of the problem. In the following we use $k \equiv k_x$. Moreover this basis allow us to write the charge conjugation matrix as $C\Gamma^{\underline{t}} = \Gamma^{\underline{r}}$.

The Γ-matrices of real and tangent space are related as explained below equation (3.51).

4.3.2 Equations of motion

The equations of motion for the fermionic field ψ is given by

$$0 = \left(\Gamma^\mu D_\mu - m_f\right)\psi - 2i\chi\,\eta_5\,\Gamma^5 C\Gamma^{\underline{t}}\psi\,. \tag{4.10}$$

As the metric only depends on the radial coordinate, the spin connection takes the simple form

$$\frac{1}{4}\omega_{ab\mu}e^\mu_c\Gamma^c\Gamma^{ab} = \frac{1}{4}\Gamma^r\partial_r\log(-gg^{rr})\,. \tag{4.11}$$

It can removed from the equations of motion by the field redefinition $\mathcal{F} = (-gg^{rr})^{1/4}\psi$ resulting in

$$0 = \left(\Gamma^\mu D'_\mu - m_f i\right)\mathcal{F} - 2i\chi\,\eta_5\,\Gamma^5 C\Gamma^{\underline{t}}\mathcal{F}\,, \tag{4.12}$$

with $D'_\mu = \partial_\mu - ie_f A_\mu$. By expanding the spinor into its Fourier modes $\mathcal{F}(x,r) = \int \mathrm{d}\omega\mathrm{d}\underline{k}\mathrm{e}^{-i\omega t + i\underline{k}\cdot\underline{x}}\mathcal{F}(\omega,\underline{k},r)$ and by decomposing the Dirac spinor into two two-component spinors $\mathcal{F} = (\mathcal{F}_1\ \mathcal{F}_2)^T$, the equations further reduce to

$$\begin{aligned}0 = &\left(\sqrt{g^{rr}}\sigma_3\partial_r + m_f \pm \sqrt{g^{xx}}i\sigma_2 k - \sqrt{g^{tt}}\sigma_1 e_f A_t\right)\mathcal{F}_{1,2}(k,r)\\ &\mp 2i\sigma_1\chi\,\eta_5\,\mathcal{F}^*_{1,2}(-k,r)\,.\end{aligned} \tag{4.13}$$

Note that the complex conjugated spinors are evaluated at minus the momentum k. It is clear that $\mathcal{F}_1$ couples to $\mathcal{F}_2^*$ and $\mathcal{F}_2$ to $\mathcal{F}_1^*$, but the two pairs decouple from each other. The two sets of equations can be mapped onto each other by applying the transformation $k \to -k$ and $\eta_5 \to -\eta_5$. This is similar to the discussion in section 3.5. We will also need the equations of motion for the complex conjugated spinor $\mathcal{F}^*$ which is obtained by simply complex conjugating the above equations of motion (4.13).

4.3.3 Green's function

The construction of the Green's function is slightly different in this case as compared to the one sketched in 3.5. The reason is the coupling to the charged conjugated spinor, which doubles the number of spinors involved. Let us review the analysis of [33] and go through the steps in detail to gain intuition about the nature of the η_5 coupling.

Given the choice of gamma matrices (4.8), the projection operators $\Gamma_\pm = \frac{1}{2}\left(1 \pm \Gamma^{\underline{r}}\right)$ on the two modes $\psi_\pm$ are

$$\Gamma_+ = \begin{pmatrix} 0 & 0 & 0 & 0 \\ 0 & 1 & 0 & 0 \\ 0 & 0 & 0 & 0 \\ 0 & 0 & 0 & 1 \end{pmatrix}, \qquad \Gamma_- = \begin{pmatrix} 1 & 0 & 0 & 0 \\ 0 & 0 & 0 & 0 \\ 0 & 0 & 1 & 0 \\ 0 & 0 & 0 & 0 \end{pmatrix}. \tag{4.14}$$

This means that the spinor $\mathcal{F}$, as opposed to equation (3.55), has the structure

$$\begin{aligned} \mathcal{F} = \left(\mathcal{F}_1\ \mathcal{F}_2\right)^T &= \left((\mathcal{F}_1)_1\ \ (\mathcal{F}_1)_2\ \ (\mathcal{F}_2)_1\ \ (\mathcal{F}_2)_2\right)^T \\ &\sim \left((\psi_-)_1\ \ (\psi_+)_1\ \ (\psi_-)_2\ \ (\psi_+)_2\right)^T , \end{aligned} \tag{4.15}$$

where the last step relates the notation in this chapter to the notation in the appendix B.1. The boundary behaviour of $\mathcal{F}$ according to the equations of motion (4.13) takes the standard form

$$\mathcal{F}(k) \sim r^{m_f} \begin{pmatrix} 0 \\ a_1 \\ 0 \\ a_2 \end{pmatrix} + r^{-m_f} \begin{pmatrix} d_1 \\ 0 \\ d_2 \\ 0 \end{pmatrix}, \tag{4.16}$$

because the coupling terms parametrised by e_f and η_5 are subleading. Note that we ommited the terms corresponding to the ones labelled by the prefactors b and c in (3.57). They do not explicitly contribute to the correlator and are directly proportional to d and a, respectively (3.58). Thus as in equation (3.59) the non-normalisable or leading mode is related to the ψ_+ mode while the normalisable or subleading mode is related to ψ_-.

The charge conjugate spinor extends the field operator map (3.52) to

$$\exp\left(iS^{\text{os}}_{\text{gravity}}\left[\chi_0,\bar{\chi}_0\right]\right)=\left\langle \exp\left(i\int \mathrm{d}^dx\left(\bar{\chi}_0\mathcal{O}+\bar{\mathcal{O}}\chi_0+\left(\bar{\chi}_c\right)_0\mathcal{O}_c+\bar{\mathcal{O}}_c\left(\chi_c\right)_0\right)\right)\right\rangle ,$$

where

$$\chi_0=\lim_{r\to\infty} r^{-m_f}\begin{pmatrix}(\mathcal{F}_1)_2\\(\mathcal{F}_2)_2\end{pmatrix},\quad \left(\chi_c\right)_0=\lim_{r\to\infty} r^{-m_f}\begin{pmatrix}(\mathcal{F}_1^*)_2\\(\mathcal{F}_2^*)_2\end{pmatrix}, \tag{4.17}$$

and $\mathcal{O}_c = C\gamma^t\mathcal{O}^*$ is the complex conjugated spinor at the boundary. At the boundary the charge conjugation operator $C\gamma^t$ can be shown to be given by the unity matrix.

Due to the coupling to the charge conjugate operator the complete Green's function is now a 4×4 matrix. It is given by

$$\begin{pmatrix}G_{\mathcal{O}\mathcal{O}^\dagger} & G_{\mathcal{O}\mathcal{O}_c^\dagger}\\ G_{\mathcal{O}_c\mathcal{O}^\dagger} & G_{\mathcal{O}_c\mathcal{O}_c^\dagger}\end{pmatrix}=\begin{pmatrix}G_{\mathcal{O}_1\mathcal{O}_1^\dagger} & 0 & 0 & G_{\mathcal{O}_1\mathcal{O}_2}\\ 0 & G_{\mathcal{O}_2\mathcal{O}_2^\dagger} & G_{\mathcal{O}_2\mathcal{O}_1} & 0\\ 0 & G_{\mathcal{O}_1^\dagger\mathcal{O}_2^\dagger} & G_{\mathcal{O}_1^\dagger\mathcal{O}_1} & 0\\ G_{\mathcal{O}_2^\dagger\mathcal{O}_1^\dagger} & 0 & 0 & G_{\mathcal{O}_2^\dagger\mathcal{O}_2}\end{pmatrix}, \tag{4.18}$$

Recall that in subsection 3.5.2 the Green's function (3.60) was a diagonal 2×2 matrix. It corresponds to the top left part of the above matrix. Moreover, just like the two entries of (3.60) can be mapped onto each other by $k\to -k$, we can map the two sectors here in the same way, if we additionally take care of the mapping prescription for the coupling η_5. There is then a small subtlety on which Green's function one should study. In [19,85,95,96], it was demonstrated that the 2-point function extracted from spinors $\mathcal{F}_1$ and $\mathcal{F}_2$ have poles for $\omega\to 0$ at different momenta. This becomes apparent by writing the spinor ψ in the Nambu-Gorkov form where in the absence of condensate, the 2-point function of one sector has a pole at $\{(\omega=0,k>0)\}$ while the other has a pole at $\{(\omega=0,k<0)\}$ [96]. Here we will focus on the Green's function which has non-trivial structure in the $k>0$ region, which can be obtained by studying the $\{\mathcal{F}_2,\mathcal{F}_1^*\}$ channel.

$$G_{R,2}=\begin{pmatrix}G_{\mathcal{O}_2\mathcal{O}_2^\dagger} & G_{\mathcal{O}_2\mathcal{O}_1}\\ G_{\mathcal{O}_1^\dagger\mathcal{O}_2^\dagger} & G_{\mathcal{O}_1^\dagger\mathcal{O}_1}\end{pmatrix}. \tag{4.19}$$

This choice essentially corresponds to focussing on the $(2,2)$ entry of the Green's function in 3.5.2. The construction of the Green's function can now be performed analogously to the procedure outlined in that subsection. However, due to the coupling of the two spinors, the 2×2 matrix is not diagonal.

The normalisable and non-normalisable modes are related by the Green's function

$$\begin{pmatrix} d_2 \\ d_1* \end{pmatrix} = G_{R,2} \begin{pmatrix} a_2 \\ -a_1* \end{pmatrix} , \tag{4.20}$$

where the index 'R' refers to the retarded Greens function and the index '2' to the fact that we are interested in the $(\mathcal{F}_2,\, \mathcal{F}_1^*)$ channel. The minus sign is a result of anti-commuting source and operator in (4.17) such that the Green's function has the correct form. To explicitly construct all four components of the retarded Green's function one needs two linearly independent sets of solutions I and II. With those we can define a 2×2 matrix

$$\mathcal{G} = \begin{pmatrix} \left(\mathcal{F}_2^I\right)_1 & \left(\mathcal{F}_2^{II}\right)_1 \\ \left(\mathcal{F}_1^{*I}\right)_1 & \left(\mathcal{F}_1^{*II}\right)_1 \end{pmatrix}^{-1} \begin{pmatrix} \left(\mathcal{F}_2^I\right)_2 & \left(\mathcal{F}_2^{II}\right)_1 \\ -\left(\mathcal{F}_1^{*I}\right)_2 & -\left(\mathcal{F}_1^{*II}\right)_2 \end{pmatrix} , \tag{4.21}$$

where we used equation (4.16). By construction $\mathcal{G}$ is related to the retarded Greens function $G_{R,2}$ by

$$G_{R,2} = \lim_{r\to\infty} r^{2m_f}\, \mathcal{G} \, . \tag{4.22}$$

The equations of motion for the 2-component spinors (4.13) can be rearranged to equations of motion for $\mathcal{G}$. This requires a dynamical equation for $\mathcal{F}^*$ which can be obtained from (4.13) by a complex conjugation and the redefinition $k \to -k$. This results in the following expression

$$\begin{aligned} 0 = &\left(\sqrt{g^{rr}}\partial_r + 2m_f\right)\mathcal{G} \\ &+ \mathcal{G}\left(\sqrt{g^{xx}}k\sigma^3 - \sqrt{g^{tt}}\left(\omega + e_f A_t \sigma^3\right) + 2i\psi \begin{pmatrix} 0 & \eta_5 \\ -\eta_5^* & 0 \end{pmatrix}\right)\mathcal{G} \\ &+ \left(-\sqrt{g^{xx}}k\sigma^3 - \sqrt{g^{tt}}\left(\omega + e_f A_t \sigma^3\right) - 2i\psi \begin{pmatrix} 0 & \eta_5 \\ -\eta_5^* & 0 \end{pmatrix}\right) . \end{aligned} \tag{4.23}$$

The analytic structure of each component in $G_{R,2}$ is qualitatively similar. We follow the logic outlined above and define the spectral density as

$$\mathcal{A}(\omega, \underline{k}) \equiv \frac{1}{\pi} \mathrm{Im}\, G_{\mathcal{O}_2\mathcal{O}_2^\dagger}(\omega, \underline{k}) = \frac{1}{\pi} \mathrm{Im}\, \left(G_{\mathrm{R},2}\right)_{1,1} , \tag{4.24}$$

in accordance with (3.61).

Solving the first order differential equation of $\mathcal{G}$ requires one boundary condition which we impose at the black hole horizon. Being interested in the causal response function we choose the ingoing boundary condition for the spinor $\mathcal{F}$. Let us go through the steps to see how those manifest themselves in $\mathcal{G}$. The ansatz for the near-horizon behaviour of $\mathcal{F}_{1,2}$ is given by

$$\mathcal{F}_1^* = (r - r_\mathrm{h})^{\alpha_1} \left(c^\mathrm{h}_{\mathcal{F}1^*,0} + c^\mathrm{h}_{\mathcal{F}1^*,1} \sqrt{r - r_\mathrm{h}} + \mathcal{O}\left(r - r_\mathrm{h}\right) \right) , \tag{4.25}$$

$$\mathcal{F}_2 = (r - r_\mathrm{h})^{\alpha_2} \left(c^\mathrm{h}_{\mathcal{F}2,0} + c^\mathrm{h}_{\mathcal{F}2,0} \sqrt{r - r_\mathrm{h}} + \mathcal{O}\left(r - r_\mathrm{h}\right) \right) , \tag{4.26}$$

where the c^hs are two-component vectors. Plugging this into the equations of motion 4.13 and solving the leading coefficients we find two possible values for each exponent $\alpha_{1,2}$

$$\alpha_{1,2} = \pm \frac{i\omega}{4\pi T} \, . \tag{4.27}$$

For $\mathcal{F}_2$ the situation is exactly the same as in (3.34). The ingoing boundary condition corresponds to $\alpha_2 = -i\omega/4\pi T$. For $\mathcal{F}_1^*$ this is slightly more subtle. We need to impose the ingoing boundary condition for the spinor $\mathcal{F}(k, r) = (\mathcal{F}_1(k, r)\, \mathcal{F}_2(k, r))^T$, but (4.26) really is an equation for $(\mathcal{F}_1(-k, r))^*$. The effects of the complex conjugation and the evaluation at minus the momentum k cancel, and thus the ingoing boundary condition is realised by $\alpha_2 = -i\omega/4\pi T$ as well. For the components leading coefficients c^h we get the relations

$$\left(c^\mathrm{h}_{\mathcal{F}1^*,0}\right)_1 = \mp i \left(c^\mathrm{h}_{\mathcal{F}1^*,0}\right)_2 , \quad \left(c^\mathrm{h}_{\mathcal{F}2,0}\right)_1 = \pm i \left(c^\mathrm{h}_{\mathcal{F}^\mathrm{h}2,0}\right)_2 . \tag{4.28}$$

The two possibilities for the relative sign are determined by the choice of the sign of the exponent α. The ingoing boundary condition corresponds to the second option. As advertised above, the set of equations has two linearly independent sets of solutions which may be constructed by

$$I \quad \left(c^\mathrm{h}_{\mathcal{F}1^*,0}\right)_1 = 1 \ \text{ and } \ \left(c^\mathrm{h}_{\mathcal{F}2,0}\right)_1 = 0 \, , \tag{4.29}$$

$$II \quad \left(c^\mathrm{h}_{\mathcal{F}1^*,0}\right)_1 = 0 \ \text{ and } \ \left(c^\mathrm{h}_{\mathcal{F}2,0}\right)_1 = 1 \, , \tag{4.30}$$

respectively. Plugging the relation between the leading order coefficients (4.28) into the definition of the Green's function matrix $\mathcal{G}$ we find

$$\mathcal{G}(r_{\rm h}) = \begin{pmatrix} i & 0 \\ 0 & i \end{pmatrix} . \qquad (4.31)$$

In the following sections we present the numerical analysis of the spectral density function for the system (4.1) and (4.4). To compute $\mathcal{A}$, we solve the equations of motion for $\mathcal{G}$ numerically by intergrating the equations starting at the horizon $r_{\rm h}$ using equation (4.31). However, in holography it is the least of cases possible to start to integrate the equations at the horizon $r_{\rm h}$ itself due to its singular nature. Instead, one starts integrating at $r_{\rm h} + \epsilon$ which is why we solve for the higher order coefficients in the horizon expansion of $\mathcal{G}$ as well. The next to leading order of the expansion is given in the appendix B.2.

4.4 Analysis

4.4.1 Model parameters

The holographic model, consisting of the AdS-RN superconductor (4.1) and the probe fermions (4.4), has five external parameters

$$\{e_b\,,\, m_b\,,\, e_f\,,\, m_f\,,\, \eta_5\}\ , \qquad (4.32)$$

We already noted that the two Maxwell charges are not independent (4.6). Moreover the setup assumes the fermions to be probe, which means that we do not consider backreaction on the superconducting background. For this assumption to be justified the coupling to the charged scalar field has to be small

$$\eta_5\ <\ 1\,. \qquad (4.33)$$

For simplicity we restrict our analysis to massless fermions

$$m_f = 0\,. \qquad (4.34)$$

This choice has proven to be sufficient to model the experimental data. Furthermore it allows us formulate another important condition in a straightforward manner. In the course of the brief discussion of the phenomenology of the normal state of high temperature superconductors, the strange metals, it was mentioned that they show marginal fermi liquid behaviour (3.14). Holographically the same behaviour is found in the case of the Green's function's IR scaling exponent $\nu = 1/2$ (3.67). To capture as many features of the experimental setup as possible with our holographic model, we engineer the parameters (4.32) such that the scaling exponent ν takes the desired value in the holographic normal state given by the AdS-RN metal. The relation (3.64) between $\nu = \nu_{k_\mathrm{F}}$, fermion charge e_f and mass m_f, however, is not sufficient. The reason is that it provides just one equation for two unknowns, the second being the Fermi-momentum $k_\mathrm{F} = k_\mathrm{F}(e_f, m_f)$. For $m_f = 0$, it is possible to obtain an analytical expression for $k_\mathrm{F}(e_f)$, see equation (6.15) in [97]

$$\frac{6\nu + i\tilde{e}}{\tilde{k}_\mathrm{F}\left(2i+\sqrt{2}\right)} = \frac{{}_2F_1\left(1+\nu-\frac{i\tilde{e}}{6}, \frac{1}{2}+\nu-\frac{\sqrt{2}\tilde{e}}{3}, 1+2\nu, \frac{2}{3}\left(1+i\sqrt{2}\right)\right)}{{}_2F_1\left(\nu-\frac{i\tilde{e}}{6}, \frac{1}{2}+\nu-\frac{\sqrt{2}\tilde{e}}{3}, 1+2\nu, \frac{2}{3}\left(1+i\sqrt{2}\right)\right)}\,, \tag{4.35}$$

where $\tilde{e}$ and $\tilde{k}_\mathrm{F}$ are related to e_f and k_F by

$$e_f = \frac{\tilde{e} r_*}{\mu_*}\,, \quad k_\mathrm{F} = \frac{\tilde{k}_\mathrm{F} r_*}{\mu_*}\,, \quad \mu_*/r_* = 2\sqrt{3}\,. \tag{4.36}$$

The origin of the appearance of μ_*, the extremal value of the chemical potential, is the fact that this relation is derived at $T = 0$ (3.21), where the Fermi momentum is properly defined. r_* is the horizon radius of the extremal black hole and ${}_2F_1$ is the hypergeometric function. Together with (3.64) we can solve for the fermion charge e_f, such that $\nu = 1/2$ we find

$$e_f \approx 0.78, \quad e_b = 2\,e_f \approx 1.56\,. \tag{4.37}$$

The predicted value for the Fermi momentum at zero temperature is then $k_\mathrm{F}/\mu_* \approx 0.48$. This implies that the spectral density exhibits a sharp peak at $\mathcal{A}(0, k_\mathrm{F})$. We confirm this numerically which at the same time provides a first test on the code we use in the following.

In trying to holographically obtain the experimental results [32] we thus are left with just two independent parameters

$$\{m_b\,,\, \eta_5\}\,. \tag{4.38}$$

The mass of the condensing scalar m_b is restricted to the range derived from the BF bounds of the UV and the IR geometry (3.45). It essentially sets the temperature T_c at which the system undergoes the phase transition to superconductivity. An ever higher mass corresponds to an ever lower critical temperature until eventually the scalar is stable at any temperature. This is the case for masses above $L^2 m_b^2 \approx -0.59$. Practically it becomes increasingly difficult to numerically construct solutions with a condensate at small temperatures. Our analysis stops therefore at $L^2 m_b^2 = -3/4$[3] at which the critical temperature is $T_c/\mu \approx 0.013$ in units of the chemical potential.

4.4.2 Procedure

Ultimately we are interested in comparing the temperature dependence of the gap $\Delta(T)$ and the pair-breaking term $\Gamma(T)$ with their experimental counterparts. In the notation of equation (3.65) they are given by

$$\Delta = \mathrm{Re}\,\Sigma \quad \text{and} \quad \Gamma = -\mathrm{Im}\,\Sigma\,, \tag{4.39}$$

respectively. The way to access the self energy is by studying poles of the spectral density function $\mathcal{A}$. Given its definition (3.61), or equivalently (4.24), it is clear that choosing $k = k_{\mathrm{F}}$, the self energy manifests itself as a peak along the real frequency axis: the location of the peak is related to the gap while its width is related to the pair breaking term. More precisely those relations can be quantified as the imaginary and real part of the location of a pole ω_{p} of $\mathcal{A}$ in the complex frequency plane

$$\Delta = \mathrm{Im}\,\omega_{\mathrm{p}} \quad \text{and} \quad \Gamma = -\mathrm{Re}\,\omega_{\mathrm{p}}\,. \tag{4.40}$$

Let us elaborate on the choice of the momentum $k =$'k_{F}'. Technically the notion of a Fermi momentum is not physically sensible for a system in the superconducting state. What we really mean is that we choose the momentum k at which the term proportional to $(k - k_{\mathrm{F}})$ in equation (3.65) vanishes. We refer to this value as k_{F}^*, the momentum which leads to a minimal size of the gap. In analysing the spectral density function, this value is naturally characterised by a peak in $\mathcal{A}(0, k)$ at $\eta_5 = 0$, as shown in figure 4.1. One expects that upon increasing $T < T_c$ it continuously merges with the value of the peak in the normal conducting (AdS-RN)

[3] We omit the factor L^2 for the scalar mass m_b in the remainder of this chapter.

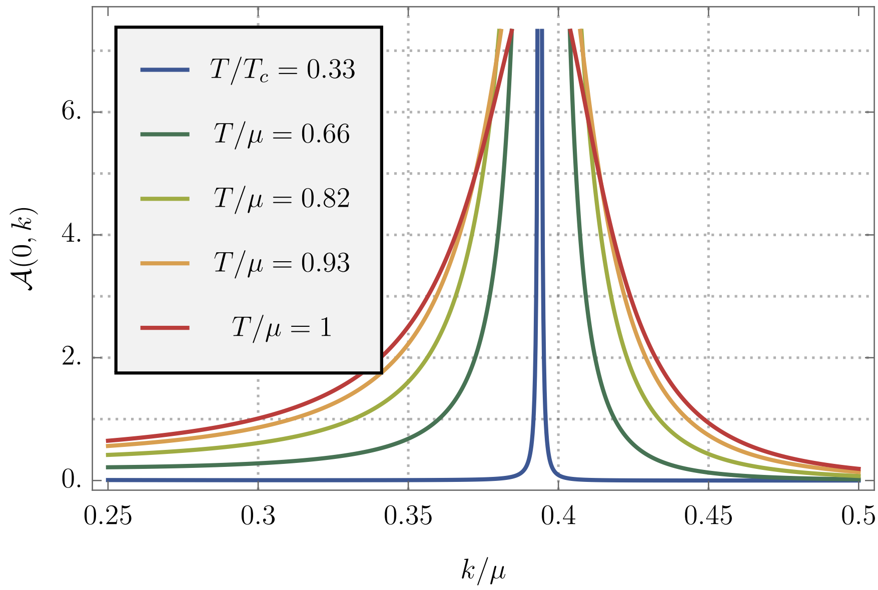

Figure 4.1: The spectral density $\mathcal{A}$ evaluated at $\omega = 0$ as a function of the momentum k for five different temperatures T/T_c, with $T_c/\mu = 0.023$. The coupling to the condensate is switched off $\eta_5 = 0$ and the mass of the scalar field is set to $m_b^2 = -5/4$.

background at the critical temperature T_c. Interestingly k_{F}^* is almost independent of the temperature T. A representative example is given by

$$k_{\mathrm{F}}^*/\mu = \begin{cases} 0.394 \;\text{ at }\; T/T_c = 0.1\,, \\ 0.395 \;\text{ at }\; T/T_c = 1 \end{cases} \qquad \text{for} \quad m_b^2 = -5/4\,. \tag{4.41}$$

For our analysis we always choose $k_{\mathrm{F}}^* \equiv k_{\mathrm{F}}^*(T/T_c = 0.1)$ which is the lowest temperature we study for each set of parameters. Note that at T_c, the spectral density function typically is already in the regime where it shows the conformal behaviour (3.62).

Once we set the value of the momentum k_{F}^*, we can proceed to find the poles ω_{p} of $\mathcal{A}(k_{\mathrm{F}}^*, \omega) \equiv \mathcal{A}_*(\omega)$ in the complex frequency plane. Figure 4.2 (a) shows a representative pole structure. To get the locations of the poles, we generate a random grid and evaluate the spectral density function on each point of the grid. Roughly speaking, the poles manifest themselves as the points, where the sign of $\mathcal{A}$ changes abruptly. We use

$$\omega_{\mathrm{p}} = \frac{1}{2}\left(\omega_{\mathrm{max}} + \omega_{\mathrm{min}}\right)\,, \tag{4.42}$$

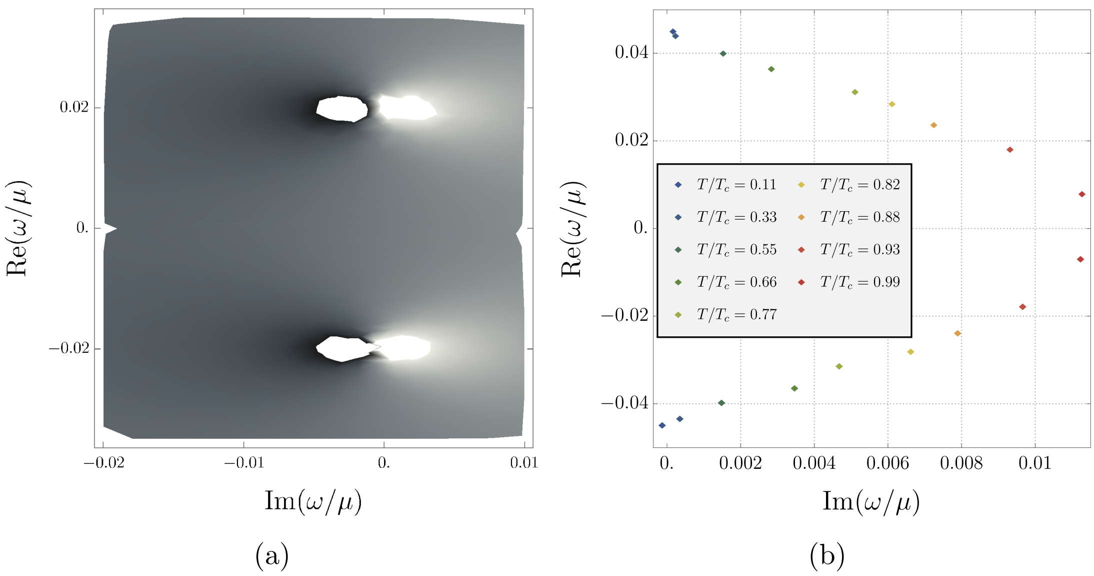

Figure 4.2: (a) $\mathcal{A}_*(\omega)$ as a function of a complex frequency. Large positive values correspond to lighter colors and small (negative) values to dark colors. The pole of the spectral density is located in the center of the two extreme regions, where the sign of $\mathcal{A}$ abruptly changes. (b) The locations of the poles depend on the temperature. The coupling to the condensate is set to $\eta_5 = 0.25$ and the mass of the scalar field is given by $m_b^2 = -5/4$.

where 'max' and 'min' refer to the values of the frequency, where $\mathcal{A}$ takes its maximal and minimal value, respectively. Here, ω is understood as a two component vector, set up by its real and imaginary part. To increase the precision of this approach we average over five different random grids for each pole. The movement of the poles through the complex frequency plane as a result of changing the temperature is shown in figure 4.2 (b). As temperature increases, the pole structure becomes more and more unreliable and the deviations of the individual data points compared to their average increases. This is something to keep in mind for the interpretation of the results.

4.5 Results

4.5.1 Behaviour of the model

In subsection 4.4.1 we established that the system we study has two independent parameters (4.38). We now analyse their effect on the gap Δ and the pair-breaking term Γ.

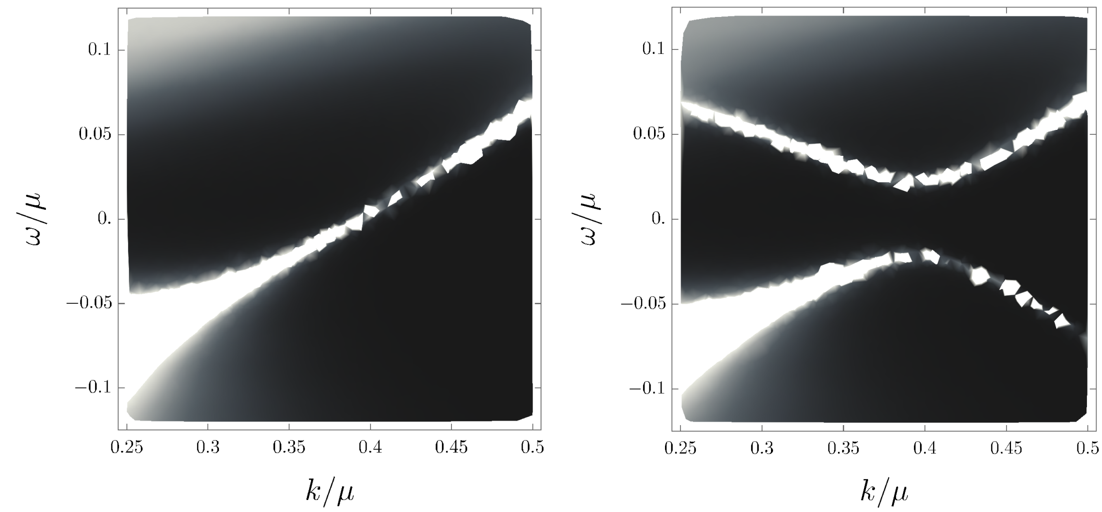

Figure 4.3: The spectral density $\mathcal{A}(\omega, k)$ for two different coupling strengths $\eta_5 = 0$ (left) and $\eta_5 = 0.125$ (right). The colour coding is the same as in figure 4.2. We fix $m_b^2 = -5/4$ and $T/T_c = 0.33$, with $T_c/\mu = 0.023$. We find that $k_\mathrm{F}^* = 0.39$.

The coupling of the condensed scalar field χ and the fermionic fields ψ parametrised by η_5 leads to the formation of a gap in the first place. Recall that a gap manifests itself as a peak in the spectral density $\mathcal{A}_*(\omega)$ along the momentum axis. This is illustrated in figure 4.3. It shows that at $\eta_5 = 0$, $\mathcal{A}_*$ peaks at $\omega = 0$. Finite η_5 breaks up the line into two 'arches', whose turning points, the point at which they are closest to the real frequency axis, are both located at k_F^*. The gap Δ is half of the distance between the two turning points which arrange themselves symmetrically with respect to the frequency axis.

Figure 4.4 illustrates the behaviour of the gap Δ as the temperature increases. The two peaks represent the two turning points of the arches at positive and negative frequencies. We observe that the two peaks approach each other as the critical temperature is approached. However, at a temperature $T/T_c < 1$ the gap is gone due to the thermal broadening of the peaks. The smaller the value of η_5, the lower is the temperature at which this effect sets in. Nonetheless the two peaks merge to just one at the critical temperature independent of η_5 or m_b. This is to be expected because the scalar condensate which multiplies η_5 in the action (4.4) vanishes at T_c. At the critical temperature we have

$$\Delta(T_c) = 0\,. \tag{4.43}$$

The overall temperature dependence closely resembles the familiar behaviour of

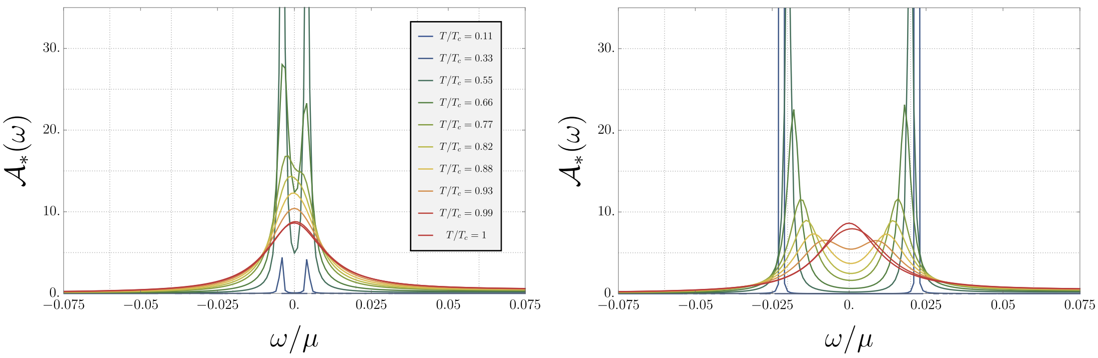

Figure 4.4: The spectral density $\mathcal{A}_*(\omega)$ for two different coupling strengths $\eta_5 = 0.025$ (left) and $\eta_5 = 0.125$ (right) evaluated at temperatures $T/T_c = 0.11, ..., 1$. With increasing temperature the gap becomes smaller. We fix $m_b^2 = -5/4$, which implies $T_c/\mu = 0.023$.

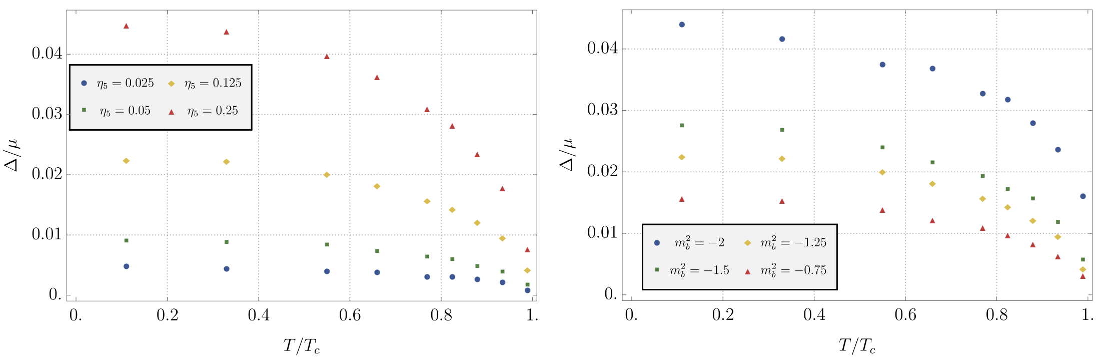

Figure 4.5: The gap Δ as a function of temperature for different values of η_5 at $m_b^2 = -5/4$ (left) and for different scalar masses m_b^2 at $\eta_5 = 0.125$ (right). The corresponding critical temperatures are $T_c/\mu = 0.060, 0.031, 0.023, 0.014$.

BCS superconductors (3.10). The maximal value of Δ at small temperatures can be varied strongly by tuning η_5, where larger values of η_5 generate larger gaps, see figure 4.5 (a). Upon varying the mass m_b, we find that larger masses lead to larger gaps.

In the view of our goal to compare those holographic results with the experimental data, the absolute values are not relevant. Instead, for each set of parameters, we need to rescale the data such that its associated 'holographic units' match the 'experimental units'. A sensible way to approach this matching in the case of the gap Δ is to normalise both, the holographic (h) and the experimental (e) at the minimal temperature $T_{\text{min}} \approx 0.1T_c$ for which an experimental result is provided.

$$\tilde{\Delta}_h = \frac{\Delta_h}{\Delta_h(T_{\text{min}})} \quad \text{and} \quad \tilde{\Delta}_e = \frac{\Delta_e}{\Delta_e(T_{\text{min}})} \, . \tag{4.44}$$

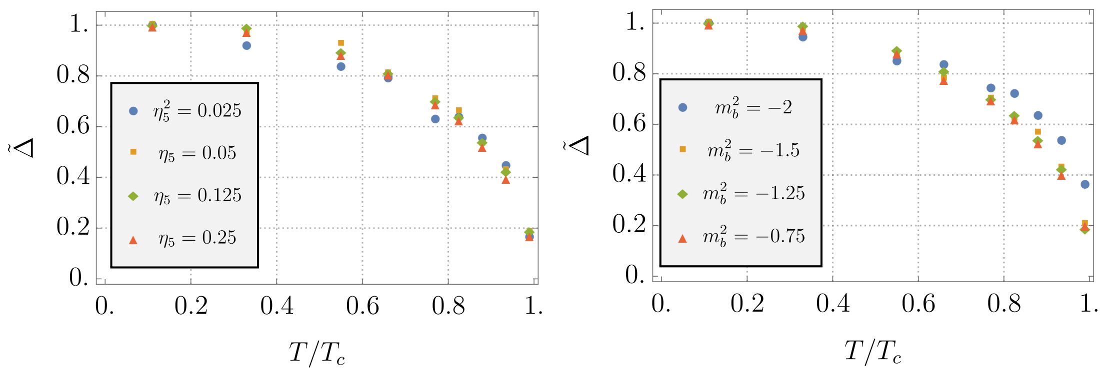

Figure 4.6: The rescaled gap $\tilde{\Delta}$ as a function of temperature for different values of η_5 at $m_b^2 = -5/4$ (left) and for different scalar masses m_b^2 at $\eta_5 = 0.125$ (right). The corresponding critical temperatures are $T_c/\mu = 0.060, 0.031, 0.023, 0.014$.

The holographic result for different values different couplings η_5 and of the mass m_f are presented in figure 4.5 (left) and (right), respectively. The previously so pronounced difference between the different couplings η_5 and masses m_b has significantly reduced. We find that the form of the temperature dependence does not strongly depend on either of the two parameters.

Let us now turn to the pair-breaking term Γ. As in the case of the gap, the pair-breaking term should continuously merge with its normal phase counterpart at the critical temperature, which is set by m_b. Furthermore, the peak in the spectral density is naturally sharper at smaller temperatures and asymptotes to zero as $T \to 0$. Combining those two insights, one expects that $\Gamma(T = 0) = 0$, increasing as temperature increases up to its final value at T_c, where larger masses m_b result in smaller values for $\Gamma(T_c)$. The right panel of figure 4.7 shows that this intuition is indeed correct. The coupling strength η_5 only marginally affects $\Gamma(T_c)$, see the left panel of figure 4.7.

For the pair-breaking term the rescaling prescription is dictated by the other end of the data, at the critical temperature. More precisely, let us define the rescaling in terms of a maximal temperature $T_{\max} \leq T_c$. The reason is that, as we mentioned before, the data close to the critical temperature becomes less reliable and possibly does not provide the best reference. The normalised pair-breaking term for the holographic data is given by

$$\tilde{\Gamma}_h = \frac{\Gamma_h}{\Gamma_h(T_{\max})} \,. \tag{4.45}$$

The analogue prescription for the experimental data is a bit more subtle and is

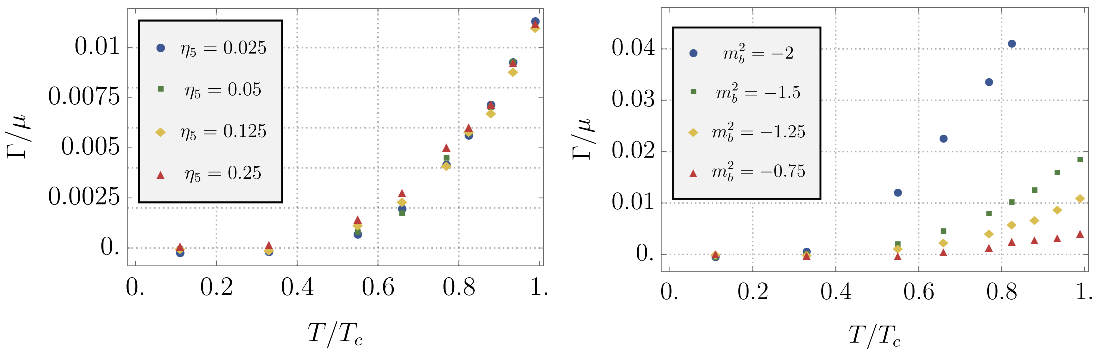

Figure 4.7: The pair-breaking term Γ as a function of temperature for different values of η_5 at $m_b^2 = -5/4$ (left) and for different scalar masses m_b^2 at $\eta_5 = 0.125$ (right). The corresponding critical temperatures are $T_c/\mu = 0.060, 0.031, 0.023, 0.014$.

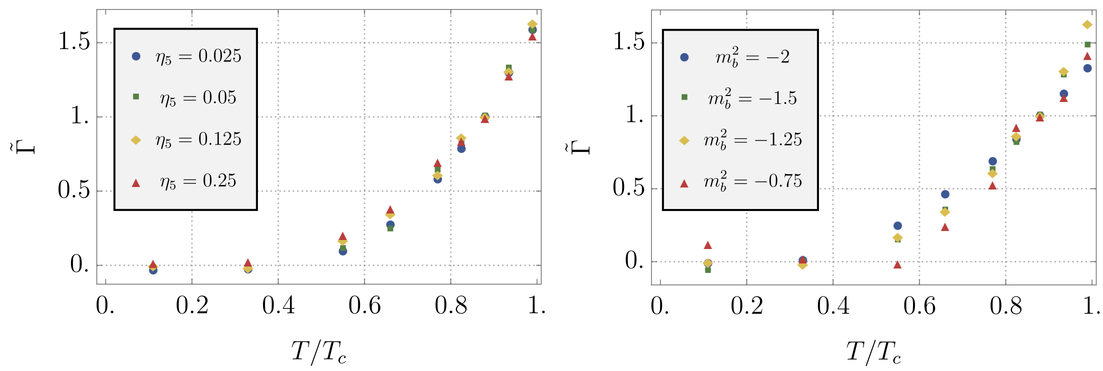

Figure 4.8: The rescaled pair-breaking term $\tilde{\Gamma}$ with $T_{\mathrm{max}} = 0.88T_c$ as a function of temperature for different values of η_5 at $m_b^2 = -5/4$ (left) and for different scalar masses m_b^2 at $\eta_5 = 0.125$ (right). The corresponding critical temperatures are $T_c/\mu = 0.060, 0.031, 0.023, 0.014$.

addressed in the next subsection. The results for $\tilde{\Gamma}_h$ are shown in figure 4.8. We observe, that also in this case, the strong dependence on m_b is merely an absolute scaling dependence than a functional one.

4.5.2 Comparison with experimental results

The analysis of the parameters' (4.38) effects on the gap Δ and the pair-breaking term Γ provide a solid ground for the attempt to imitate the experimental results [32] with holographic methods. In particular we are interested in the optimally doped case presented in the top right of figure 2 therein. This choice is due to the general assumption that holographic strange metals and high-temperature

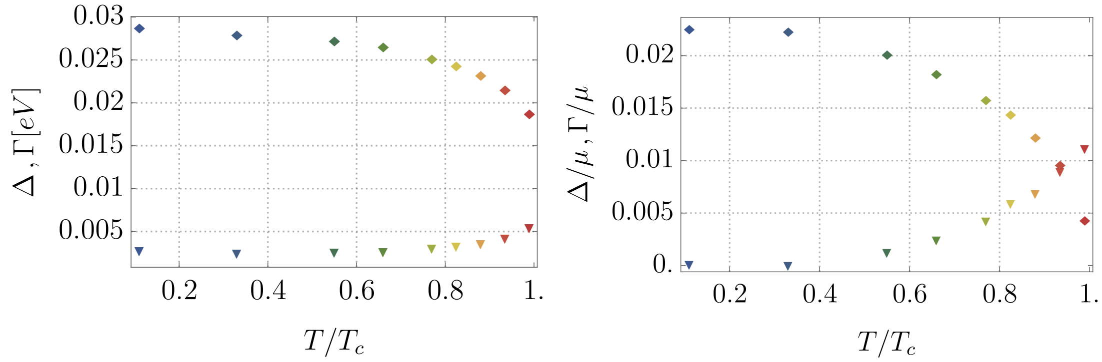

(a) experimental data (b) holographic data

Figure 4.9: (a) Experimental data taken from figure 2 (top right) in [32] for the gap Δ (♦) and Γ (▼) in units of eV as a function of temperature T/T_c where $T_c = 91K$. (b) The corresponding holographic data at $\eta = -0.125$ and $m_b^2 = -5/4$, where $T_c/\mu = 0.023$.

superconductors are likely most similar to the optimally doped case, where the unfamiliar properties, such as the high critical temperature are most pronounced. This choice is, however, not crucial for our results.

We should mention that, just like in our holographic analysis, the data towards the critical temperature becomes more and more noisy and hence we will not compare the last two data points at $T/T_c \approx 0.93$ and $T/T_c \approx 0.99$. Figure 4.9 shows the experimental data (a) contrasted with a representative sample of the holographic data (b). Even though they look qualitatively similar, we immediately observe two features of the experimental data that can definetely not be immitated by our holographic model. The first is the finite gap Δ at the critical temperature, which we established in the previous subsection to vanish by definition for all values of the parameters m_b and η_5. We discuss the physical interpretation of this feature given in [32] in section 4.6. The second is the finite value of the pair-breaking term towards zero temperature. And even more strangely it is $\Gamma(0.22T_c) > \Gamma(0.33T_c)$. Although we did not analyse our model all the way down to $T = 0$ we argued that holography predicts $\Gamma(T = 0) = 0$. The numerical analysis for small temperatures confirms this picture. The offset's origin in the experiment is not explained by the authors.

Given those limitations of our endavour we focus on comparing the pair-breaking term Γ. After all, it is its strong temperature dependence and its large absolute size that constitute the main result of the experiment as it is vastly different from conventional superconductors. As a start let us note that we also find that gap

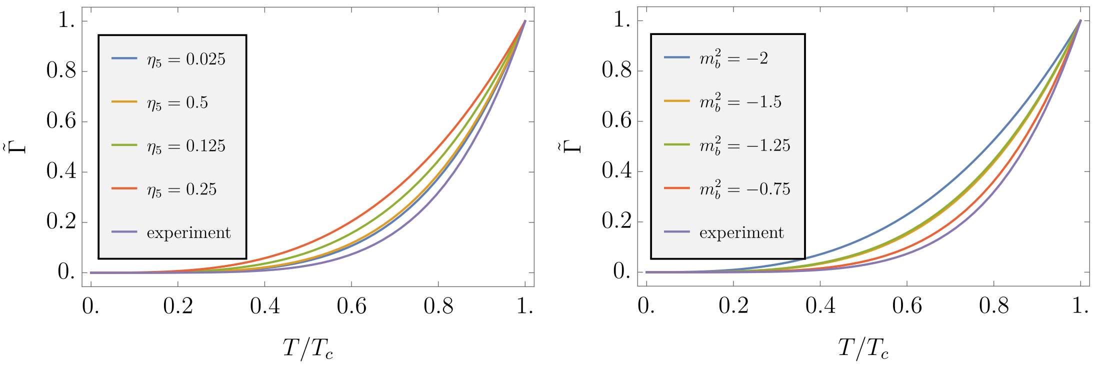

Figure 4.10: The fitted rescaled pair-breaking term $\tilde{\Gamma}$ with $T_{\max} = 0.88T_c$ as a function of temperature compared to the fitted experimental data for different values of η_5 at $m_b^2 = -5/4$ (left) and for different scalar masses m_b^2 at $\eta_5 = 0.125$ (right). The corresponding critical temperatures are $T_c/\mu = 0.060, 0.031, 0.023, 0.014$.

and width are of the same order of magnitude

$$\Delta_h \sim \Gamma_h \,. \tag{4.46}$$

In order to go beyond the qualitative resemblance 4.9 and (4.46), we introduce a fit function for the rescaled pair-breaking term

$$\tilde{\Gamma}_{\text{fit}}(T) = (T/T_{\max})^{\alpha} \,, \tag{4.47}$$

where $\tilde{\Gamma}(T)_h$ given by equation (4.45) and the experimental version given by

$$\tilde{\Gamma}_e(T) = \frac{\Gamma_e - \Gamma_e(T_{\min})}{\Gamma_e(T_{\max}) - \Gamma_e(T_{\min})} \,. \tag{4.48}$$

This definition has the effect of artificially shifting the experimental data such that $\tilde{\Gamma} \to 0$ as the temperature goes to zero. Extrapolating the data we find $\Gamma_e(T_{\min}) \approx 0.0028$eV. Moreover as announced above we ignore the last two data points at $T/T_c \approx 0.93$ and $T/T_c \approx 0.99$ for both, the holographic and the experimental dataset.

As the next step let us apply the fit function for the results presented in figure 4.8, to pronounce the effect of the scalar mass m_b and coupling η_5. Plotting the fit functions in figure 4.10, we observe both increasing m_b and decreasing η_5 bring us closer to the fitted experimental data for the pair-breaking term.

We end this section by presenting the holographic data set 4.11 that is the most

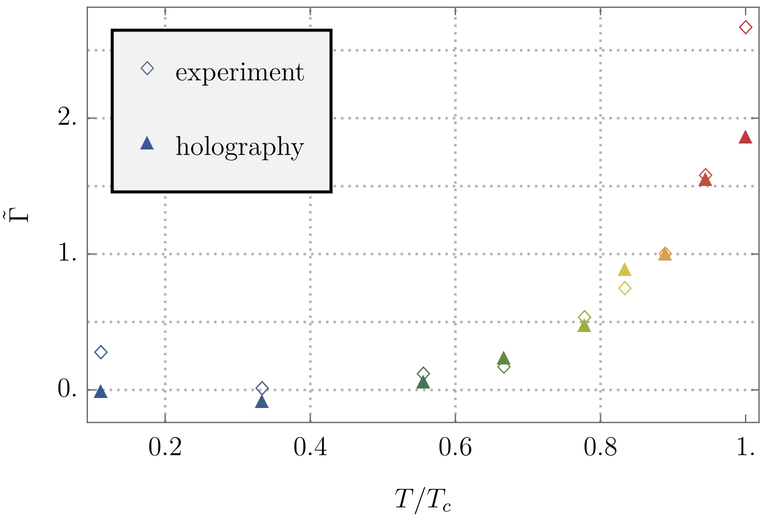

Figure 4.11: Comparison between the rescaled experimental (4.48) and holographic (4.45) temperature evolution of the rescaled pair-breaking term $\tilde{\Gamma}$. For generating the holographic data we used $\eta_5 = 0.025$ and $m_b^2 = -3/4$, with $T_c = 0.013$.

similar to the experimental one, while at the same time is about the best we can do with our numerical method: $m_b^2 = -3/4$ and $\eta_5 = 0.025$. Albeit a small remaining difference in the scaling exponent $\alpha_e \approx 5.12$ and $\alpha_h \approx 4.85$, the two temperature evolutions are remarkably similar.

4.6 Summary and outlook

In this chapter we studied the properties of holographic probe fermions in the background of the AdS-RN superconductor. The goal was to describe experimental results about the temperature dependence of the gap Δ and the pair-breaking term Γ for an optimally doped high-temperature superconductor with holographic methods. The gap represents the minimal energy which is necessary to excite the coherent superconducting ground state. The pair-breaking term parametrises the inverse lifetime of the pairs which compose that ground state.

The experimental data showed three characteristic features. The first is that the gap vanishes at a temperature $T_{\text{pair}} > T_c$ higher than the critical temperature. This is unfamiliar from any to date available theoretical description of superconductors. The intuitive picture presented in [32] is that the critical temperature in high-temperature superconductors is not determined by the mere possibility for the electrons to pair up, but that there has to be a critical density of pairs long lived enough to form a coherent state. This is directly related to the second characteristic feature. The pair-breaking term was measured to be strongly temperature dependent and to be of the same order of magnitude as the gap, in particular at the critical temperature they found that $\Delta \approx 3\Gamma$. Recall that the pair-breaking term of BCS like superconductors is almost temperature independent and negligibly small compared to the gap (3.12). This phenomenon can be utilised to furnish the above intuitive picture. At temperatures above T_c, the pairs break up rapidly, preventing the formation of a superconducting ground state. Below the critical temperature it is still strong enough to break up enough pairs to be responsible for a filling of the gap instead of let it close. The third feature, albeit not of the same relevance, is that the pair-breaking term seems to be non-zero at zero temperature, equivalent of a persisting finite width of the peak.

Backed up with the encouraging results of probe fermions in a holographic strange metal and holographic setup capable of generating a gap in the spectrum of a probe fermion in a superconducting background at $T = 0$, we studied the temperature evolution of Δ and Γ in the background of what supposedly could be a holographic high-temperature superconductor. We derived the finite temperature ansatz of the model constructed in [33] in the background of the simplest holographic superconductor (3.42). By demanding that the normal state, realised by the AdS-RN theory, behaves as effectively as possible like a marginal fermi liquid, we reduced the number of external parameters to only two. The mass m_b of the condensing charged scalar field and the coupling strength η_5 between the probe fermion and that scalar.

We then studied how the gap and the pair-breaking term are affected by changes of those two parameters and which of the characteristic features can be mimicked with our holographic model. We find that $\Delta(T_c) = 0$ for all of the parameter configurations. This is result is to be expected because above the critical temperature the ground state reduces to the AdS-RN strange metal which does not show a gap. Moreover, one expects a continuous transition between the normal and superconducting state due to the continuously vanishing scalar condensate, which effectively multiplies the term in the action responsible for the gap. However, on top of this, we observed that the peaks spread out thermally such that at temperatures $T < T_c$ the gap has filled before it closed. This effect is stronger for smaller values of η_5. This was presented in [33] as well. It is not clear whether the superposition of the thermal broadening of the peaks and the closing of the gap can be related to the new interpretation of Δ in high-temperature superconductors put into play by in [32].

We did find the strong temperature dependence of the pair-breaking term. Moreover, we also observed that $\Gamma \sim \Delta$, both in accordance with the experiment. We were able to quantitatively approach to temperature evolution of Γ, which we mathematically formulated as a powerlaw behaviour (4.47). Knowing the effect of the two external parameters, we were able to identify a set of parameters $\{m_b^2, \eta_5\} = \{-3/4, 0.025\}$ which leads to a remarkably similar pair-breaking term. Note that the value for the scalar mass is comparably high and scratches the bound above which the system no longer exhibits a phase transition to superconductivity and that the value of the pair-breaking term at the critical temperature is controlled by the critical temperature. In order to go beyond the scalar mass $m_b^2 = -3/4$, one should resort to a different numerical method to both, solve the background and also solve the equations of motion for the probe fermion. A possible approach in this direction is to implement a pseudo-spectral method.

Figure 4.11 shows one of the major achievements of this thesis, as a quantitative matching of properties of real physical systems and holographic models is very rare in AdS/CMT. Importantly, this result is directly related to the superconducting state on both sides and shows for the first time a close relation between real and holographic high temperature superconductors. Our results 'close' the square consisting of the normal and superconducting state of real and holographic strange metals: the relation between the metallic phases already passed two tests on a quantitative level, namely the linear increase of the electrical resistivity with temperature [34] and a power-law dependence of the electrical conductivity in a mid-infrared regime [71]. The holographic metal and superconductor are directly connected by construction and the relation between the real strange metal and high-temperature superconductor is a widely accepted idea. In this picture this thesis explicitly furnishes the assumed relation between the two superconducting states.

The good qualitative and and also quantitative agreement between the holographic and experimental data for $\Gamma(T)$ is the main result of this chapter. Note however that, in the bottom-up approach, there is no clear procedure to determine the action for bulk fermion. In fact, various effects other than the one studied here can be obtain by adding couplings between fermion and other fields (allowed by gauge invariance), see e.g. [96, 98–101]. Likewise, it is not entirely clear what exactly the coupling between probe fermion and charged scalar utilised in this chapter represents on the dual boundary field theory. A proper understanding of the η_5-coupling we implemented in our model in terms of a top-down interpretation should certainly be a goal of future research in this direction.

One of the most abvious questions is addressed in the next chapter 5, namely is it possible to obtain similar results with a different holographic superconductor? Of particular interest naturally are superconductors with a normal phase closer to the real world strange metals as for example the model studied in [34].

Chapter 5

A holographic superconductor with momentum relaxation

5.1 Introduction and summary

Ever since the first holographic realisation of a superconductor [16], holographic superconductivity has been an active and fruitful field of research. The original model is a bottom-up construction starting with the 'minimal' holographic model (2.34) supplemented with a $U(1)$ gauge field and a charged scalar. By now countless models have been developed and investigated among which are also top-down constructions, see for example [102].

The goal of describing real high-temperature superconductors in mind, one has to include a mechanism of momentum dissipation to the boundary field theory. This is equivalent of breaking translational invariance in the bulk because it leads to a non-conservation of the dual stress-energy tensor. Recall that without momentum dissipation the DC conductivity is infinite also in the normal conducting or metallic phase, see 3.3.2.

The first mechanism to implement momentum dissipation into holographic models were holographic lattices [71, 103–107]. Another way is to explicitly break bulk translation invariance by including a mass term for the graviton [108]. It is however, not clear how those massive gravity theories should be interpreted from the quantum field theory perspective. Reference [109] suggested a relation between lattice models and a specific massive gravity theory.

A comparably simple, yet effective way to realise a breaking of translational symmetry is to include spatially dependent sources within the boundary field theory in the form of massless scalar fields $\xi_i \sim \alpha x^i$, with $i = 1, ..., d-1$, suggested in [110]. Such a scalar shift symmetry has the advantage that the geometry of the bulk is still isotropic and homogeneous. Note that the on-shell gravity action in the presence of those scalar fields looks exactly like the on-shell action of the massive gravity theories in a holographic context. From the boundary field theory perspective, those scalar fields may be regarded as linearised exponential potentials analogous to the electrostatic periodic potentials in a lattice [111]. Holographic superconductors with this method of breaking translational invariance are presented in [35, 36].

In this thesis we study a holographic superconductor model based on the model investigated in [34]. Its distinguishing feature is the origin of the linear increase of the DC electrical resistivity ρ_{DC} with temperature: This model has the property that $\rho_{\mathrm{DC}} \sim \eta \sim s$, where η is the shear viscosity and s the entropy density. From a (non-holographic) hydrodynamic perspective this is true for a system which has minimal viscosity, a property directly related to intrinsic strong coupling. The above relation requires in particular that the entropy density scales linearly in temperature as well and vanishes at $T = 0$. Such a hydrodynamic behaviour in metals can be motivated from [112]. Recall from the discussion in 3.2, that this feature cannot be realised by a model based on the AdS-RN background. Instead the model presented in [34] includes a dilaton field acting as a dynamical gauge coupling and leading to the vanishing of the black hole at $T = 0$, i.e. $s(T = 0) = 0$ due to the relation given in (2.33). We add a charged scalar which as we show causes a phase transition to superconductivity and change the mechanism for momentum dissipation from a massive graviton in [34] to the neutral scalar fields ξ_i mentioned above. Close to when we were finishing our analysis of the superconductor work on similar holographic superconductors appeared [35, 36]. We emphasise that there are many more requirements for the action to faithfully represent strange metals. For example the holographic model cannot reproduce the temperature dependence of Hall angle found in such materials. It is pointed out in [113] that the correct temperature dependence of DC resistivity and Hall angle can be obtained in more complicated Einstein-Maxwell-dilaton theories with momentum relaxation. Such a setup has been found recently in [114] and is arguably consistent once one relaxes the constraint from the null energy condition [115].

The encouraging results of the previous chapter about the accordance of the temperature dependence of the pair-breaking term $\Gamma(T)$ between the minimal holographic and a real high-temperature superconductor are the main motivation to investigate this more complicated but also more realistic model. We find the same qualitative behaviour of $\Gamma(T)$ in the current chapter indicating that it is a more general feature of holographic superconductors.

We start by discussing the action of the holographic model we use in section 5.2. Section 5.3 contains a review of the properties of the normal conducting state of the model as well as own results. The superconducting ground state is analysed in section 5.4. The analysis of the fermionic spectral density analogous to the analysis in previous chapter is presented in 5.5. We summarise and suggest directions for future research in the last section 5.6 of this chapter.

The author's contribution to the results presented in this chapter is writing the code to numerically construct the superconducting state and to investigate its properties such as the free energy and the eletrical conductivity. The analytic groundwork presented in subsection 5.4.2 is original work done by the author of this thesis, as well as the generalisation of the methods used in chapter 4 and the corresponding analysis of the fermionic spectral density.

5.2 Holographic model

5.2.1 Setup

The superconductor we investigate in this chapter is based on the following action for the normal conducting state

$$S_{\text{dilaton}} = \int \mathrm{d}^4x\sqrt{-g}\left[R - \frac{1}{4}e^{\phi}F^2 - \frac{3}{2}\left(\nabla\Phi\right)^2 + \frac{6}{L^2}\cosh\left(\Phi\right)\right]. \tag{5.1}$$

This Einstein-Maxwell-dilaton model was studied from the holographic perspective in [72] and further analysed in [34]. It is the low energy limit of a solution to eleven dimensional supergravity [116]. The ansatz for the solution is given by

$$\begin{aligned}
&\mathrm{d}s^2 = -\frac{r^2}{L^2}h(r)\mathrm{d}t^2 + \frac{r^2}{L^2}g(r)\mathrm{d}x^2 + \frac{r^2}{L^2}g(r)\mathrm{d}y^2 + \frac{L^2}{r^2}h(r)^{-1}\mathrm{d}r^2, \\
&A = A_t(r)\mathrm{d}t, \quad \Phi = \Phi(r)\,.
\end{aligned} \tag{5.2}$$

As in the previous chapter, this ansatz implies the radial gauge for the Maxwell field: $A_r = 0$.

One of the main reasons we are interested in this model is that its entropy density vanishes at zero temperature, see 5.3.1. This is in contrast to the AdS-RN metal, which has a degenerate ground state (3.22) hinting at a severe instability of the system. The vanishing entropy density is due to the dilaton. In fact the exponent with which the entropy density close to $T = 0$ scales with temperature can be varied depending on the form of the gauge coupling and the dilaton potential [74], which in our case are given by e^{Φ} and $\cosh\Phi$, respectively.

In reference [34] this model was studied in the context of realising a linear increase of the electrical resistivity with temperature. We explained in section 3.3 that a physically sensible electrical conductivity requires breaking of translational invariance of the boundary field theory. This can be realised by an explicit breaking of translational invariance of the bulk ground state which was implemented in references [108,110,117] by including mass terms for the graviton. In this thesis we add two neutral scalar fields to the gravity theory, which break translational invariance in an isotropic and homogeneous way

$$S_{\text{axion}} = \int \mathrm{d}^4x\sqrt{-g}\Big[-\frac{1}{2}\sum_{i=1,2}\left(\nabla\xi_i\right)^2\Big]\,, \tag{5.3}$$

with

$$\xi_i\left(x^i\right) = \alpha x^i\,. \tag{5.4}$$

Explicitly writing out the massive gravity term used in the above references yields the same terms in the on-shell gravity action as using adding S_{axion} to S_{dilaton}. The advantage of using the neutral scalar fields is to avoid possible issues with ghosts which are present in massive gravity theories, see e.g. [118]. The breaking of translational invariance is now controlled by the parameter α, to which we also refer as strength of momentum dissipation.

As the last ingredient to our holographic superconductor model we add a charged scalar field χ, minimally coupled to gravity and the $U(1)$ gauge field, similarly to the original holographic superconductor 3.4

$$S_{\text{scalar}} = -\int \mathrm{d}^4x\sqrt{-g}\left[g^{\mu\nu}\left|D\chi\right|^2 + m^2\left|\chi\right|^2\right]\,. \tag{5.5}$$

The action of the holographic superconductor model subject of this chapter is given by

$$S = S_{\text{dilaton}} + S_{\text{axion}} + S_{\text{scalar}} + S_{\text{bdy}}\,, \tag{5.6}$$

where S_{bdy} contains the boundary terms, necessary to give the bulk theory a well defined variational principle and at the same time renormalises the theory

$$S_{\text{bdy}} = \int_{\partial\text{aAdS}} \mathrm{d}^3x\sqrt{-\gamma}\left[2\mathcal{K} - \frac{4}{L} - \frac{|\chi|^2}{L} - \frac{3}{2L}\phi^2 + \frac{1}{2L}\sum_{i=1,2}\left(\partial_{[\gamma]}\alpha_i\right)^2\right]. \tag{5.7}$$

The first two terms are related to the gravity part of the action. They are the Gibbons-Hawking terms and the so-called infinite-volume term, see [55, 59] for detailed explanations. Note that as in (4.2), there is an additional factor of 2 compared to the analysis in [59]. This is due to our convention to rescale the fields of the gravity theory in such a way that the prefactor $1/2\kappa^2$ of the gravity part disappears. The remaining three terms renormalise the one-point functions of the operators dual to the fields on the boundary. γ is the induced metric on the asymptotically AdS (aAdS) boundary of the bulk.

In the remainder of this section we establish the necessary background and tools to numerically construct the solutions of the fields appearing in the action (5.6) which are dual to a superconductor. The novelty of this model is that its normal conducting state, i.e. (5.6) without the charged scalar was shown in [34] to resemble the real strange metals which are the normal state of high-temperature superconductors. Other models with the same implementation of translational symmetry breaking are investigated in references [35, 36, 119].

5.2.2 Equations of motion

In order to study the properties of this holographic model in thermodynamic equilibrium we need to construct its ground state by solving the equations of motion

$$
\begin{aligned}
0 &= A_t'' + \left(\frac{2}{r} + \frac{g'}{g} - \phi'\right) A_t' - \frac{2L^2 e^2 e^{-\phi} \chi^2 A_t}{r^2 h}\,, \\
0 &= \phi'' + \left(\frac{4}{r} + \frac{g'}{g} + \frac{h'}{h}\right)\phi' + \frac{2\sinh(\phi)}{r^2 h} + \frac{L^2 e^{\phi} A_t'^2}{6 r^2 h}\,, \\
0 &= \chi'' + \left(\frac{4}{r} + \frac{g'}{g} + \frac{h'}{h}\right)\chi' - \left(\frac{L^2 m^2}{r^2 h} - \frac{e^2 L^4 A_t^2}{r^4 h^2}\right)\chi\,, \\
0 &= g'' - \frac{g'^2}{4g} + \left(\frac{4}{r} + \frac{h'}{2h}\right) g' + \left(\frac{3}{r^2} - \frac{2\cosh(\phi)}{r^2 h} + \frac{e^2 L^4 A_t^2 \chi^2}{2 r^4 h^2} + \frac{L^2 \alpha^2 \chi^2}{2 r^2 h}\right. \\
&\quad \left. + \frac{L^2 e^{\phi} A_t'^2}{4 r^2 h} + \frac{h'}{rh} + \frac{3\phi'^2}{4} + \frac{\chi'^2}{2}\right) g + \frac{L^4 m^2}{2 r^4 h}\,, \\
0 &= h'' + \left(\frac{5}{r} + \frac{g'}{2g}\right) h' + \left(\frac{3}{r^2} - \frac{g'^2}{4g^2} + \frac{3\phi'^2}{4} + \frac{\chi'^2}{2}\right) h - \frac{2\cosh(\phi)}{r^2} - \frac{L^4 \alpha^2}{2 r^4 g} \\
&\quad + \frac{L^2 m^2 \chi^2}{2 r^2} - \frac{3 e^2 L^4 A_t^2 \chi^2}{2 r^4 h} - \frac{3 L^2 e^{\phi} A_t'^2}{4 r^2}\,, \\
0 &= \frac{3}{r^2} - \frac{\cosh(\phi)}{r^2 h} + \frac{L^4 \alpha^2}{2 r^4 g h} + \left(\frac{L^2 m^2}{2 r^4 h^2} - \frac{e^2 L^4 A_t^2}{2 r^4 h^2}\right)\chi^2 + \frac{L^2 e^{\phi} A_t'^2}{4 r^2 h} + \frac{2g'}{rg} \\
&\quad + \frac{g'^2}{4g^2} + \frac{h'}{rh} + \frac{g'h'}{2gh} - \frac{3\phi'^2}{4} - \frac{\chi'^2}{2}\,.
\end{aligned}
\tag{5.8}
$$

Note that choosing the radial gauge for the Maxwell field $A_r = 0$, by the radial component of the Maxwell equation, demands a constant phase of the charged scalar field which we fixed to zero $\chi^* = \chi$. The UV BF bound on the charged scalar mass is the same as for the AdS-RN metal (2.31). As in the original holographic superconductor 3.4 we choose to work with the scalar $m^2 L^2 = -2$.

There are five second order differential equations and one contraint equation whose radial derivative can be shown to vanish by using the remaining equations. It represents a conserved quantity. Taking a closer look at the equations, we see that it has three scaling symmetries which we can utilise to simplify our numerical analysis of the model

$$
\begin{aligned}
&I && g \to \lambda\, g\,,\ \alpha \to \sqrt{\lambda}\,\alpha\,, \\
&II && r \to \lambda\, r\,,\ A_t \to \lambda\, A_t\,,\ \alpha \to \lambda\, \alpha\,, \\
&III && L \to \lambda^{-1} L\,,\ m \to \lambda\, m\,,\ \alpha \to \lambda^2 \alpha\,,\ e \to \lambda\, e\,,\ A_t \to \lambda\, A_t\,.
\end{aligned}
\tag{5.9}
$$

In particular, we can use the third relation to fix the AdS radius $L = 1$ and the second relation to set the horizon radius $r_\mathrm{h} = 1$. Note that as mentioned in chapter 3.2, the Maxwell field A_t, and hence the chemical potential, and also the translational symmetry breaking parameter α scale in the same way as the radial coordinate. This explicitly shows that it is consistent to express the energy dimensions of quantities in units of the chemical potential.

5.2.3 Boundary expansion

The boundary behaviour of the background fields whose solution constitutes the systems ground state reveals information about the model's structure. The system is described by five second order equations of which one can consistently be replaced by the first order constraint equation. Thus a priori there are $2 \times 5 - 1 = 9$ boundary conditions that have to be fixed in order to uniquely determine a solution.

For an expansion of the fields close to the black hole horizon, we start by introducing ten coefficients, two for each field. Demanding regularity at the horizon for all of those five fields, yields five conditions which fix five of the ten coefficients. As the constraint equation vanishes automatically at the horizon when the regularity conditions are met, it does not provide additional information. The horizon expansion is then parametrised by five coefficients c^h

$$\begin{aligned}
&A_t(r) = c^\mathrm{h}_{A_t,1}\,(r - r_\mathrm{h}) + \mathcal{O}\big(\,(r - r_\mathrm{h})^2\,\big)\,, \quad \chi(r) = c^\mathrm{h}_{\chi,0} + \mathcal{O}\,(r - r_\mathrm{h})\,,\\
&\phi(r) = c^\mathrm{h}_{\phi,0} + \mathcal{O}\,(r - r_\mathrm{h})\,, \quad h(r) = c^\mathrm{h}_{h,1}\,(r - r_\mathrm{h}) + \mathcal{O}\big(\,(r - r_\mathrm{h})^2\,\big)\,,\\
&g(r) = c^\mathrm{h}_{g,0} + \mathcal{O}\,(r - r_\mathrm{h})\ ,
\end{aligned} \tag{5.10}$$

where the index $i = 0, 1$ of the coefficients refers to the order in $(r - r_\mathrm{h})$ they accompany. For the UV boundary at $r \to \infty$ let us also start with the initial set of ten coefficients c^b

$$\begin{aligned}
A_t(r) &= c^\mathrm{b}_{A_t,0} + c^\mathrm{b}_{A_t,1} r^{-1} + \mathcal{O}\left(r^{-2}\right)\ ,\\
\chi(r) &= c^\mathrm{b}_{\chi,1} r^{-1} + c^\mathrm{b}_{\chi,2} r^{-2} + \mathcal{O}\left(r^{-3}\right)\ ,\\
\phi(r) &= c^\mathrm{b}_{\phi,1} r^{-1} + c^\mathrm{b}_{\phi,2} r^{-2} + \mathcal{O}\left(r^{-3}\right)\ ,\\
h(r) &= c^\mathrm{b}_{h,0} + \tilde{c}^\mathrm{b}_{h,1} r^{-1} + \tilde{c}^\mathrm{b}_{h,2} r^{-2} + c^\mathrm{b}_{h,3} r^{-3} + \mathcal{O}\left(r^{-4}\right)\ ,\\
g(r) &= c^\mathrm{b}_{g,0} + \tilde{c}^\mathrm{b}_{g,1} r^{-1} + \tilde{c}^\mathrm{b}_{g,2} r^{-2} + c^\mathrm{b}_{g,3} r^{-3} + \mathcal{O}\left(r^{-4}\right)\ ,
\end{aligned} \tag{5.11}$$

where again the index $i = 0, 1, 2, 3$ of the coefficients refers to the corresponding order of r^{-1}. The coefficients $\tilde{c}^{\mathrm{b}}$'s are functions of the independent ones c. The relations are given in the appendix in equation (C.30). As predicted by the holographic dictionary, each field has a non-normalisable and a normalisable mode and their scaling dimension with respect to the radial coordinate is fixed by the nature of the field, its mass and the number of dimensions. At the boundary the constraint equation indeed provides additional information and automatically fixes $c^{\mathrm{b}}_{h,0} = 1$. To recapitulate, we already imposed five conditions at the horizon. This means that in order to completely specify a solution four more conditions are needed at the boundary. The minimal condition at $r \to \infty$ is that the space asymptotes to AdS space which demands $c^{\mathrm{b}}_{g,0} = 1$. Moreover we impose the following three conditions at infinity

$$c^{\mathrm{b}}_{A_t,0} = \mu\,, \quad c^{\mathrm{b}}_{\chi,1} = 0\,, \quad c^{\mathrm{b}}_{\phi,1} = \phi_0\,. \tag{5.12}$$

The first condition really means that when constructing the solutions numerically, we demand a certain value for the chemical potential μ. The second condition assures that the charged scalar field is not sourced at the boundary but rather spontaneously acquires a profile as the temperature is lowered. The third condition expresses that in order to completely specify a solution we need to fix the normalisable mode of the dilaton as well.

The equations of motion (5.8) are solved with a standard procedure called shooting method. The first step is to express the value the fields and their derivative at the horizon, given a set of numerical values for the independent coefficients at the horizon. With this information the solution can be integrated starting at $r_{\mathrm{h}} + \epsilon$ all the way to the AdS boundary at $r \to \infty$. At the same time, one needs to check that the solution to the five second order differential equations also obeys the extra first order constraint equation. A solution generated like gives a numerical value for nine of the ten coefficients c^{b} in (5.11), recall that one coefficient $c^{\mathrm{b}}_{h,0} = 1$ automatically takes the correct value. The numerical values for the other nine coefficients will typically not obey the boundary conditions (5.12). To meet those conditions, one has to vary the five horizon parameters c^{h} until (5.12) is satisfied. This is implemented with a 'find root' routine.

Of course the above numerical procedure requires numerical values for the horizon radius and the AdS radius which are fixed without loss of generality to $r_{\mathrm{h}} = L = 1$ with the help of the scaling symmetries (5.9). To speed up the search for a solution which meets the imposed boundary conditions one can also relax the condition for $c^{\mathrm{b}}_{g,0}$ and restore it afterwards by applying the first scaling symmetry. The external parameters α and e have to be assigned a numerical value as well. In summary the solutions to (5.8) are parametrised by

$$T/\mu\,, \quad \bar{\phi}_0 \equiv \phi_0/\mu\,, \quad e \quad \text{and} \quad \bar{\alpha} \equiv \alpha/\mu\,, \tag{5.13}$$

where we traded the chemical potential μ for the temperature T and consequently express all the dimensionful quantities in units of μ.

5.3 Normal state

We now summarise the properties of the holographic model (5.6) in the normal state by which we refer to the solutions where the charged scalar is zero $\chi \equiv 0$. As found in [34] they resemble the properties of a real strange metal in many ways. Moreover we apply the method outlined in [117] to our setup in order to obtain an explicit expression for the DC resistivity and analyse the frequency dependence of the electrical conductivity.

5.3.1 In thermal equilibrium

The equations of motion (5.8) have the following analytical solution

$$\begin{aligned}
h(r) &= g(r)\left(1 - \frac{L^4\alpha^2}{2\,(r+Q)^2} - \frac{(r_\mathrm{h}+Q)\left(2\,(Q+r_\mathrm{h})^2 - L^4\alpha^2\right)}{2\,(r+Q)^3}\right)\,,\\
A_t(r) &= \frac{\sqrt{3Q}}{L^2}\left(1 - \frac{r_\mathrm{h}+Q}{r+Q}\right)\sqrt{\frac{2\,(Q+r_\mathrm{h})^2 - L^4\alpha^2}{2\,(r_\mathrm{h}+Q)}}\,,\\
g(r) &= \left(1+\frac{Q}{r}\right)^{3/2}\,, \qquad \phi(r) = \frac{1}{3}\log\left(g(r)\right) \qquad \chi(r) = \chi^*(r) = 0\,.
\end{aligned} \tag{5.14}$$

It is parametrised by the translational symmetry breaking parameter α and the parameter Q associated to the Maxwell field A_t. Note that based on the analysis in the previous subsection (5.13) one would expect three parameters in absence of the scalar. The above solution thus cannot represent the most general solution.

Instead the non-normalisable mode of the dilaton is fixed to

$$\phi_0 = \frac{Q}{2}\,. \tag{5.15}$$

The Bekenstein-Hawking temperature and hence the temperature of the field theory dual to (5.14) according to (2.38) is given by

$$T = \frac{\sqrt{r_\mathrm{h}}\left(6\left(r_\mathrm{h}+Q\right)^2 - L^4\alpha^2\right)}{8\pi L^2\left(r_\mathrm{h}+Q\right)^{3/2}}\,, \tag{5.16}$$

and the chemical potential according to equation (3.19) evaluates to

$$\mu = \frac{1}{L^2}\left(3Q(Q+r_\mathrm{h})\big(1-\frac{\alpha^2L^4}{2(Q+r_\mathrm{h})^2}\big)\right)^{1/2}\,. \tag{5.17}$$

For the chemical potential to be real valued one has to demand $2\left(Q+r_\mathrm{h}\right)^2 \geq L^4\alpha^2$. The physically sensible parameter, however, is the ratio of T/μ, referred to as temperature in the remainder of this section. In contrast to the AdS-RN solution, the holographic model discussed here can reach small temperatures only by a small horizon radius and scales as

$$T/\mu \sim \sqrt{r_\mathrm{h}/Q}\,. \tag{5.18}$$

In particular, zero temperature is reached for $r_\mathrm{h} = 0$.

The IR geometry of (5.14) is different from the one of the AdS-RN metal (3.23). To construct it, we start by setting $r_\mathrm{h} = 0$, as it represents zero temperature and then expand the radial coordinate around zero. Redefining the radial coordinate by $r = \frac{L^2\gamma}{\zeta}$ the metric becomes

$$\mathrm{d}s^2 = -\frac{L^4\left(6\alpha^2 - L^4\alpha^2\right)\gamma^3}{2Q^{3/2}\zeta^3}\mathrm{d}t^2 + \frac{Q^{3/2}\gamma}{\zeta}\mathrm{d}x^2 + \frac{Q^{3/2}\gamma}{\zeta}\mathrm{d}y^2 + \frac{8L^4Q^{3/2}\gamma}{6Q^2 - L^4\alpha^2}\mathrm{d}\zeta^2\,. \tag{5.19}$$

We now define γ in such a way that the temporal and radial part represent a conformal-to-AdS$_2$ spacetime. This is realised by

$$\gamma = \frac{4Q^{3/2}}{6Q^2 - L^4\alpha^2}\,. \tag{5.20}$$

where we used the positivity constraint from the chemical potential $2Q^2 > L^4\alpha^2$.

Finally, the IR geometry of the dilaton strange metal is given by

$$\mathrm{d}s^2 = \frac{4Q^3L^2}{\left(6Q^2 - L^4\alpha^2\right)^2\zeta}\left[\frac{8L^2}{\zeta^2}\left(-\mathrm{d}t^2 + \mathrm{d}\zeta^2\right) + \frac{6Q^2 - L^4\alpha^2}{L^2}\left(\mathrm{d}x^2 + \mathrm{d}y^2\right)\right]. \quad (5.21)$$

which is conformal to $\mathrm{AdS}_2 \times \mathbb{R}^2$. As such it transforms as $\mathrm{d}s^2 \to \lambda^{-1}\mathrm{d}s^2$ under a scaling transformation of the temporal coordinate which leaves the spatial ones untouched [34]

$$t \to \lambda\, t\,, \quad x_i \to x_i\,, \quad \zeta \to \lambda^{-2}\,\zeta\,. \quad (5.22)$$

This amounts to a local quantum critical state with hyperscaling violation. More presicely, we have $z \to \infty$ and $\theta/z = -1$, where θ is the hyperscaling violation exponent [74]. It also determines the scaling of the entropy density with temperature. Calculating it from the corresponding entry of the AdS/CFT dictionary (2.33) gives

$$s/\mu^2 = \frac{r_\mathrm{h}^2 g(r_\mathrm{h})}{4GL^2\mu^2} = \frac{2\pi L^2}{3\kappa^2}\sqrt{r_\mathrm{h}/Q}\sqrt{1 + r_\mathrm{h}/Q}\left(1 + \frac{3\bar{\alpha}^2}{2(1 + r_\mathrm{h}/Q)}\right) \sim T/\mu\,, \quad (5.23)$$

where the units are properly taken care off by the chemical potential. For small temperatures, i.e. small r_h, it scales linearly in temperature as advertised in the introduction to this chapter.

The charge density $\langle\varrho\rangle \equiv \varrho$ according to the prescription in (3.20) is given by

$$\varrho/\mu^2 = -L^2 r_\mathrm{bdy}^2 A_t'(r_\mathrm{bdy})/\mu^2 = \frac{1}{\sqrt{3}L}\sqrt{1 + r_\mathrm{h}/Q}\sqrt{1 + \frac{3\bar{m}^2}{2\left(1 + r_\mathrm{h}/Q\right)}} \sim (T/\mu)^0\,, \quad (5.24)$$

and is independent of temperature in the small temperature regime.

5.3.2 Electrical conductivity

In section 3.3 we explained the concept of transport coefficients and how they can be computed using the holographic methodology. In short, we have to perturb the equilibrium and calculate the linear respone functions which in holography are equal to Green's functions of the appropriate perturbations. In most cases this requires an often numerically constructed solution for the perturbations. However, sometimes it is possible to make use of the membrane paradigm which allows to determine the low energy or IR behaviour of the transport coefficient solely in terms of horizon parameters [11]. Reference [117] showed that the membrane paradigm is applicable to the holographic strange metal with broken translational invariance for firstly a metal based on the AdS-RN solution and secondly for the present model with a dilaton field. In [117] the breaking of the translational symmetry in the bulk is realised by a mass term for the graviton which is conceptually different from (5.6), albeit, when evaluated on-shell the actions of the two models are the same. For the calculation of the optical conductivity this difference between the models results a different set of fluctuations that are relevant. While the in the massive gravity approach apart from the Maxwell fluctuation δA_x only the gravity fluctuations δg_{tx} and δg_{xr} need to be taken into account, our approach requires to additionally consider the scalar field fluctuation $\delta\xi_x$.

We will now present the procedure for our model. Let us start by perturbing the thermal equilibrium described by the analytic solution (5.14) on the gravity side. Just as in section 3.3, the field theory dual is isotropic and without loss of generality we can focus on the conductivity along the x-direction. For zero spatial momentum, there are four perturbations that couple to the perturbation of interest which is the one of the Maxwell field δA_x. Their linearised equations of motion are given by

$$\begin{aligned}
0 &= \left(e^{\phi} r^2 h \delta A_x'\right)' + L^2 e^{\phi} r^2 g A_t' \left(\frac{\delta g_{tx}}{r^2 g}\right)' + \frac{L^4\omega^2 e^{\phi}\delta A_x}{r^2 h} + iL^2\omega e^{\phi} A_t' \delta g_{xr}, \\
0 &= \left(r^4 g h \delta\xi_x'\right)' - L^2\alpha\left(r^2 h\delta_{xr}\right)' + \frac{L^4\omega^2 g\delta\xi_x}{h} - \frac{i\mathrm{L}^6\alpha\omega\delta g_{tx}}{r^2 h}, \\
0 &= \Big(r^2 g\delta g_{tx} - \left(r^2 g\right)' + e^{\phi} r^2 g A_t' \delta A_x + i r^2 g \delta g_{xr}\Big)' - \frac{iL^2 m\omega\delta\xi_x}{h} - \frac{L^4\alpha^2\delta g_{tx}}{r^2 h}, \\
0 &= \Big(r^2 g\delta g_{tx} - \left(r^2 g\right)' + e^{\phi} r^2 g A_t' \delta A_x + i r^2 g \delta g_{xr}\Big) - \frac{i\alpha^2 r^2 h \delta g_{xr}}{\omega} - \frac{i\alpha r^4 g h \delta\xi_x'}{L^2\omega}.
\end{aligned} \tag{5.25}$$

Following [117], we start by eliminating δg_{tx} with the constraint

$$0 = \left(r\delta\tilde{g}_{xr}\right)' + \frac{iL^4\omega\delta g_{tx}}{r^2 h} - \frac{L^2\omega^2 g\delta\xi_x}{h\alpha^2} \tag{5.26}$$

which is simply the second equation along with the definition $\delta\tilde{g}_{xr} = r^2 h(\delta g_{xr} - r^2 g\delta\alpha_x'/L^2\alpha)$. Using this constraint equation the system reduces to two equations which only depend on δA_x and $\delta\tilde{g}_{xr}$ plus one equation with all three remaining fluctuations. As we are interested in the dynamics of δA_x only, it is sufficient to focus on the former. They are given by

$$
\begin{aligned}
0 &= r^2 e^{-\phi}\left(r^2 e^{\phi} h \delta A_x'\right)' + \frac{L^4\omega^2}{h}\delta A_x - \frac{e^{-\phi}}{g^2}\left(\frac{L^2\mathcal{Q}^2}{r^2}\delta A_x + \frac{L^2\alpha^2\mathcal{Q}}{i\omega r^2}\delta\tilde{g}_{xr}\right),\\
0 &= r^4 g\left(\frac{h}{g}\delta\tilde{g}_{xr}'\right)' + \frac{L^4\omega^2}{h}\delta\tilde{g}_{xr} - \frac{1}{g}\left(i\omega L^4\mathcal{Q}\delta A_x + L^4\alpha^2\delta\tilde{g}_{xr}\right).
\end{aligned}
\tag{5.27}
$$

We introduced the conserved charge density $\mathcal{Q}$

$$
\mathcal{Q} = r^2 e^{\phi} g A_t' \quad \text{with} \quad \mathcal{Q}' = 0\,, \tag{5.28}
$$

where the conservation equation is actually the Maxwell equation from (5.8). These equations can now be mapped to the equations of motion on page 13 in [117] with the identifications

$$
f = h/g\,, \quad Z(\phi) = g\mathrm{e}^{\phi}\,, \quad \text{and} \quad \chi = 0\,. \tag{5.29}
$$

The left hand sides of those identifications corresponds to the notation in [117] where the right hand sides to our notation. The additional factors of g^2 do not alter the form of the conserved current. Note that in contrast to their convention we work in a coordinate system where the AdS boundary is at $r \to \infty$. Conclusively the logic of the original work applies here as well and the remaining calculations can be mapped onto each other by (5.29). The crucial observation that allows the membrane paradigm to take it from here, is that the determinant of the mass-matrix in (5.27) vanishes. The two eigenstates are

$$
\begin{aligned}
\delta\lambda_1 &= \left(e^{\phi}g + \frac{\mathcal{Q}}{\alpha^2 r^2}\right)^{-1}\left(e^{\phi}g\delta A_x - \frac{\mathcal{Q}}{i\omega L^2}\delta\tilde{g}_{tx}\right).\\
\delta\lambda_2 &= \left(e^{\phi}g + \frac{\mathcal{Q}}{\alpha^2 r^2}\right)^{-1}\left(\frac{1}{i\omega}\delta\tilde{g}_{rx} + \frac{L^2\mathcal{Q}}{\alpha^2}\delta A_x\right).
\end{aligned}
\tag{5.30}
$$

where $\delta\lambda_1$ is the massless mode obeying the following equation of motion

$$
\begin{aligned}
0 = r^2 g &\left(\left(e^{\phi}g + \frac{\mathcal{Q}}{\alpha^2 r^2}\right)\frac{hr^2}{g}\delta\lambda_1' - \frac{\mathcal{Q}h}{L^2 r^2 g}\left(r^2 e^{\phi} g\right)'\delta\lambda_2\right)'\\
&+ \frac{L^4\omega^2}{h}\left(e^{\phi}g + \frac{\mathcal{Q}}{\alpha^2 r^2}\right)\delta\lambda_1\,.
\end{aligned}
\tag{5.31}
$$

In the zero frequency limit this reduces to a conservation equation for the current

$$\Pi = \left(e^{\phi}g + \frac{\mathcal{Q}}{\alpha^2 r^2}\right)\frac{hr^2}{g}\delta\lambda_1' - \frac{\mathcal{Q}h}{L^2 r^2 g}\left(r^2 e^{\phi} g\right)'\delta\lambda_2\,. \tag{5.32}$$

One can now define a radially dependent conductivity

$$\sigma_{\mathrm{DC}}(r) = \lim_{\omega\to 0}\frac{\Pi(r)}{i\omega\delta\lambda_1(r)}\,. \tag{5.33}$$

which at the boundary reduces to the standard form of the conductivity in holography (3.37). In the zero frequency limit σ_{DC} is constant and hence be evaluated at the horizon, where the $\delta\lambda_2$ part of the conserved current does not contribute, as it has a double zero at r_{h}. The result is given by

$$\sigma_{\mathrm{DC}} = \lim_{\omega\to 0}\frac{\Pi(r_{\mathrm{h}})}{i\omega\delta\lambda_1(r_{\mathrm{h}})} = e^{\phi}\left(1 + \frac{\mathcal{Q}e^{-\phi}}{\alpha^2 r^2 g}\right)\,, \tag{5.34}$$

An expansion in α for small momentum relaxation of the electrical resistivity, the inverse of the conductivity, results in

$$\rho_{\mathrm{DC}} = \frac{r_{\mathrm{h}}^2 g(r_{\mathrm{h}})}{\mathcal{Q}^2}\alpha^2 + \mathcal{O}\left(\alpha^4\right) = \frac{\bar{\alpha}^2}{\sqrt{1 + r_{\mathrm{h}}/Q}}\sqrt{r_{\mathrm{h}}/Q} + \mathcal{O}\left(\bar{\alpha}^4\right) \sim T/\mu. \tag{5.35}$$

We see that even though in our case we have the additional neutral scalar field responsible for the momentum dissipation the result is exactly the same. In particular the proportionality $\rho \propto T \propto s$ also holds here. Note that comparing $\sigma_{\mathrm{DC}} = \rho_{\mathrm{DC}}^{-1}$ with the DC conductivity in (3.40) in the context of discussing the Drude model, it is clear that referring to $\bar{\alpha}$ as the scale of momentum relaxtion is justified, because it is related to the average time τ between collision through $\tau \sim \bar{\alpha}^{-1}$.

A investigation of the full (non-expanded) resistivity reveals that the linear behaviour with temperature is a good approximation up to temperatures of about $T/\mu \sim 0.05$. Moreover, the physical reasoning behind [34] demands the momentum relaxation to be weak. We will therefore restrict our analysis to small values of $\bar{\alpha}$ as well.

5.4 Superconducting state

5.4.1 Superconducting instability

Due to the Maxwell field the mass of the charged scalar is effectively lowered (5.8)

$$m_{\text{eff}}^2 L^2 = m^2 L^2 - \frac{e^2 L^4 A_t^2}{r^2 h} \,. \tag{5.36}$$

We established earlier in this thesis, that this term is more relevant as temperature is decreased and eventually causes the scalar to become unstable. Recall that in this chapter we fix $m^2 L^2 = -2$. The closer the scalar mass is to the UV BF bound $m_{\text{BF}}^2 L^2 = -9/4$, the higher is the critical temperature.

One way to investigate the precise temperature where the instability sets in, is to compute the quasinormal modes. The idea to treat the scalar as a time dependent fluctuation around the normal conducting ground state (5.14). The corresponding equation of motion for the Fourier modes of $\chi(t,r) = \int \mathrm{d}\omega \mathrm{e}^{-i\omega t} \chi_k(r)$ reads as follows

$$0 = \chi_k'' + \left(\frac{4}{r} + \frac{g'}{g} + \frac{h'}{h}\right) \chi_k' - \left(\frac{L^2 m^2}{r^2 h} - \frac{L^4 \left(e A_t + \omega\right)^2}{r^4 h^2}\right) \chi_k \,. \tag{5.37}$$

The quasinormal modes are given by the poles of the retarded two-point function G^{R}, which in the case of the scalar fluctuation by the method outlined in 3.3.1 is proportional to

$$G_{\chi\chi}^{\text{R}} \propto \left.\frac{r \chi_k'}{\chi_k}\right|_{r\to\infty} , \tag{5.38}$$

where it is understood that the scalar fluctuation satisfies the ingoing boundary conditions (3.34). In general, there are several quasinormal modes, whose locations ω_{QNM} in the complex frequency plane change in temperature. The one which triggers the instability is the one crossing the real axis, i.e. changing the sign of the imaginary part $\operatorname{Im} \omega_{\text{QNM}}$, at $\omega = 0$. The then positive imaginary part of the pole by $\chi \sim \exp(-i\omega_{\text{QNM}})$ represents an exponential growth of the scalar and hence indicates the instability. The temperature at which this happens is the critical temperature T_c.

We find that T_c increases as the scalar's charge is e increased, i.e. the instability sets in at a higher temperature. This is not surprising because the effective mass m_{eff} is lowered by finite values for the charge (5.36). Upon changing the parameter $\bar{\alpha}$ which controls the breaking of translational symmetry, we observe that higher values lead to a smaller critical temperature. This behaviour is less obvious from the above mass relation, because the background fields explicitly depend on $\bar{\alpha}$ in a nontrivial way. However, plugging in the normal state solution (5.14), one finds that

$$\partial_{\bar{\alpha}} m_{\text{eff}} \propto -\bar{\alpha} + \mathcal{O}\left(\bar{\alpha}^2\right) , \tag{5.39}$$

i.e. the effective mass m_{eff} is increased due to small values of $\bar{\alpha}$. Let us give a few examples for the critical temperature

$$\begin{aligned}
T_c/\mu &= 0.043 \quad \text{for} \quad e = 2.0\,,\ \bar{\alpha} = 0.08\,,\\
T_c/\mu &= 0.041 \quad \text{for} \quad e = 2.0\,,\ \bar{\alpha} = 0.16\,,\\
T_c/\mu &= 0.023 \quad \text{for} \quad e = 2.0\,,\ \bar{\alpha} = 0.35\,,\\
T_c/\mu &= 0.100 \quad \text{for} \quad e = 2.5\,,\ \bar{\alpha} = 0.08\,,\\
T_c/\mu &= 0.175 \quad \text{for} \quad e = 3.5\,,\ \bar{\alpha} = 0.08\,.
\end{aligned} \tag{5.40}$$

Given that the DC resistivity ρ_{DC} is only linear in temperature for temperatures up to $T \sim 0.05$ we will restrict to $e = 2$ in the following. The monotonous behaviour of the critical temperature depending on the two external parameters e and $\bar{\alpha}$ agrees with the analysis in [36] holographic superconductor model based on an AdS-RN geometry but with the same mechanism of breaking translational invariance. For values of the charge investigated here, it moreover agrees with the results in [35]. However, they find that the critical temperature increases for very small values of the charge.

5.4.2 Superconducting ground state

For the superconducting instability to actually cause a phase transition to a superconductor the thermodynamic state associated to the condensate has to be thermodynamically preferred. This can be checked by comparing the grand potential of the normal conducting solution (5.14) to the one of solutions with a charged scalar profile. The holographic dictionary states that the grand potential of a thermal field theory is proportional to the Euclidean on-shell action of the gravity theory (2.36). For the model that we are discussing in this chapter (5.6), the on-shell action can be expressed in two different ways

$$S_1^{\mathrm{os}}/\beta V_2 = \frac{r^6 g^2}{L^4}\left(\frac{1}{g\,r^2}\right)'\Bigg|_{r_\mathrm{h}}^{1/\epsilon} - \alpha^2\left(\frac{1}{\epsilon} - r_\mathrm{h}\right) + S_{\mathrm{bdy}}/\beta V_2\,, \tag{5.41}$$

$$S_2^{\mathrm{os}}/\beta V_2 = \frac{r^2 g}{L^2}\left(e^{\phi}A_t A_t' - \left(\frac{r^2 h}{L^2}\right)'\right)\Bigg|_{r_\mathrm{h}}^{1/\epsilon} + S_{\mathrm{bdy}}/\beta V_2\,, \tag{5.42}$$

where V_2 represents the integral over the boundary coordinates x and y and β the integral over the compactified time coordinate. The parameter $\epsilon \sim 1/r$ is the UV cut-off and is taken to $\epsilon \to 0$ when the whole expression, including the boundary terms which act as a renormalisation, is evaluated. To obtain those expressions, one has to rewrite the action as a total radial derivative plus a term which is proportional to the equations of motion. It is a generic feature that there are two versions of the total derivative leading to $S_1^{\mathrm{os}} = S_2^{\mathrm{os}}$. To understand this feature's origin it is instructive to write out (5.41) and (5.42) in terms of the boundary coefficients $c^{\mathrm{b,h}}$ introduced in subsection 5.2.3, see equations (5.11) and (C.30),

$$S_1^{\mathrm{os}}/\beta V_2 = \frac{c_{g,0}^{\mathrm{b}} c_{h,3}^{\mathrm{b}}}{L^4} + \alpha^2\left(\frac{c_{g,3}^{\mathrm{b}}}{c_{h,3}^{\mathrm{b}}(c_{\phi,1}^{\mathrm{b}})^2} + \frac{c_{\phi,2}^{\mathrm{b}}}{c_{\phi,1}^{\mathrm{b}}} - r_\mathrm{h}\right), \tag{5.43}$$

$$S_2^{\mathrm{os}}/\beta V_2 = -\frac{c_{g,0}^{\mathrm{h}} c_{h,1}^{\mathrm{h}} r_\mathrm{h}^4}{L^4} + \frac{c_{A_t,0}^{\mathrm{b}} c_{A_t,1}^{\mathrm{b}} c_{g,0}^{\mathrm{b}}}{L^2} + \frac{3c_{g,3}^{\mathrm{b}}}{L^4} - \frac{2c_{g,0}^{\mathrm{b}} c_{h,3}^{\mathrm{b}}}{L^4}\,. \tag{5.44}$$

On the other hand, the thermodynamic quantities of the model can be expressed in terms of those coefficients as well

$$T = \frac{r_\mathrm{h}^2 c_{h,1}^{\mathrm{h}}}{4\pi L^2}\,, \quad s = S/V_2 = \frac{2\pi r_\mathrm{h}^2 c_{g,0}^{\mathrm{h}}}{\kappa^2 L^2} \quad \mu = c_{A_t,0}^{\mathrm{b}}\,, \quad \varrho = -\frac{c_{A_t,1}^{\mathrm{b}}}{L^2}\,, \tag{5.45}$$

where we used (2.38) to compute the temperature T, (2.33) for the entropy density s, (3.19) for the chemical potential μ and the appropriate adaption of equation (3.20) for the charge density ϱ. There is a small subtlety in computing the entropy density. The reason is that the general formula for the entropy in the holographic context (2.33) requires the canonical normalisation of the gravity action which we omitted here. Thus when we check the thermodynamic relation we have to compensate for it by including a factor of $2\kappa^2$.

And there is one last ingredient for the physical interpretation of the two expressions of the on-shell action. It is the stress energy tensor of the field theory which is sourced by the bulk metric. Applying the field-operator map (2.30) we obtain

$$\langle T^{tt}\rangle = \frac{3c^{\mathrm{b}}_{g,3}}{L^4 c^{\mathrm{b}}_{g,0}} - \frac{2c^{\mathrm{b}}_{g,0}c^{\mathrm{b}}_{h,3}}{L^4}\,, \qquad \langle T^{xx}\rangle = \langle T^{yy}\rangle = -\frac{c^{\mathrm{b}}_{g,0}c^{\mathrm{b}}_{h,3}}{L^4}\,. \tag{5.46}$$

It is now clear that the two expressions for the grand potential density Ω/V_2 simply represent the thermodynamic relation for the grand potential

$$\Omega_1/V_2 = -S^{\mathrm{os}}_1/\beta V_2 \equiv -p\,, \tag{5.47}$$

$$\Omega_2/V_2 = -S^{\mathrm{os}}_2/\beta V_2 = \varepsilon - T\,s - \mu\,\varrho\,. \tag{5.48}$$

where the energy density is defined as $\varepsilon = \langle T^{tt}\rangle$. The pressure p of the thermodynamic equilibrium state of the field theory is appropriately defined by the grand potential density (5.47). Note that in our model the pressure is not given by the spatial component of the stress energy tensor

$$p = \langle T^{xx}\rangle - \alpha^2\left(\frac{c^{\mathrm{b}}_{g,3}}{c^{\mathrm{b}}_{h,3}(c^{\mathrm{b}}_{\phi,1})^2} + \frac{c^{\mathrm{b}}_{\phi,2}}{c^{\mathrm{b}}_{\phi,1}} - r_{\mathrm{h}}\right). \tag{5.49}$$

The difference is sourced by the translational invariance breaking parameter α. This can be regarded as analogous to a situation where a constant magnetic field is applied leading to a magnetisation [120]. Another observation is that the trace of the stress-energy tensor does not vanish

$$\langle T^{\mu}_{\mu}\rangle \neq 0\,. \tag{5.50}$$

This is a clear sign that the UV conformal symmetry is broken, i.e. the microscopic quantum field theory dual to our holographic model is deformed from conformality, see for example [121, 122].

When comparing the grand potential Ω it is important to take care of the units and compare the appropriate pair of solutions . The former can be summarised to

$$(T/\mu)_s = (T/\mu)_n\,, \quad \bar{\alpha}_s = \bar{\alpha}_n\,, \quad \left(\Omega/\mu^3\right)_s \text{ vs. } \left(\Omega/\mu^3\right)_n\,, \tag{5.51}$$

where the indices refer to what will soon be identified as the normal conducting state (n) and the superconducting state (s). Note that the normalisation with respect to the chemical potential denoted by the bar has to be performed with the value of the chemical potential in the respective branch of solutions. Morevoer

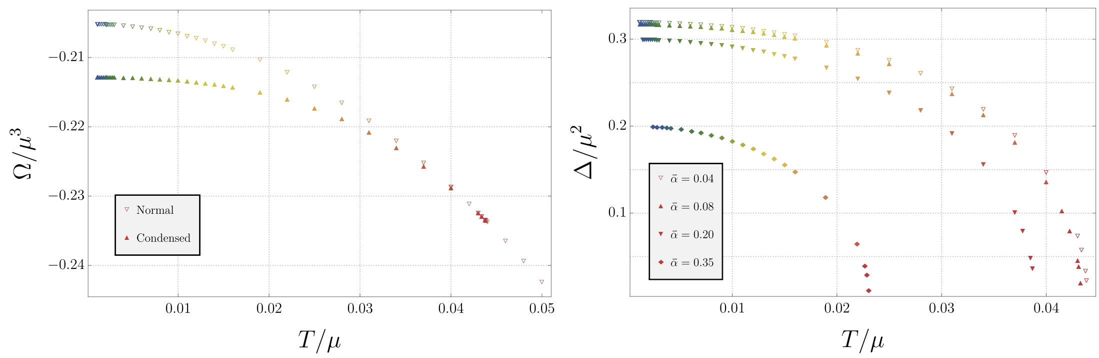

(a) (b)

Figure 5.1: (a) The grand potential Ω as a function of temperature for the normal conducting state and the superconducting state, which is identified to be thermodynamically preferred for $T/\mu < T_c/\mu \approx 0.044$. We fix $e = 2$ and $\bar{\alpha} = 0.04$. (b) The scalar condensate Δ as a function of temperature for four different values of $\bar{\alpha} = 0.04$, 0.08, 0.2, 0.3 at $e = 2$.

there is a subtlety related to the non-normalisable mode ϕ_0 of the dilaton field. We identified ϕ_0 as one of the free parameters which has to be fixed in order to completely specify the solution (5.13). At the same time, the normal state solution (5.14) corresponds to a special solution, where ϕ_0 is already fixed, effectively as a function of the temperature (5.15). If we are to compare the numerical superconducting state solution to the special analytic normal state solution this function has to be matched

$$\left(\bar{\phi}_0\left(T/\mu\right)\right)_s = \left(\bar{\phi}_0\left(T/\mu\right)\right)_n \,, \tag{5.52}$$

Using the boundary condition for the dilaton Φ, we numerically construct solutions with a non-trivial charged scalar profile below the critical temperature T_c using the shooting method explained in 5.2.3.

Figure 5.1(a) shows that the numerically constructed solution with a non-vanishing charged scalar representing the superconducting state, is indeed thermodynamically preferred over the normal state solution below a certain critical temperature T_c.

The condensate of the charged scalar by equation (3.47) close to the critical temperature exhibits a mean-field behaviour (3.48)

$$\Delta/\mu^2 = c^{\mathrm{b}}_{\chi,2}/\mu^2 \sim \left(1 - T/T_c\right)^{1/2} \,, \tag{5.53}$$

as shown in figure 5.1(b). We also observe the decreasing value for the critical temperature for increasing values of $\bar{\alpha}$, discussed in the previous subsection 5.4.1.

It remains to show that this new phase really describes a superconductor in a sense that the conductivity shows a δ pole at zero frequency.

5.4.3 Electrical conductivity

We now turn to the electrical conductivity in the supposedly superconducting ground state of the holographic model (5.6) studied in this chapter. The goal is to see a pole of the form $1/i\omega$ in the imaginary part $\mathrm{Im}\,\sigma(\omega)$ at zero frequency. This pole, by the Kramers-Kronig relation is equivalent to a δ-peak of the DC conductivity $\mathrm{Re}\,\sigma_{\mathrm{DC}}$.

To compute the electrical conductivity we use the holographic method explained in detail in 3.3.1. As for the normal conducting state analysis, we choose without loss of generality to focus on the conductivity in the x-direction. The first step, perturbing the ground state really means adding perturbations to every component of every field present in the gravity background (5.2). In general, the fluctuation δA_x does not decouple from the rest of the fluctuations. Thus before we can follow the prescription, we have to identify to which of the fluctuations it couples. This can be done based on symmetry considerations. Being interested in the time-dependence only, we do not consider a spatial dependence and the set of perturbations we need to take into account to compute the optical conductivity is

$$\{\delta A_x,\, \delta g_t^x,\, \delta g_r^x,\, \delta\xi_x\}\,. \tag{5.54}$$

In this thesis we work with a gauge invariant approach. By this we mean that we consider only field combinations of (5.54) which are invariant under symmetry transformations of the $U(1)$ symmetry and diffeomorphism transformations. This has the advantage that at any time we can be sure that the quantities we compute are physical and not influenced by specific gauge choices. We explain this approach in detail in appendix C. The gauge invariant combinations, $\Phi_{1,2}$, in terms of the original perturbations are given by

$$\Phi_1(\omega,r) = \delta g_t^x(\omega,r) + \frac{i\omega}{\alpha}\delta\xi_x(\omega,r)\,, \quad \Phi_2(\omega,r) = \delta A_x(\omega,r) \tag{5.55}$$

where $\Phi(t,r) = \int \mathrm{d}\omega e^{-i\omega t}\Phi(r)$. Note that Φ_2 now represents the relevant Maxwell field fluctuation. Our set of fluctuations can then by described as $\{\Phi_1,\ \Phi_2,\ \delta g_r^x,\ \delta\xi_x\}$, however all of the physical information is now encoded in the dynamics of the two gauge invariant combinations $\Phi_{1,2}$. Their equations of motion decouple from the ones for the other two and read

$$
\begin{aligned}
0 =&\Phi_1'' + \left(\frac{4}{r} + \frac{g'}{g} + \frac{\alpha^2 h^2 g' + \omega^2 g h'}{\omega^2 g^2 h - \alpha^2 g h^2}\right)\Phi_1' + \frac{L^2 e^{\phi} A_t'}{r^2 g}\Phi_2' + \frac{L^4\left(\omega^2 g - \alpha^2 h\right)}{r^4 g h^2}\Phi_1 \\
&+ \left(\frac{2L^4\alpha^2 A_t\left|\chi\right|^2}{r^4 g h} + \frac{L^2\omega^2 e^{\phi} A_t'\left(-g'h + gh'\right)}{r^2 g h\left(\omega^2 g - \alpha^2 h\right)}\right)\Phi_2\,, \qquad (5.56)\\
0 =&\Phi_2'' + \frac{\alpha^2 g A_t'}{-\omega^2 g + \alpha^2 h}\Phi_1' + \left(\frac{2}{r} - \frac{g'}{g} + \frac{h'}{h} + \phi'\right)\Phi_2' \\
&+ \left(\frac{L^4\omega^4}{r^4 h^2} - \frac{2L^2 e^{-\phi}\left|\chi\right|^2}{r^2 h} - \frac{L^2\omega^2 e^{\phi} A_t'^2 g}{r^2 h\left(\omega^2 g - \alpha\, h\right)}\right)\Phi_2\,.
\end{aligned}
$$

The equations for δg_r^x and $\delta\xi_x$ are given in the appendix (C.28). This implies that in order to compute the conductivity we only need to solve (5.56). We can now apply the procedure of 3.3.1.

First, we first impose the ingoing boundary conditions at the horizon

$$
\Phi_i(\omega, r) = \left(r - r_{\mathrm{h}}\right)^{-\frac{i\omega}{4\pi T}}\left(c^{\mathrm{h}}_{\Phi i,0} + \mathcal{O}\left(r - r_{\mathrm{h}}\right)\right)\,. \qquad (5.57)
$$

Then, in order to obtain the on-shell action as in (3.37) we investigate the behaviour of $\Phi_{1,2}$ at the asymptotically AdS boundary at $r \to \infty$

$$
\begin{aligned}
\Phi_1(\omega, r) &= c^{\mathrm{b}}_{\Phi 1,0}(\omega) + \tilde{c}^{\mathrm{b}}_{\Phi 1,1}(\omega) r^{-2} + \tilde{c}^{\mathrm{b}}_{\Phi 2,2}(\omega) r^{-2} + c^{\mathrm{b}}_{\Phi 1,3}(\omega) r^{-3} + \mathcal{O}\left(r^{-4}\right) \qquad (5.58)\\
\Phi_2(\omega, r) &= c^{\mathrm{b}}_{\Phi 2,0}(\omega) + c^{\mathrm{b}}_{\Phi 2,1}(\omega) r^{-1} + \mathcal{O}\left(r^{-2}\right)
\end{aligned}
$$

where $\tilde{c}^{\mathrm{b}}$ are functions of the c^{b}'s, the independent boundary coefficients.

Using the groundwork presented in the appendix, in particular equation (C.29), we find that the on-shell action is given by

$$
S^{\mathrm{os}}/V_2 = \int \mathrm{d}\omega\left[-\frac{3\alpha^2 c_{\Phi 1,0} c_{\Phi 1,3}}{2L^4\left(\alpha^2 - \omega^2\right)} + \frac{c_{\Phi 2,0} c_{\Phi 2,1}}{2L^2} + \text{contact terms}\right]\,, \qquad (5.59)
$$

where the contact terms represent further terms proportional to the product of different boundary values of all perturbations $\Phi_{1,2}$, $\delta\xi_x$ and δg_{xr}. They would appear as a constant shift and thereby not contributing to the pole structure of the retarded Green's function. From a physical perspective, because those terms do not contain a subleading or normalisable term which corresponds to the sourced operator of the boundary field theory, they do not represent any dynamical information about the response of the field theory to external perturbations.

The comparison with equation (3.37) reveals $c = 1/2L^2$ and tells us that the electrical conductivtiy of the system dual to the gravity model with action (5.6) is given by

$$\sigma(\omega) = \left. \frac{c_{\Phi 2,1}(\omega)}{i\omega L^2 c_{\Phi 2,0}(\omega)} \right|_{c^{\mathrm{b}}_{\Phi 1,0}=0}, \tag{5.60}$$

where the condition that $c^{\mathrm{b}}_{\Phi 1,0} = 0$ makes sure we do not source a heat current dual to Φ_1. Sourcing Φ_1 alters the subleading term $c_{\Phi 2,1}$ in a way, that it can no longer be traced back to an external electrical field $c_{\Phi 2,0}$ only. A detailed elaboration on this holographic operator mixing is presented in [78]. On a technical level the condition $c^{\mathrm{b}}_{\Phi_1,0} = 0$ can be obtained by tuning the ratio of free parameters of the near horizon expansions $c^{\mathrm{h}}_{\Phi_1,0}/c^{\mathrm{h}}_{\Phi_2,0}$ to an appropriate value.

We numerically solve the equations of motion (5.56) and compute the optical conductivity for different scales of momentum dissipation and different temperatures. We find that the imaginary part shows a $1/i\omega$-peak, and hence the real part has a delta pole at zero frequency $\mathrm{Re}(\sigma) \sim \delta(\omega)$. This proves that the new ground state identified in the previous subsection, indeed is a superconducting state, see figure 5.2. Moreover, increasing the temperature towards the critical temperature has the effect, that the real part of the conductivity more and more resembles the Drude-like behaviour of the normal phase.

5.5 Fermionic correlators

In the previous chapter 4 we found a remarkably good agreement between a holographic and a real high-temperature superconductor in the context of a (holographic) photoemission experiment. More precisely, we investigated the pole structure of a probe fermion's spectral density in the superconducting state of the simplest holographic superconductor model 4.2. Comparing the so-called pair-breaking term Γ, which has the interpretation as the inverse lifetime of a generalised version of Cooper pairsn, revealed a agreement on a quantitative level between the holographic results and the results of [32]. Part of the motivation to study this more complicated superconductor was to investigate whether this

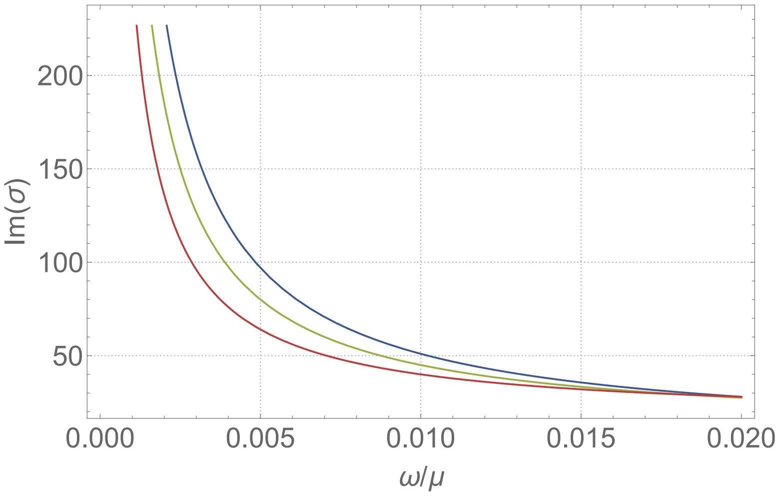

Figure 5.2: Imaginary part of the conductivity $\mathrm{Im}(\sigma)$ in the superconducting phase at three different temperatures $T/\mu = 0.0033, 0.007, 0.0014$ (top to bottom). We fix $e = 2$ and $\bar{\alpha} = 0.35$ and thus $T_c/\mu = 0.023$.

accordance is restricted to the simpler but also less realistic model based on the AdS-RN setup or whether the similarity is a more general feature of holographic superconductors. The Einstein-Maxwell-dilaton superconductor is of particular interest since its normal conducting state behaves similar to real strange metals in many ways.

We work with exactly the same setup for probe fermion as in chapter 4. For convenience we repeat the corresponding action (4.4)

$$S_{\text{fermion}} = \int \mathrm{d}x^4 \sqrt{-g} \Big[i\,\overline{\psi}\,(\Gamma^\mu D_\mu - m_f)\,\psi \\ + \left(\eta_5^* \chi^* \psi^T C \Gamma^5 \psi \,+\, \eta_5 \chi \overline{\psi} C \Gamma^5 \overline{\psi}^T \right) \Big] . \tag{5.61}$$

The discussion of section 4.3 is independent of the background and in order to apply the ansatz to the present holographic model, we simply use the solutions for the metric $g_{\mu\nu}$, Maxwell field A_t and charged scalar χ constructed in 5.4, which alters the horizon expansion of the Green's function matrix $\mathcal{G}$, albeit not to leading order, see (B.9)-(B.12).

In the context of this chapter we do not aim for a quantitative comparison of the holographic and experiment results. The issue is that the IR scaling of the spectral density can be computed analytically for the AdS RN strange metal which allowed us to fix the model parameters in such a way that this scaling matches the experimentally observed marginal Fermi liquid behaviour. This is not the case

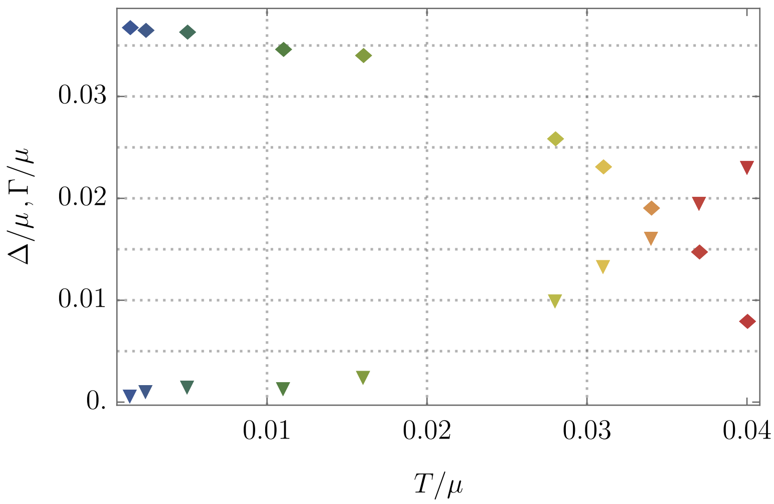

Figure 5.3: The figure shows a representative data set for the gap Δ (♦) and pair-breaking term Γ (▼). We use $\eta_5 = 0.125$ and $e = 2$, $\bar{\alpha} = 0.16$ with $T_c/\mu = 0.041$.

for the holographic strange metal including the dilaton 5.1. Instead, we show the effect of the coupling η_5 between the charged scalar and the probe fermion and the momentum dissipation scale α on the a qualitative level.

First of all, we note that the qualitative picture shown in figure 5.3 of the gap $\Delta(T)$ and the pair-breaking term $\Gamma(T)$ as a function of temperature is similar to the result in the right panel of figure 4.9 in the previous chapter.

Moreover, we observe the same effect of the coupling η_5 on the increase rate of the pair-breaking term as compared to the results for the AdS-RN superconductor, compare the right panels of figures 4.9 and 5.3. Again, increasing η_5 results in a flattened growth of Γ. To obtain the data shown in figure 5.3 we rescaled the temperature and pair-breaking term as described in equation (4.45) and fitted the data as in (4.47), choosing $T_{\max} = T_c$. Figure 5.4(a) shows $\Gamma(T)$ for three different values of $\bar{\alpha}$ which are chosen such that they roughly exhaust the allowed range. Similarly to the effect of η_5, increasing $\bar{\alpha}$ leads to a smaller value of the exponent of the fitted curve.

We can regard this result as a proof of principle, that the experimentally observed temperature dependence of the pair-breaking term for high-temperature superconductors can also be described in the context of the holographic model (5.6) investigated in this chapter. This suggests that this behaviour could be a more general feature of holographic superconductors. In combination with the experimental observation that this behaviour also seems to be a more general feature of

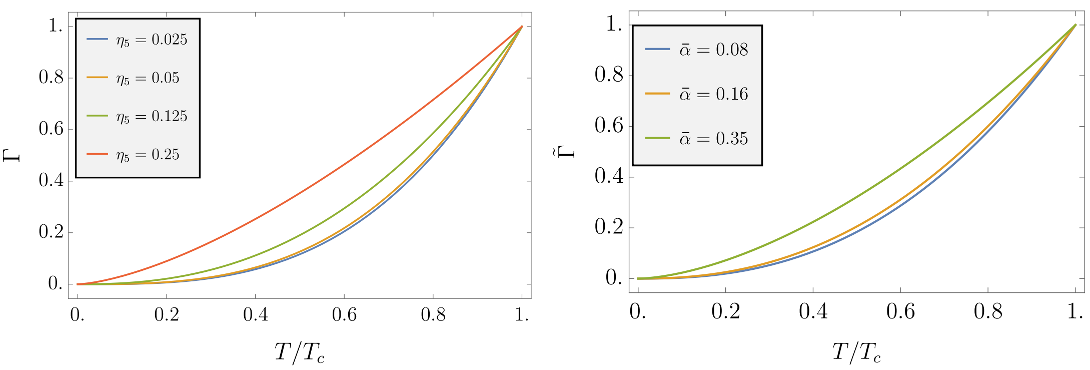

(a) $e = 2$, $\bar{m} = 0.16$ (b) $e = 2$, $\eta_5 = 0.125$

Figure 5.4: Fitted (4.45) and rescaled (4.47) pair-breaking term $\tilde{\Gamma}(T)$ for different values of the coupling η_5 (left) and for the momentum dissipation scale $\bar{\alpha}$ (right). To rescale and fit the data we use $T_{\text{max}} = T_c$, where T_c is the respective value of the critical temperature given in (5.40).

real high-temperature superconductors [32], our results furnish the idea that they are intrinsically related to their holographic counterparts.

5.6 Summary and outlook

In this chapter we studied a model of a holographic superconductor whose normal state is characterised by the linear increase of the DC resistivity at small temperatures and a Drude like behaviour of the electrical conductivity, as observed for real strange metals. This is in contrast to the AdS-RN model investigated in the previous chapter, where $\sigma_{\text{DC}} \sim \delta(\omega)$ in the normal state as well. The origin of the linear scaling of ρ_{DC} and the resolution of the δ-peak into a Drude peak is the implementation of a mechanism breaking translational invariance. The mechanism we chose here, is to include $d - 1 = 2$ neutral massless scalar fields ξ_i explicitly breaking translational invariance of the gravity theory's ground state while leaving it isotropic and homogeneous.

We first established the holographic model including a dilaton field (5.6) and then reviewed its most important features in the normal or metallic state where the charged scalar field is identically zero $\chi \equiv 0$. In particular we repeated the analysis of [34] showing the entropy density scales linearly in temperature as well and vanishes for $T = 0$ (5.23).

Based on this holographic strange metal we added a charged scalar field minimally coupled to the $U(1)$ gauge field and gravity. In section 5.4 we showed that the scalar becomes unstable at a critical temperature T_c which triggers a phase transition to a new ground state, with $\chi \neq 0$ and which is thermodynamically preferred to the $\chi \equiv 0$ state. The value of critical temperature depends on the two external parameters, the scalar charge e and the scale of momentum relaxation $\bar{\alpha}$. The behaviour of T_c upon changing those parameters, agrees with the results of [35,36] in the overlapping parameter regimes, where holographic superconductors with the same mechanism of breaking translational invariance but based on the AdS-RN metal. Studying the electrical conductivity confirmed that the new ground state has a δ-peak at $\omega = 0$ and hence is a superconducting state.

Aside from the interest in the properties of a holographic superconductor whose normal phase resembles real strange metallic phases, the main reason for our analysis was to investigate the fermionic spectral density in exactly the same way as in the previous chapter 4. More precisely, our goal was to see whether the remarkable agreement between the temperature dependence of the pair-breaking term $\Gamma(T)$ in holography and experimentally studied high-temperature superconductors, holds up for a more realistic model as well. In the previous chapter though, due to the simple AdS-RN metallic state, we were able to engineer the charge of the probe fermion such that the IR scaling of the fermionic spectral density resembles the marginal Fermi liquid behaviour of strange metals. We could not realise this for the dilaton model of this chapter and therefore restricted our analysis to a qualitative level, investigating the effect of the momentum dissipation scale $\bar{\alpha}$ and the coupling η_5 between probe fermion and charged scalar χ. We find that the overall qualitative behaviour of the energy gap $\Delta(T)$ and the pair-breaking term $\Gamma(T)$ is the same as for the AdS-RN superconductor and also changing the parameter η_5 still has the same effect. As for the momentum dissipation scale $\bar{\alpha}$ we find that the it leads to an analogous change of $\Gamma(T)$ as η_5. Increasing $\bar{\alpha}$ flattens the profile of the pair-breaking term's temperature dependence. To summarise, we can regard this as an indication that a quantitative matching with the experimental data is possible with the holographic superconductor model including the dilaton field as well. This requires a way of fixing the fermion parameters to achieve marginal Fermi liquid behaviour in the normal state which is an interesting subject for further research.

Based on the results of the previous and the present chapter, it is tempting to speculate that the behaviour of $\Gamma(T)$ in [32] is generic for holographic superconductors. However, in order to make such a claim more classes of holographic superconductors would have to be studied.

As for the holographic superconductor itself a direction for future research is to investigate *Homes' relation*, which is an empirical law stating a universal relation between the superconducting charge density ϱ_s at zero temperature and the DC conductivity σ_{DC} at the critical temperature

$$\varrho_s(T=0) = c\,\sigma_{\mathrm{DC}}(T_c)\,T_c\,, \tag{5.62}$$

where in the case of high-temperature superconductors the constant is experimentally found to be $c \approx 4.4$. Recall that it is the universal behaviours of whole classes of strongly coupled systems which are predestined to be investigated from a holographic perspective. An example of a holographic study of Homes' relation is presented in [123]. It would be interesting to see whether this relation is realised in our model.

Chapter 6

Quantum information in far from equilibrium systems

6.1 Introduction and summary

The subject of the previous two chapters were systems in thermal equilibrium, slightly perturbed by external sources. Studying the correlators of the sourced operators, allowed us to gather information about the transport properties and the 'electronic structure' of the field theory duals. As advertised in the introduction, the applications of the gauge/gravity duality are impressively diverse. We now turn to a different application, or rather we pose a different set of questions about the quantum field theory. In this chapter we are interested in away from equilibrium situations and instead of local correlators we study the long-range quantum entanglement.

Gauge/gravity duality has the useful property that there is no conceptual problem to study strongly systems far away from equilibrium, albeit in practise, solving Einstein's equations for a time dependent setup can be a challenge. The crucial difference to for example the lattice method is that the duality allows us to work with real instead of Euclidean time. Investigating strongly coupled out of equilibrium systems is thus a popular field of research [21–24], see [124–126] for reviews. More specifically, there is a great interest in *quantum quenches*, which in the context of holography are classified as 'global' when the entire gravity dual evolves from an initial non-equilibrium configuration and as 'local' in the case of a sudden change at a specificed locus in spacetime. Important results on holographic global quenches are given in references [127–135] and on local quenches in [136–145].

In this thesis we are interested in a situation similar to a local quench in many ways. More specifically we investigate the time evolution of an initial configuration given by two semi-infinite heat baths at two different temperatures T_L and T_R. At time $t = 0$ they are connected at $x = 0$, such that the initial temperature profile is given by

$$T(t = 0, x) = T_\mathrm{L}\theta(-x) + T_\mathrm{R}\theta(x)\,. \tag{6.1}$$

From then on the two heat baths are allowed to interact resulting in a heat current $\langle J_E \rangle$, which transports energy from the hotter reservoir to the colder one in an attempt to thermally equilibrate the system. However, as the two heat baths are assumed be at a constant temperature, the system never reaches thermal equilibrium. The rate of the energy transport is constant in time, while the region over which the current extends is growing. Eventually, at late times, the steady heat current conquers the whole space. The setup is illustrated in figure 6.1. It is

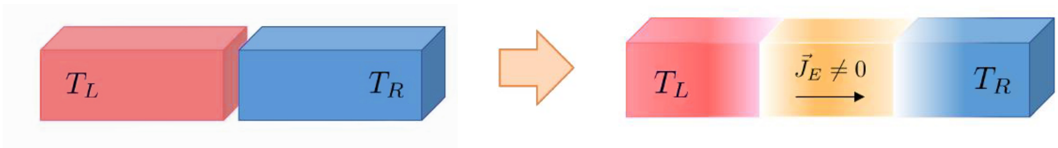

Figure 6.1: The initially seperated heat baths, equilibrated at temperatures T_L and T_R are connected and a heat current J_E emerges. Figure taken from [1].

straight forward to construct the holographic dual of the initial state, knowing that a finite temperature of the boundary field theory is dual to a black hole geometry in the bulk, see 2.3.4. The bulk setup equivalent to the initial temperature profile (6.1) is thus given by cutting two black hole geometries with Bekenstein-Hawking temperatures T_L and T_R at $x = 0$ and gluing together one part of each. Of course, such a spacetime is not a solution to general relativity, just like the field theory setup is not a thermodynamic equilibrium state. Einstein's equations then dictate the time evolution of the geometry and hence allow to draw conclusions on the field theory dual.

We focus on the case of $d = 2$, i.e. we are interested one-dimensional heat baths with a gravity dual in three spacetime dimensions. Three-dimensional gravity is special in the sense that it is not-dynamical and at every point in spacetime the geometry can be transformed to locally look like the vacuum, in our case AdS_3. Due to this special property our holographic model has an exact analytical solution describing the time evolution of the setup's gravity dual [37]. As we discuss in the next section, this solution is characterised by two infinitely sharp 'shockwaves' moving at the speed of light away from the connection point at $x = 0$. In between the two wavefronts a region characterised by a steady heat current emerges, to which we refer as 'steady state regime'.

Previous work on this setup is presented in [38–40], where the authors showed that the asymptotic steady state can be described by a thermal distribution at a shifted temperature. This result can be regarded as the holographic dual to the finding that the steady state region on the boundary is dual to a boosted black hole geometry in the bulk [37] at temperature $\sqrt{T_\mathrm{L} T_\mathrm{R}}$.

An interesting tool to study the quantum properties of this far away from equilibrium system is entanglement entropy. Entanglement entropy can be regarded as a measure of long range quantum entanglement and as such is generally hard to compute in particular in strongly coupled systems. Utilising the holographic prescription which unsurprisingly translates the problem to a geometrical problem, we investigate the time evolution of the entanglement entropy in this setup.

The next section 6.2 provides a brief introduction to holographic entanglement entropy. In section 6.3 we establish the initial state and time evolution of the holographic setup dual to the specific system we are interested in (figure 6.1). Section 6.4 presents the analytic approach to compute the entanglement entropy and the analytically obtained results. The numerical methods and the numerically obtained results are explained in section 6.5. We summarise our work presented in this chapter in section 6.6 and give an outlook on possible future research.

The author of this thesis contributed to the development and implementation of the numerical methods used to study the time evolution of the entanglement entropy. Moreover she developed the basis for the analytical approach.

6.2 Holographic entanglement entropy

Entanglement entropy is a relatively simple measure of quantum entanglement, a fundamental property of any quantum system. In contrast to the correlators we focused on in the previous two chapters, it is a non-local quantity. More precisely, it is a measure of the entanglement or quantum correlation of a subsystem A and its complement A_c. It is defined as the *von Neumann entropy* of the reduced density matrix $\rho_A = \mathrm{Tr}_{A_c}[\rho]$ of A

$$S_A = -\mathrm{Tr}_A[\rho_A \log \rho_A] \,. \tag{6.2}$$

The reduced density matrix can be thought of as a density matrix, where the degrees of freedom of A_c are made unreadable for an observer in the subsystem A. In this picture, the von Neumann entropy or entanglement entropy is the entropy of A taking this restriction into account. Note that this logic is similar to the logic leading to the Bekenstein-Hawking entropy (2.33) of black holes.

Recall that the AdS/CFT correspondence is a duality between a quantum field theory and a classical gravity theory, in particular, properties of the former are given a geometric interpretation. Somehow the information contained in the boundary field theory must be encoded in the higher dimensional bulk. The first concrete prescription was given in references [29, 30] by Ryu and Takayanagi. The idea is essentially to simulate a horizon in the bulk hiding the information contained in A_c [146]. This imaginary horizon is constructed as a co-dimension one hypersurface in a time slice of the bulk, anchored at the boundary $\partial A_c = \partial A$ of the region A_c. According to the prescription the entanglement entropy is, inspired by the Bekenstein-Hawking entropy, given by the area of the *minimal surface* divided by $4G_N$

$$S_A = \frac{\mathrm{Area}\,(\gamma_A)}{4G_N}\,, \tag{6.3}$$

where Newton's constant G_N is understood to be evaluated for the number of bulk dimensions $d+1$. The hypersurface Σ with minimal area is characterised a vanishing variation of the area functional

$$S = \int_{\gamma_A} \mathrm{d}^{d-1}y\,\sqrt{\gamma}\,. \tag{6.4}$$

y are the coordinates of Σ and γ is the induced metric on that surface. If there is more than one extremum the one with the minimal surface is chosen to be γ_A. The conjectured equality between the quantum field theory entanglement entropy and (6.3) was proven in [31]. The original RT prescription is restricted to static systems. The covariant generalisation, the *HRT prescription* was given in [63]. In this case, the equal time co-dimension one hypersurface γ_A in the bulk and region A at the boundary are generalised to be a spacelike hypersurface and region, respectively.

In the case of a two dimensional boundary, the boundary regions are one-dimensional and so are the co-dimension one hypersurfaces. Thus one is really looking for a geodesic whose endpoints at the boundary are located at the endpoints of the interval. In a general background with metric g, geodesics obey the equation

$$0 = \frac{d^2 x^\mu}{\mathrm{d}s^2} + \Gamma^\mu_{\nu\lambda} \frac{\mathrm{d}x^\nu}{\mathrm{d}s} \frac{\mathrm{d}x^\lambda}{\mathrm{d}s} \,. \tag{6.5}$$

This form of the geodesic equation implies that s is the so-called affine parameter, which is characterised by attributing a unit tangent vector $|x'|^2 = 1$ to the geodesic and by $\det(\gamma) = 1$. According to equation (6.4) this implies that s really is the length of the geodesic. The geodesic equations do not have an analytic solution in general. However, for the BTZ black hole geometry we are interested in this chapter, they do, see for example equations (3.25)-(3.27) in [147]. The resulting entanglement entropy is

$$S_{\mathrm{BTZ}} = \frac{L}{4G_{\mathrm{N}}} \log \left[\frac{1}{\pi^2 \epsilon^2 T^2} \left(\cosh(2\pi T \Delta x) - \cosh(2\pi T \Delta t) \right)^2 \right] \,, \tag{6.6}$$

where the integration was stopped at a cutoff surface at $r = 1/\epsilon$, as the expression is a priori divergent. Once again one has to employ a holographic renormalisation procedure to obtain a finite expression. A common renormalisation scheme in the context of holographic entanglement entropy is the minimal subtraction scheme, where only the divergent part of (6.6) is removed

$$S^{\mathrm{ren}}_{\mathrm{BTZ}} = S_{\mathrm{BTZ}} - \frac{2L}{4G} \log \epsilon \,. \tag{6.7}$$

The equal time limit $\Delta t = 0$ is given in (6.25) and its renormalised version, obtained with the minimal subtraction scheme, in equation (6.26).

Later in this chapter 6.5.3 we will be interested in the situation of several intervals. As an instructive example, let us briefly discuss the case of $n = 2$ intervals. Attempting to compute the entanglement entropy of the union $A \cup B$ of two non-adjacent intervals A and B and its complement $(A \cup B)_c$, one has to find the appropriate configuration for the minimal bulk surface attached to those intervals. There are, in principle, three different ways of connecting the four endpoints with two geodesics. They are illustrated in figure 6.2. The entanglement entropy is given by the option which leads to the minimal area [148–150]

$$S(A \cup B) = \min \left\{ S(A) + S(B), S(AB_1) + S(AB_2) \right\} \,. \tag{6.8}$$

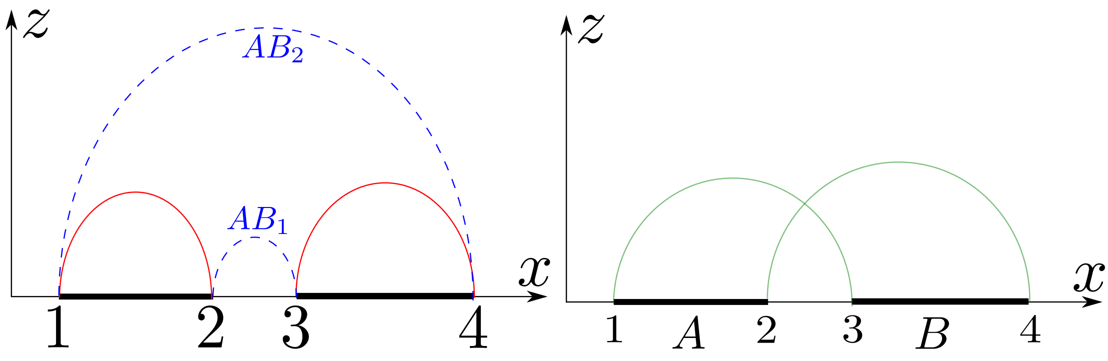

Figure 6.2: There are two physical ways to construct the minimal surface as the holographic dual of the entanglement entropy $S(A \cup B)$ for two intervals (left). The third possible option for connecting the endpoints of the intervals is unphysical (right). Figure taken from [1].

The third option, shown on the right in figure 6.2 can be shown to never yield the smallest surface and is therefore ignored in (6.8) and described as unphysical. Depending on the specific configuration of the two intervals A and B, AB_1 or AB_2 yields the the correct value for the holographic entanglement entropy. The result has to obey two entanglement inequalities: the *subadditivity* and the *triangle* or *Araki-Lieb inequality*

$$S(A \cup B) \leq S(A) + S(B)\,, \quad \text{and} \quad S(A \cup B) \geq |S(A) - S(B)|\,. \tag{6.9}$$

It is straight forward to prove that they indeed hold in holography as well [151].

6.3 Holographic thermal steady state

6.3.1 Setup and initial geometry

The idea of this chapter is to study the time evolution of a system which at $t = 0$ is set up as two semi-infinite heat baths at temperatures T_{L} and T_{R} spread over $x < 0$ and $x > 0$, respectively, which then are allowed to interact. Such a situation can in principle be studied at arbitrary dimensions d with a $(d-2)$-dimensional contact area. In this chapter we discuss the special case of a $d = 2$ dimensional boundary spacetime, where the contact area consequently is zero-dimensional.

We established in subsection 2.3.4 that a field theory at finite temperature is dual to a black hole geometry. Black holes in three dimensional AdS space are referred to as BTZ black holes [152, 153]. They appear as a solution of

$$S = \frac{1}{2\kappa^2} \int \mathrm{d}^3 x \sqrt{-g} \left(R + \frac{2}{L^2} \right) \tag{6.10}$$

and are described by the AdS-Schwarzschild metric (2.37). For the three dimensional case it is given by

$$\mathrm{d}s^2 = \frac{r^2}{L^2} \left(-f(r)\mathrm{d}t^2 + \mathrm{d}x^2 \right) + \frac{L^2}{r^2 f(r)} \mathrm{d}r^2 \quad \text{with} \quad f(r) = 1 - \left(\frac{r_\mathrm{h}}{r} \right)^2 , \tag{6.11}$$

and the associated temperature by $T = r_\mathrm{h}/2\pi$. Connecting two semi-infinite heat baths is then dual to the following geometry

$$\mathrm{d}s^2 = \begin{cases} \mathrm{d}s^2_{T_\mathrm{L}} & \text{for } x < 0 \, , \\ \mathrm{d}s^2_{T_\mathrm{R}} & \text{for } x > 0 \, , \end{cases} \qquad \text{at} \quad t = 0 \, . \tag{6.12}$$

In the next step, we discuss the time evolution of this geometry.

6.3.2 Time evolution of the geometry

Bringing two heat baths at different temperatures into contact clearly is not an equilibrium situation and a current transporting heat from the hotter to the colder region will emerge immediately. What does this process look like from the perspective of the dual bulk geometry? This question is best addressed in Fefferman-Graham coordinates where the dynamical solution to this problem for any temperature profile is given by [37, 154]

$$\mathrm{d}s^2 = \frac{\tilde{r}^2}{L^2} \tilde{g}_{\mu\nu}(\tilde{t}, \tilde{x}, \tilde{r}) + \frac{L^2}{\tilde{r}^2} \mathrm{d}\tilde{r}^2 \, . \tag{6.13}$$

The metric components are

$$\tilde{g}_{tt} = - \left[1 - \frac{L^2}{\tilde{r}^2} \left(f_\mathrm{R} + f_\mathrm{L} \right) \right]^2 + \left[\frac{L^2}{\tilde{r}^2} \left(f_\mathrm{R} - f_\mathrm{L} \right) \right]^2 , \tag{6.14}$$

$$\tilde{g}_{tx} = -2 \frac{L^2}{\tilde{r}^2} \left(f_\mathrm{R} - f_\mathrm{L} \right) , \tag{6.15}$$

$$\tilde{g}_{xx} = \left[1 + \frac{L^2}{\tilde{r}^2} \left(f_\mathrm{R} + f_\mathrm{L} \right) \right]^2 - \left[\frac{L^2}{\tilde{r}^2} \left(f_\mathrm{R} - f_\mathrm{L} \right) \right]^2 , \tag{6.16}$$

in terms of left moving $f_{\rm L}(x+t)$ and right-moving $f_{\rm R}(x-t)$ wavefunctions. Their explicit form is determined by the initial condition that there is no heat current $\langle T^{tx}\rangle = 0$ at the time $t=0$. The one point function of the boundary stress energy tensor for the above metric with equations (2.30) and (2.32) are given by

$$\left\langle T^{tt}\right\rangle = \langle T^{xx}\rangle = \frac{c}{6\pi^2 L^2}\left(f_{\rm R}+f_{\rm L}\right) , \qquad \left\langle T^{tx}\right\rangle = \frac{c}{6\pi L^2}\left(f_{\rm R}-f_{\rm L}\right) , \tag{6.17}$$

where c is the central charge of the dual CFT. The initial condition thus demands that $f_{\rm L}(v) = f_{\rm R}(v)$ at $t=0$, were their arguments both reduce to $v=x$. Plugging this into the metric (6.14)-(6.14), taking the initial temperature profile (6.1) into account and comparing it with the AdS-Schwarzschild metric in Fefferman-Graham coordinates, one finds

$$f_{\rm L,R}(v) = \frac{\pi^2 L^2}{2}\left(T_{\rm L}^2 + \left(T_{\rm R}^2 - T_{\rm L}^2\right)\theta(v)\right) , \tag{6.18}$$

in terms of the step function θ. As time evolves, a growing region $t > x > -t$ with a non-vanishing and constant heat current $\langle T^{tx}\rangle$ emerges. The infinitely sharp wavefronts with which this region supersedes the two heat baths move at the speed of light. For higher dimensions $d > 2$ the nature of those shockwaves is quite different. We briefly discuss this at the end of this chapter. In section 6.5 we work with two different methods, of which one requires a smooth geometry, which can be realised by

$$f_{\rm L,R}(v) = \frac{\pi^2 L^2}{4}\left(\left(T_{\rm L}^2 + T_{\rm R}^2\right) + \left(T_{\rm R}^2 - T_{\rm L}^2\right)\tanh(\alpha v)\right) . \tag{6.19}$$

In the limit $\alpha \to \infty$ this solution reduces to the discontinuous version (6.18).

Going back the Schwarzschild coordinates, the metric describing the steady state region takes the form of a boosted black hole

$$\begin{aligned} \mathrm{d}s^2_{\rm boost} = &\frac{r^2}{L^2}\left[-f(r)\left(\cosh\theta\,\mathrm{d}t - \sinh\theta\,\mathrm{d}x\right)^2 + \left(\cosh\theta\,\mathrm{d}x - \sinh\theta\,\mathrm{d}t\right)^2\right] \\ &+ \frac{L^2}{r^2 f(r)}\mathrm{d}r^2 , \end{aligned} \tag{6.20}$$

at the effective temperature T given by

$$T = \sqrt{T_L T_R} , \quad \chi = \frac{T_L}{T_R} , \quad \beta = \frac{\chi - 1}{\chi + 1} , \quad \beta = \operatorname{arctanh}\beta . \tag{6.21}$$

In this notation the full geometry can be expressed as

$$\mathrm{d}s^2 = \begin{cases} \mathrm{d}s^2_{T_\mathrm{L}} & \text{for } x < -t\,, \\ \mathrm{d}s^2_{\text{boost}} & \text{for } -t < x < t\,, \\ \mathrm{d}s^2_{T_\mathrm{R}} & \text{for } x > t\,. \end{cases} \tag{6.22}$$

The discontinuous geometry is a result of gluing together the three different spacetime regions along co-dimension one hypersurfaces. Those hypersurfaces are the bulk extension of the boundary shockwaves bounding the steady state region. The geometrically appropriate way to glue regions in general relativity is to study the Israel junction conditions [155]. When two hypersurfaces Σ_1 and Σ_2 are to be identified, they have to have the same topology and induced metric γ_{ij}. This is assured by the following equation for the stress-energy tensor S_{ij} defined on the hypersurface

$$\left(K^+_{ij} - \gamma_{ij}K^+\right) - \left(K^-_{ij} - \gamma_{ij}K^-\right) = -\kappa S_{ij}\,. \tag{6.23}$$

The extrinsic curvatures of the hypersurface are computed with the induced metrices of the left and the right side, respectively. For our setup those Israel junction conditions are satisfied and in particular, S_{ij} vanishes identically. It is worth pointing out the subtlety that in our case the glued spacetimes involve a black hole horizon appearing to be cut into three pieces. This is explained in detail in section 2 in [1] with the aid of a Kruskal diagram (see figure 2 therein). In short, the result of the discussion is that the shockwaves do not touch any of the 'three horizons' in a problematic way. Moreover in the coordinates we are using, the hypersurfaces are spacelike and from a bulk perspective thus seem to be superluminal. Recalling that general relativity in three dimensions is not dynamical, i.e. does not contain propagating degrees of freedom, it becomes clear, that in the bulk theory no information is transported in the traditional sense. This feature is essentially a manifestation of the fact that the BTZ black hole locally looks like empty AdS space everywhere.

6.4 Entanglement entropy: analytic approach

6.4.1 Essential analytic ingredients

In the context of this chapter we are interested in the entanglement entropy between equal time regions at the boundary, which are either completely contained in the $x < 0$ or the $x > 0$ region and their complements. The two endpoints of an interval of length ℓ are denoted by x_l and x_r with $\ell = |x_r - x_l|$. In this chapter we always work with the following boundary conditions

$$x_l^> > x_r^> > 0 \quad \text{or} \quad 0 > x_l^< > x_r^< \qquad \text{and} \qquad t_l^{>,<} = t_r^{>,<} = t^{>,<}\,. \tag{6.24}$$

As a consequence, the entanglement entropy of an interval ℓ and its complement at the initial time $t = 0$ is simply given by the AdS-Schwarzschild or BTZ expression

$$S_{\mathrm{BTZ}} = \frac{L}{4G_{\mathrm{N}}} \log\left[\frac{1}{\pi^2\epsilon^2 T_{\mathrm{L,R}}^2} \sinh^2\left(\pi\ell_{\mathrm{L,R}} T_{\mathrm{L,R}}\right)\right]\,, \tag{6.25}$$

for an interval located in the left (L) or right (R) heat bath, respectively. Renormalising the expression with the minimal subtraction scheme cancels the factor of ϵ^2

$$S_{\mathrm{BTZ}}^{\mathrm{ren}} = \frac{L}{4G_{\mathrm{N}}} \log\left[\frac{1}{\pi^2 T_{\mathrm{L,R}}^2} \sinh^2\left(\pi\ell_{\mathrm{L,R}} T_{\mathrm{L,R}}\right)\right]\,. \tag{6.26}$$

The steady state region, growing with time, eventually conquers the whole space at $t \to \infty$. Knowing that this region is appropriately described by a boosted black hole geometry, one can take the general expression for the entanglement entropy in the unboosted geometry (6.6) and engineer the value of the time difference Δt in such a way, that the boost leads to an equal time interval. This is the case for

$$\Delta t = \frac{T_{\mathrm{L}} - T_{\mathrm{R}}}{2\sqrt{T_{\mathrm{L}} T_{\mathrm{R}}}}\ell\,, \quad \Delta x \frac{T_{\mathrm{L}} + T_{\mathrm{R}}}{2\sqrt{T_{\mathrm{L}} T_{\mathrm{R}}}}\ell\,, \tag{6.27}$$

where ℓ is the length of the interval we actually interested in. Plugged into equation (6.6) this yields

$$S_{\mathrm{boost}}^{\mathrm{ren}} = \frac{L}{4G} \log\left[\frac{1}{\pi^2 T_{\mathrm{L}} T_{\mathrm{R}}} \sinh\left(\pi\ell T_{\mathrm{L}}\right) \sinh\left(\pi\ell T_{\mathrm{R}}\right)\right]\,. \tag{6.28}$$

Note that looking at two intervals A and B arranged symmetrically around $x = 0$, relations (6.26) and (6.28) imply

$$S_A(t = 0) + S_B(t = 0) = S_A(t \to \infty) + S_B(\to \infty)\,. \tag{6.29}$$

This relation may be referred to as some sort of conservation of entanglement entropy, albeit the sum depends nontrivially on time while the shockwaves move through the interval. The same relation was obtained in [156] for a slightly different setup. We discuss this in section 6.5.2. The time period during which the interval is traversed by the shockwave, $x_l^< < t < x_r^<$ or $x_l^> > t > x_r^>$, is the only time period where the entanglement entropy of that interval changes in time. Note that this precise limitation is of course only true for infinitely sharp shockwaves (6.18) and (6.22). The smoothened version (6.19) can only asymptotically be described by those static spacetime regions.

Moreover, given the initial (6.26) and final (6.28) value of the entanglement entropy of an interval A, the average entropy increase rate is bounded. The bound is fixed by the temperature difference, see section 5.4 in [1] for a detailed discussion. Note that (6.29) implies that while for one region the entanglement entropy increases in time, it decreases for the other. It increases for an interval originally located in the colder heat bath and decreases for an interval originally located in the warmer heat bath.

Let us finally address this time dependent regime. In $d + 1 = 3$ bulk dimensions many problems are solvable and we are given an analytic expression for the background. One might hope, that similarly to the gluing of spacetime regions it is also possible to create a piecewise defined geodesic and obtain an analytic expression for the time evolution of the entanglement entropy. It turns out, that this is not quite the case, but it is possible to hold on to the analytic approach for a bit longer. Recall that we are interested in intervals of the form (6.24). Those intervals will at most host two of the three regimes. Hence the geodesic connecting the endpoints through the bulk will at most pass through two of the three spacetimes (6.22) as well. One is always the ordinary BTZ spacetime (6.11) and the other its boosted analogue (6.20).

The idea is to connect a geodesic with one endpoint at the boundary located in one regime at $\{t_*, x_l^>\}$ to a geodesic in a different regime with endpoint $\{t_*, x_r^>\}$. For concreteness we restrict to intervals at $x > 0$. As before, we define $\ell = |x_r^> - x_l^>|$. The two geodesics are connected (c) on the hypersurface separating the two associated bulk spacetimes which is characterised by $x_c = t_c$. Note that neither of the geodesic is an equal time geodesic. It is only required that the two endpoints of the final composite geodesic reach the boundary at the same time t_*. The procedure is inspired by [157] and makes use of the peculiar properties of general relativity in three dimensions. In order to resort to results of [157], we switch to Fefferman-Graham coordinates $\tilde{x}^\mu$, which at the boundary are equal to the Schwarzschild coordinates[1]. The final expression for the renormalised length of the composite curve as a function of the connecting point $\tilde{x}_c^\mu$ is given by

$$\begin{aligned} d_{\mathrm{R}}(z_c, x_c) = &\log\left[\zeta_+^{\mathrm{RR}}\cosh\left(2\pi T_{\mathrm{R}}(x-\ell)\right) - \zeta_-^{\mathrm{RR}}\cosh\left(2\pi T_{\mathrm{R}}(t-x)\right)\right] \\ &+ \log\left[\zeta_+^{\mathrm{LR}}\cosh\left(\pi\left(T_{\mathrm{L}}-T_{\mathrm{R}}\right)t + 2\pi T_{\mathrm{R}}x\right)\right. \\ &\left. - \zeta_-^{\mathrm{LR}}\cosh\left(\pi\left(T_{\mathrm{L}}+T_{\mathrm{R}}\right)t - 2\pi T_{\mathrm{R}}x\right)\right] - \frac{1}{2}\log\left[16\pi^8 T_{\mathrm{L}}^2 T_{\mathrm{R}}^6 \tilde{z}_j^4\right], \end{aligned} \tag{6.30}$$

where the AdS radius is set to one, $L = 1$, and

$$\zeta_\pm^{\mathrm{XY}} = 1 \pm \pi^2 T_{\mathrm{X}} T_{\mathrm{Y}} \tilde{z}_c^2\,, \quad x = \tilde{x}_c - x_l \quad \text{and} \quad t = t_* - x_l^> \,. \tag{6.31}$$

The latter is the time that passed since the shockwave entered the boundary interval of interest. A similar expression d_{L} can be obtained for an interval located at $x < 0$. In order to turn this composite curve, consisting of two geodesics in two different spacetimes, into a geodesic in the composite spacetime, d has to be minimised with respect to the connecting point, i.e. $\{\tilde{x}_c, \tilde{z}_c\}$ or equivalently $\{x, \tilde{z}_c\}$

$$\partial_{\tilde{z}_c} d_{\mathrm{R}} = 0\,, \quad \partial_x d_{\mathrm{R}} = 0\,. \tag{6.32}$$

Those equations do not have analytical solutions and in order to study the entanglement entropy's time evolution in full generality one has to resort to numerical methods, see section 6.5. There are, however, two limits which allow an analytical advance. They are presented in the two following subsections. Note that the entanglement entropy is related to the length of the geodesic through $S = Ld/4G_{\mathrm{N}}$.

6.4.2 Universal behaviour

The first case in which we can proceed to solve equation (6.32) analytically, is realised when both temperatures are small. This can be implemented by introducing

[1]in addition to switching to Fefferman-Graham coordinates all of the analytic formulae related to equation (6.30) are written in terms of the an inverted radial coordinate $z = L/r$.

a small factor δ

$$T_{\mathrm{L,R}} \to \delta\, T_{\mathrm{L,R}}\,, \tag{6.33}$$

keeping the relative order of magnitude of the two temperatures as it is. The artificially introduced smallness is to be understood in relation to the inverse interval length. Expanding d_{R} and its 'left analogue' d_L in δ, one finds for the leading order

$$\partial_x d_{\mathrm{R}} \propto \partial_{\tilde{z}_c} d_{\mathrm{L}} \propto (\ell - t)\,(\ell + 2t - 4x)\,t - (l - 2t)\,\tilde{z}_c^2\,, \tag{6.34}$$

$$\partial_{\tilde{z}_c} d_{\mathrm{R}} \propto \partial_x d_{\mathrm{L}} \propto (\ell - t)\,(t - 2x)\,(\ell + t - 2x)\,t + \tilde{z}_c^4\,. \tag{6.35}$$

Those expressions are extremised by

$$x = t\,, \qquad \tilde{z}_c = \sqrt{(\ell - t)\,t}\,. \tag{6.36}$$

We define the normalised entanglement entropy f as a function of the normalised time ρ to be

$$f_A(\rho) = \frac{S_A(t) - S_A(t=0)}{S_A(t \to \infty) - S_A(t=0)} \quad \text{with} \quad \rho = t/\ell\,. \tag{6.37}$$

Note that ρ parametrises the time which passed between the arrival of the shockwave at the interval and the time at which the entanglement entropy is studied. It is bounded by $0 \le \rho \le 1$, where the maximal value is reached, when the shockwave leaves the interval. The simple solution of (6.36) leads to the following universal time evolution

$$f(\rho) = 3\rho^2 - 2\rho^3 + \mathcal{O}(\delta) \tag{6.38}$$

to lowest order in the expansion parameter δ. This behaviour is universal in the sense that it does not depend on the location or the length ℓ of the interval for which the entanglement entropy is computed. The limitations of the universality are dicussed in 6.5.2 by means of the numerical analysis. Interestingly, the above time evolution of f has proven to be a good approximation beyond the analytic validity of the expansion.

6.4.3 Zero temperature limit

The second analytically tractable limit is the one where one of the temperatures is zero, say $T_{\mathrm{R}} = 0$. In this case the geodesic length (6.30) is extremised by

$$x = \frac{\pi t T_{\mathrm{L}}(\ell - t)\coth(\pi t T_{\mathrm{L}}) + (\ell + t)}{2 + 2\pi T_{\mathrm{L}}(\ell - t)\coth(\pi t T_{\mathrm{L}})}, \quad z_c^2 = \frac{\ell(\ell - t}{1 + \pi T_{\mathrm{L}}(\ell - t)\coth(\pi t T_{\mathrm{R}})}. \tag{6.39}$$

For a high temperature of the left heat bath $T_{\mathrm{L}}\ell \gg 1$ the entanglement entropy of the interval A with length ℓ increases linearly in time

$$S_A = \frac{L}{4G_{\mathrm{N}}}\pi t T_{\mathrm{L}}\,. \tag{6.40}$$

It is tempting to discuss this result in the context of *entanglement tsunamis*, see e.g. [127, 131–133], which refers to the linear growth of the entanglement entropy after a global quench of a sufficiently large region and an initial quadratic growth [127–129,131–133,158]. Note however that our setup does not admit a quasiparticle picture.

6.5 Enganglement entropy: numerical approach

6.5.1 Two complementary methods

Let us now turn to the numerical analysis of the entanglement entropy's time evolution. To this end we employ two different methods, the 'shooting' and the 'matching method'[2]. The results in the regime where the two methods overlap agree.

The shooting method, as the name already suggests, is similar to the shooting method we described in the context of the holographic superconductor 5.2. The idea is to integrate the geodesic equation (6.5) in the smoothened version of the bulk geometry (6.19), starting from a specific locus in the bulk, in both directions to the two endpoints of the geodesics $x^\mu_{\mathrm{L}} = x^\mu(s \to -\infty)$ and $x^\mu_{\mathrm{R}} = x^\mu(s \to \infty)$ at the boundary, s is the affine parameter. The set of initial conditions is provided by $x^\mu(s_0)$ and $(x^\mu)'(s_0)$. We chose to start the integration at the geodesic's turning

[2]We attempted a third method, called the 'relaxation' method, which is based on approaching the solution by iteratively relaxing an initial guess, see e.g. [159]. It turned out, however, that this method is not very effective nor stable for the equations we needed to solve.

point $s_0 = 0$. However, at the start of the procedure their numerical values are unknown. Thus the solving procedure is the search for the correct set of numerical values for $x^\mu(s_0)$ and $(x^\mu)'(s_0)$, which result in the desired endpoints (6.24). On a technical level this is implemented with a 'find root' method which requires an acceptable initial guess. For similar temperatures $T_{\mathrm{L,R}}$, a reasonable choice is to take the analytically known values of $x^\mu(s_0)$ and $(x^\mu)'(s_0)$ for a geodesic in the simple AdS-Schwarzschild spacetime given in equations (3.25)-(3.27) in [147]. Those initial conditions used in the dynamical spacetime (6.19) do not result in a geodesic which satisfies the boundary conditions, but the endpoints will not be far off either. This works very reliably for small temperature differences $\Delta T \equiv (|T_{\mathrm{L}} - T_{\mathrm{R}}|)/(T_{\mathrm{L}} + T_{\mathrm{R}}) \sim 0.05$ and for a not too sharp transition between the three regions, i.e. $\alpha \leq 30$. Those requirements restrict the applicability of the the shooting method in this setup. For the shooting method we used the minimal substraction renormalisation scheme (6.7).

The second method, which we refer to as matching method is the numerical completion of the analytic approach in the previous section 6.4. Recall that the idea is to construct the geodesic ranging from one point at the boundary x^μ_{L}, located in one region to the other x^μ_{R}, located at a different but neighbouring region, as a piecewise defined trajectory. The expression for the resulting length of the trajectory as a function of the boundary conditions $x^\mu_{\mathrm{L,R}}$ and the point x^μ_c at which the two pieces meet is given in (6.30). This is the furthest we get analytically. From here it remains to minimise $d_{\mathrm{L,R}}$ with respect to the matching point to obtain the trajectory of minimal length, the actual geodesic. This requires to find a numerical solution of (6.32). Note that to derive this expression we used the minimal subtraction scheme as well. Briefly, this undertaking can be split into two steps. The first step is to find approximate solutions and check which of them result in a positive length. The approximate solutions passing this test are then refined using Newton's method. The final answer is given by the minimal positive geodesic length between the two endpoints $x^\mu_{\mathrm{L,R}}$. Note that solutions which correspond to a geodesic going beyond the horizon were shown to be unphysical, i.e. they do not result in a positive geodesic length. Furthermore the minimal distance $d_{\mathrm{L,R}}$ becomes complex valued for solutions which correspond to a null or timelike separation. The matching method is not constrained by restrictions similar to the ones of the shooting method. It can be employed for large temperature differences in relative and absolute values as well. It does however, rely on the assumption that the coordinates x^μ smoothly parametrise the border between the different

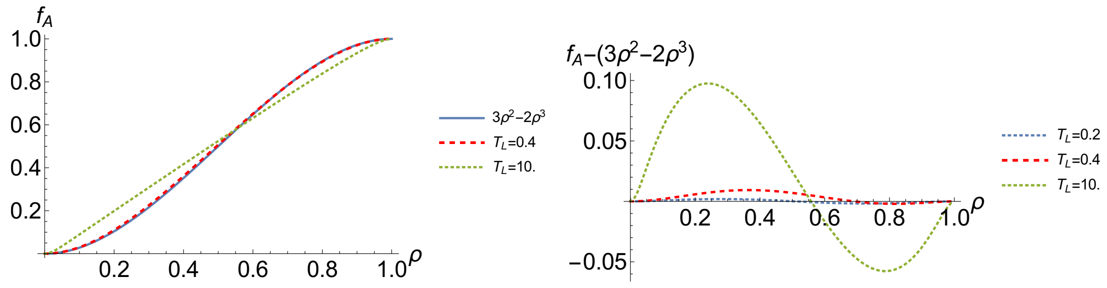

Figure 6.3: Normalised entanglement entropy f_A for the interval A in temperatures $T_L = 0.4$ and $T_L = 10$ compared to the universal formula (6.38) (left) and deviations from it for $T_L = 0.2,\ 0.4,\ 10.$ (right). The interval is chosen to $\Delta x_A \in [0.175, 1.35]$ and $T_\mathrm{R} = 1.95$. Figure taken from [1].

regions and that the metric components take care of possible discontinuities. The Mathematica code used for this method in a supplementary file together with [1].

In the parameter regimes where both methods are applicable, the results agree, providing a consistency check for each other. Note that the interval length is understood to be measured in units of the AdS radius L and the temperatures in units of its inverse L^{-1}. For the numerical analysis we set $L = G_\mathrm{N} = 1$.

6.5.2 Corrections to the universal behaviour

Let us first address the universal behaviour for small temperatures and temperature differences. In section 6.4 we presented an analytic formula for the universal time evolution of the normalised entanglement entropy $f_A(\rho)$ of a region A (6.38). The normalised time $0 \leq \rho \leq 1$ (6.37) parametrises the time interval during which the shock wave passes through the interval of interest. This formula is restricted to the limit of small temperatures $\ell T_{\mathrm{L,R}} < 1$ and temperature differences $\ell\,|T_\mathrm{L} - T_\mathrm{R}| < 1$. The universality refers to the fact that this expression is independent of the interval length ℓ and the location of the interval. The numerical analysis confirms this universal behaviour and in addition to it allows to go beyond the small temperature and temperature difference limit. Note that is was actually those numerical results which inspired the analytical treatment.

Figure 6.3 shows the deviation from the universal time evolution upon increasing the temperature of the left heat bath and thereby also increasing the difference between the two temperatures, as we set $T_\mathrm{R} = 1.95$. Moreover at $T_\mathrm{L} = 10$ the data hints at the linear time dependence of the normalised entanglement entropy (6.40). Recall that the latter was derived at $T_\mathrm{R} = 0$. This situation is mimicked

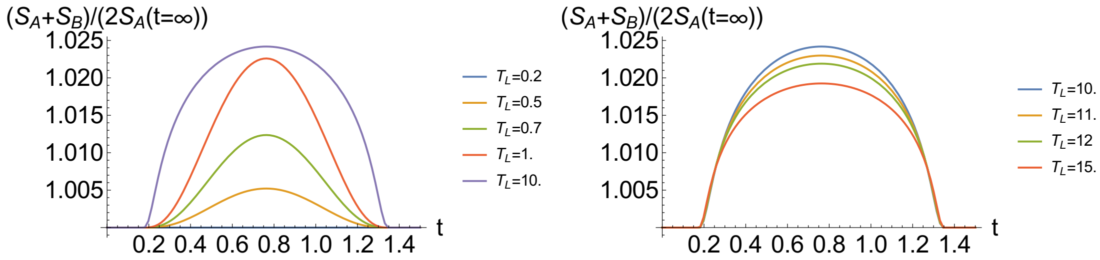

Figure 6.4: The normalised sum $S_A + S_B$ (6.42) as a function of boundary time. The deviation of the sum's initial and final value seems to be bounded. Figure taken from [1].

here by $T_{\rm L} \gg T_{\rm R}$.

Another way to quantify the deviations from the universal behaviour (6.38) is to look at the sum of the entanglement entropies of two intervals A and B. The two intervals are assumed to be of the same length ℓ and are arranged symmetrically around $x = 0$. If the time evolution were truly independent of also the location of the interval, the sum of S_A and S_B would have to be constant. This conclusion becomes clear by inverting the definition of the normalised entanglement entropy f (6.37)

$$S_A(\rho) = S_A(0) + [S_A(t \to \infty) - S_A(0)]\, f(\rho)\,, \tag{6.41}$$

where $S_A(t \to \infty) = S_A(\rho = 1)$ for any interval A, since S is constant as soon as the shockwave passed through the interval. Now we know from the analytical perspective that the sums of the entanglement entropies of two symmetric intervals A and B at $t = 0$ and $t \to \infty$ agree (6.29) and $S_A(t)+S_B(t) = \text{const}$ if $f_A = f_B = f$. The fact that this is not the case is illustrated in figure 6.4. Interestingly, the normalised sum

$$\frac{S_A(t) + S_B(t)}{2S_A(\infty)} \tag{6.42}$$

appears to be bounded from above by approximately 1.025.

6.5.3 Entanglement inequalities

Let us now turn to a very interesting usage of the matching method, explained in the beginning of this section. When it comes to the discussion of entanglement entropy, inequalities often play a role. They arise in the context of more than just one region A and its complement A_c. In 6.2 we already mentioned two examples in the case of two different regions: subadditivity and triangle or Araki-Lieb inequality. Three regions, A, B and C, already give rise to more complicated inequalities. Among those the *strong subadditivity* is one of the most prominent examples

$$S(AB) + S(BC) - S(ABC) - S(B) \geq 0\,, \tag{6.43}$$

where combinations of A, B and C indicate the union of the respective regions. Note that there is a second inequality which sometimes is also referred to strong subbadditivity. It is given in equation (6.10) in [1]. Another common example is the *monogamy of mutual information*, also referred to as *negativity of tripartite information*

$$\begin{aligned} I_3(A:B:C) \equiv\, & S(A) + S(B) + S(C) - S(AB) - S(BC) \\ & - S(AC) + S(ABC) \leq 0\,. \end{aligned} \tag{6.44}$$

Inequalities for the entanglement entropies of several regions are of particular interest from the perspective of holography. Given that they have to be obeyed from a quantum physics point of view, it is interesting to see whether they are obeyed in a holographic setup as well. It turned out that those inequalities are intricately related to the energy conditions in the bulk. Thus they promise to give further inside into both the details and the bigger picture of the holographic duality.

The matching method allows us to study inequalities in the context of the steady state setup whose peculiarity it is to provide a simple yet nontrivial time dependent framework. In this work we are interested in checking the strong subadditivity (6.43) and monogamy of mutual information (6.44) for $n = 3$ regions, the positivity of the four-partite information given in equation (6.18) in [1] for $n = 4$ regions as well as the negativity of the five partite function (6.19) and further inequalities given in equations (6.12)-(6.16) for $n = 5$ regions. This is the maximum number of regions studied in [1].

The first challenge for that purpose is to construct the holographic duals of the different unions of regions or intervals, as our setup only has one spatial dimension at the boundary. Figure 6.2 illustrates that even in the case of two intervals one has to think carefully about which of theoretically possible ways to connect the intervals' boundaries through bulk geodesics. The authors of [1] developed an algorithm which allows to enumerate all of the possible configurations taking physical considerations into account. It turns out that their number is given by the Catalan numbers. Furthermore, depending on which inequality one studies, some of the configurations are equivalent to others upon a relabelling of the intervals A, B, C, ... This topic is presented in detail in section 6.1 of [1].

Having established the possible configurations it remains to explicitly choose intervals and temperatures at which the inequalities mentioned above are to be studied. The idea is to choose a fixed number $N = 20$ of different locations at the boundary and subsequently construct up to $n = 5$ non-adjacent intervals ending on those points. In order to cover many orders of magnitude for the distances between the boundary points, they are positioned in a fractal way

$$x = 0,\, 1 - \frac{2}{\alpha},\, 1 - \frac{4}{\alpha^2},\, 1 - \frac{8}{\alpha^3},\, ...,\, 1 + \frac{8}{\alpha^3},\, 1 + \frac{4}{\alpha^2},\, 1 + \frac{2}{\alpha},\, 2\,. \tag{6.45}$$

The choice $T_{\mathrm{L}} = 9$ and $T_{\mathrm{R}} = 1$ gives representative results.

After studying several hundred thousands of different cases, we find that none of the studied inequalities for $n = 3$ intervals are violated for any of those, as expected based on [160,161]. The positivity of the four-partite function is violated for a number of examples, which was also the result of [162] and [163] in a static geometry. The same is true for the five-partite information. The inequalities of [164], where they were proven in the static case, given in (6.12)-(6.16) in [1] are satisfied for every single example that was studied.

6.6 Summary and Outlook

In this chapter we investigated a system far away from thermal equilibrium with holographic methods. The system is characterised by an emergent steady heat current between two initially separated heat reservoirs, see figure 6.1. In particular we studied the time dependence of the entanglement entropy which measures the information flow between the subsystems.

The choice to work with a $d = 2$ dimensional boundary theory provided us with an exact analytic solution for the time evolution of the dual bulk spacetime, which in turn allowed to partially employ analytical methods to study the entanglement entropy 6.4. We then took two different limits of the initial temperature configuration resulting in two manifestly distinct behaviours. The first is the limit, where both temperatures are small. In this case we find a ‘S’-shaped increase/decrease of the entanglement entropy of an interval initially located in the colder/warmer heat bath. To leading order this behaviour is universal, by which we mean that it does not depend on the length of the interval nor on its location. In the second limit we set one of the temperatures to zero, while the other is assumed to take large values in units of the inverse interval length. The entanglement entropy then changes linearly in time. This behaviour resembles the entanglement tsunami behaviour in systems experiencing a global quench, see e.g. [127, 131–133]. In analogy with this one could think of the 'S'-shape as an *entanglement tide*.

Outside those two limits, we resorted to numerics to complete the analytic approach 6.4. Firstly the numerical analysis confirms the two analytically obtained results and shows, that the entanglement tide characterises the time evolution of the entanglement entropy beyond the limits on the order of magnitude for which the analytical computation is valid, see figure 6.3. Furthermore we checked the validity of entanglement inequalities, in particular the inequalities for a large number of subsystems proven in [164] for the static case. Explicitly analysing them for up to five subsystems on our time-dependent system, we did not find any example where they are violated. However, our setup seems to violate the definiteness of four- and five-partite information. This is surprising in the context that as our system locally looks like the AdS_3 vacuum everywhere, it satisfies most common energy conditions. It would be interesting to explore this further to track the origin of the violations in our setup.

Another subject for further research is certainly the higher dimensional $d > 2$ generalisation of the system studied in this work. The system itself was already investigated in different contexts [37, 165–168]. A crucial difference is that in contrast to the two-dimensional case addressed in this thesis, the waves pushing back the heat baths are no longer sharp shockwaves. A natural generalisation would be to think of smoothened shock waves. However, reference [167] pointed out that due to the 'entropic condition' a shock-rarefaction wave solution is physically preferred over the double-shock solution. A rarefaction wave is much wider in space and it is a priori not clear whether it extends to the shockwave on the other side and thereby excluding a formation of a steady state. Reference [168] argued, based on numerical considerations, that this is not the case and a steady state region still emerges in the higher dimensional case. It would be interesting to see whether it is possible to obtain a shock-rarefaction solution with gauge/gravity duality.

Chapter 7

Conclusion

This thesis investigated two different classes of applications of gauge/gravity duality. One of them are holographic superconductors in their ground state or thermal equilibrium, probed by external perturbations like an electric current or a holographic version of a photoemission experiment. The other is a system far away from thermal equilibrium investigated through the properties of its entanglement structure during the system's evolution in time.

We motivated and reviewed the origin of the duality in chapter 2 and established the holographic dictionary. Chapter 3 provides a review of the methods and entries of the holographic dictionary used for applications of the duality to condensed matter systems, often referred to as AdS/CMT.

In chapter 4 we investigated a holographic superconductor by the means of a 'holographic photoemission experiment' which refers to studying the spectral density of probe fermions added to the superconductor model. Our goal was to compare our results with the results of a recent experiment about the temperature dependence of the gap Δ and pair-breaking term Γ of a high-temperature superconductor [32] on a quantitative level. We worked with the simplest model of a holographic superconductor, first proposed in [16]. The interaction of the probe fermions with the superconductor were chosen such that a gap forms in the spectral density as soon as the superconducting state is entered below the critical temperature [33]. Imposing a condition on the behaviour of the spectral density in the normal conducting state, allowed us to reduce the number of parameters to only two. We then investigated the effect of those two parameters, the coupling strength between fermion and superconducting condensate and a parameter regulating the critical temperature, on the temperature dependence of Δ and Γ. They manifest themselves as the imaginary and real part of a pole of the spectral density in the complex frequency plane, respectively. Given our holographic model, the gap vanishes unsurprisingly at the critical temperature, unlike the behaviour observed in the experiment. However, we find that the experimentally measured temperature dependence of the pair-breaking is effortlessly described by the holographic setup. Tuning the two parameters of our model appropriately, we were able to get a remarkably good accordance between our holographic results on $\Gamma(T)$ and the experimental ones on a quantitative level.

We presented our results on a new holographic model of a superconductor in chapter 5. The unique characteristic feature of our model is that its normal state is built on the basis of a model [34] which has proven to share two important properties with experimentally observed strange metals, the supposedly normal state of a high temperature superconductor. The first is that its resistivity increases linearly in temperature at small temperatures and the second is the appropriate scaling of the entropy density as zero temperature is approached. The former requires a holographic mechanism to break translational invariance to avoid momentum conservation in the dual field theory. This is implemented by an additional scalar field in the gravity setup, whose magnitude gives the scale of the momentum dissipation. We numerically show that there is a phase transition to superconductivity and investigate the effect of the momentum dissipation on the critical temperature, the temperature dependence of the superconducting condensate and the electrical conductivity. We then probe this holographic superconductor with external fermions with the same approach as in chapter 4 and show that the non-conservation of momentum does not qualitatively alter the results obtained with the simpler model of chapter 4. Thus this model generates a temperature evolution of the pair-breaking Γ, similar to what was experimentally observed, as well.

The results of chapter 4 and 5 join the ranks of similarities between 'holographic metals' and the ones studied in condensed matter laboratories. Showing the quantitative similarity of the fermionic spectral density of a superconductor is one of the major achievements of this thesis. It would certainly be interesting to actually fit the holographic results to experimental data and find the best fit parameters. It should be noted that the best accordance found in the context of this thesis is reached towards the boundaries of our numerical code. One therefore needs to choose a method other than the shooting method to generate the backgrounds close to zero temperature. At the same time, a different numerical method to investigate the pole structure of the spectral density function is required. Moreover, there is the possibility to add further coupling terms to the holographic model between the superconducting condensate and the probe fermions to improve the fit. Another important direction of further study is to better understand the origin of the coupling employed in this thesis from a top-down string theory perspective. This is important to answer the still unsettled question what the holographic duality, despite of all the remarkable similarities between AdS/CFT and real world physics, is capable of contributing to resolve real world physical puzzles.

In chapter 6 we studied the time evolution of two infinite heat baths, each of which equilibrated at different temperatures and brought into contact at initial time. This relatively simple setup facilitates a good theoretical handle on the system, while at the same time revealing non-trivial properties. Out of the contact area of the two heat baths, a steady heat current emerges and expands as time evolves. The regime of the steady state was shown to allow for a description as a thermal state at a shifted temperature both with field theoretical and holographic methods [37–40]. In this thesis we focused on the case of one-dimensional heat baths, i.e. they are defined in 1+1 dimensions with a holographically dual gravity theory in 2+1 dimensions. The eminently simple properties of gravity in three dimensions made it possible to approach the system analytically to a certain extend. After a brief review of the concept of holographic entanglement entropy, where the field theory entanglement entropy is established to be dual to the area of a minimal surface in the bulk, we apply this technique to the 'steady state setup'. We find that the entanglement entropy exhibits two distinct behaviours depending on the absolute magnitude and the relative size of the two temperatures. In the case where both temperatures are small, the entanglement entropy increases/decreases in a universal 'S'-shaped way for entangling regions located in the initial colder/warmer heat bath. In contrast, in the case where one temperature is manifestly smaller than the other, the 'S' shape flattens and asymptotes to a linear increase/decrease. As the latter resembles the behaviour of so-called entanglement tsunamis, we named the former 'entanglement tide'. Furthermore, we numerically checked entanglement inequalities for three, four and five entangling regions. The inequalities, proposed by [164] in the case of five regions, are to be understood as generalisations of the well known inequalities for two intervals like the subadditivity. This is particularly interesting for our time-dependent setup. While some of the addressed inequalities are clearly violated, others are not.

One very interesting subject for further study is the generalisation to a higher dimensional setup. While the holographic dual of the asymptotic state is the same, a boosted black hole geometry, the details of the system's evolution to this final state are different. Most notably, the wavefronts with which the steady state regime expands, are no longer sharp but diffuse as time proceeds. It would be worthwhile to find out whether the two limits of the entanglement entropy's time evolution are a universal feature of the system irrespective of the number of dimensions. In order to approach this question, one has to rely on numerical methods to solve Einstein's equations in higher dimensions, as an exact solution is not available for $d > 3$, which is a technically challenging problem.

Acknowledgements

I would like to express my gratitude to my supervisor Johanna Erdmenger for her continuous support, reassurance and advice and for the opportunity to be part of her research group. I am indebted to Dieter Lüst for providing the inspiring environment at the Max-Planck-Institut für Physik and for being the second referee of this thesis. I am grateful to my colleagues and everyone I worked with in the past years for many interesting discussions and the chance to learn from them. I would like to thank my friends and my family for their support, without which this thesis would not have been possible.

Ich möchte mich außerdem ganz herzlich bei den beiden großartigen Omas und vor allem dem wundervollen Papa von Oskar für ihre tatkräftige Unterstützung bedanken. Lieber Max, danke für Deinen vorbehaltlosen Rückhalt in den vergangenen Jahren.

Appendix A

Einstein relation

In this appendix we present a method to incorporate the Einstein relation [76] to the holographic picture. It relates the electrical conductivity to the charge diffusion constant, similarly to the relation between shear viscosity and the momentum diffusion constant [169]. It allows to express the DC conductivity entirely in terms of equilibrium quantities. Note that although we use them in the context of this appendix, we do not introduce the ideas and methods of the hydrodynamic gradient expansion and fluid/gravity duality in detail. See [170, 171] for pedagogical reviews. Note that in this appendix we refer to the DC conductivity as the finite part, ignoring the δ-peak contribution at zero frequency in absence of momentum dissipation.

A.1 Einstein relation for a conformal fluid

The theory of hydrodynamics is an effective theory to describe long wavelength fluctuations around thermal equilibrium. Starting from equilibrium expressions for the stress-energy tensor and charge current as functions of quantities such as temperature T, pressure p and chemical potential μ, one explicitly gives them a space-time dependence and expands the stress energy tensor and charge current in the gradients of those quantities. By using conservation equations one can then solve iteratively for those gradients. Whilst the zeroth order describes an ideal fluid, higher orders include dissipative effects.

The first order of the hydrodynamic expansion of the charge current J^μ for an ordinary charged fluid can be written in two different ways, in terms of the charge diffusion constant D or the DC conductivity $\sigma \equiv \sigma_{\mathrm{DC}}$. Unlike the optical conductivity, the charge diffusion constant is a natural quantity to appear in a hydrodynamic consideration. The Einstein relation is based on the conversion of those two expressions into each other and is given by [76]

$$\sigma = D\chi. \tag{A.1}$$

χ is the charge susceptibility that thermodynamically is derived from the charge density $\varrho(\mu, T)$ as a function of the chemical potential μ and the temperature T by

$$\chi = \left(\frac{\partial \varrho}{\partial \mu}\right)_T , \tag{A.2}$$

where $(x)_T$ tells us to take the derivative, keeping the temperature fixed. In this section we derive an expression for the charge susceptibility for a conformal fluid in d dimensions with the help the the Einstein relation (A.1). The two versions of the hydrodynamic expansion of the charge current to first order are given by

$$\mathcal{J}^{\mu}_{(1)} = \varrho u^{\mu} - DP^{\mu\nu}\partial_{\nu}\varrho + \tilde{\gamma}P^{\mu\nu}\partial_{\nu}\varepsilon \, , \tag{A.3}$$

$$J^{\mu}_{(2)} = \varrho u^{\mu} - \sigma T P^{\mu\nu}\partial_{\nu}\left(\frac{\mu}{T}\right) + \gamma P^{\mu\nu}\partial_{\nu}T \, , \tag{A.4}$$

where the projector $P_{\mu}\nu = \eta_{\mu\nu} + u_{\mu}u_{\nu}$ projects on the space perpendicular to the fluid velocity u^{μ}, normalised as $u^{\mu}u_{\mu} = -1$. The contributions $\tilde{\gamma}$ and γ represent the contribution of the energy density to the charge current and vanish in the case of a conformal fluid. Moreover for conformal fluids the charge current $\mathcal{J}^{\mu}$ has to transform homogeneously

$$\mathcal{J}^{\mu} \to e^{-d\phi}\tilde{\mathcal{J}}^{\mu} \tag{A.5}$$

under a Weyl transformation $g_{\mu\nu} \to e^{2\phi}\tilde{g}_{\mu\nu}$ in d spacetime dimensions and hence it has to be built from Weyl-covariant terms only. It is therefore convenient to introduce the Weyl-covariant derivative $\mathcal{D}_{\mu}$ that for a scalar φ with weight w, i.e. $\varphi \to e^{-w\phi}\tilde{\varphi}$ is given by

$$\mathcal{D}_{\mu}\varphi = \nabla_{\mu}\varphi + w\varphi\left(u^{\nu}\nabla_{\nu}u_{\mu} - \frac{1}{d-1}u_{\mu}\nabla_{\nu}u^{\nu}\right) . \tag{A.6}$$

Note that $u^\mu \to e^{-\phi}\tilde{u}^\mu$. In flat spacetime $\mathcal{J}^\mu_{(1)}$ is then given by

$$\mathcal{J}^\mu_{(1)} = \varrho u^\mu - D_R P^{\mu\nu}\mathcal{D}_\nu\varrho = \varrho u^\mu - D_R P^{\mu\nu}\left[\partial_\nu\varrho + (d-1)\varrho u^\lambda\partial_\lambda u_\nu\right] , \tag{A.7}$$

as the charge density ϱ has the weight $w_\varrho = d-1$. Realising that μ/T has weight $w=0$, because $\mu \to e^{-\phi}\tilde{\mu}$ and $T \to e^{-\phi}\tilde{T}$, it is clear that (A.4) already has the desired form.

The next step is to convert $\mathcal{J}^\mu_{(2)}$ into $\mathcal{J}^\mu_{(1)}$ which essentially requires to exchange the two variables μ and T for ϱ and u^μ. A convenient method is to employ the conservation equation for the stress energy tensor $\partial_\mu T^{\mu\nu} = 0$ in the direction transversal to u^μ

$$P^\mu_\lambda\partial_\nu T^{\nu\lambda} = P^{\mu\nu}\partial_\nu p + d\,p P^{\mu\nu}u^\lambda\partial_\lambda u_\nu = P^{\mu\nu}\partial_\nu\varepsilon + d\,\varepsilon\, P^{\mu\nu}u^\lambda\partial_\lambda u_\nu = 0\,. \tag{A.8}$$

with the stress-energy tensor of an ordinary fluid $T^{\mu\nu} = \varepsilon u^\mu u^\nu + pP^{\mu\nu}$ in terms of the energy density ε and the pressure $p = \varepsilon/(d-1)$ for conformal fluids. As the energy density has weight $w_\varepsilon = d$, i.e. $\varepsilon \to e^{-d\phi}\tilde{\varepsilon}$, a combination of ε and ϱ with weight zero is given by $\varepsilon^{d-1}/\varrho^d$ and we have

$$\begin{aligned}\partial_\nu\left(\frac{\varepsilon^{d-1}}{\varrho^d}\right) &= \left(\frac{\varepsilon^{d-2}}{\varrho^{d+1}}\right)\left[(d-1)\varrho\partial_\nu\varepsilon - d\,\varepsilon\,\partial_\nu\varrho\right] \\ &= \left(\frac{\varepsilon^{d-2}}{\varrho^{d+1}}\right)\left[(d-1)\varrho\left(\frac{\partial\varepsilon}{\partial\mu}\right)_T - d\varepsilon\left(\frac{\partial\varrho}{\partial\mu}\right)_T\right]T\partial_\nu\left(\frac{\mu}{T}\right)\,.\end{aligned} \tag{A.9}$$

Using the projected conservation equation (A.8) one obtains

$$TP^{\mu\nu}\partial_\nu\left(\frac{\mu}{T}\right) = \left[\left(\frac{\partial\varrho}{\partial\mu}\right)_T + \frac{(d-1)\varrho}{d\varepsilon}\left(\frac{\partial\varepsilon}{\partial\mu}\right)_T\right]^{-1} P^{\mu\nu}\mathcal{D}_\nu\varrho. \tag{A.10}$$

The Einstein relation (A.1) we find that the appropriate definition of the charge susceptibility in the case of a conformal fluid is given by

$$\chi_{\mathrm{CFT}} = \left(\frac{\partial\varrho}{\partial\mu}\right)_T + \frac{(d-1)\varrho}{d\varepsilon}\left(\frac{\partial\varepsilon}{\partial\mu}\right)_T . \tag{A.11}$$

A.2 Einstein relation in AdS/CFT

We are now ready to set up the Einstein relation for holographic fluids, which are conformal by construction. The simples holographic model qualified for this taks is the AdS-RN setup introduced in section 3.2. At the same time this choice allows us to resort to existing results in reference [172]. The idea is to compute the charge susceptibility χ_{CFT} in thermodynamic equilibrium and the charge diffusion constant D via the holographic version of the hydrodynamic expansion, known as fluid/gravity correspondence. Assuming the Einstein relation (A.1) to hold we can then derive an expression for the DC conductivity σ in d dimensions.

It is useful to extend our pool of thermodynamic variables, so far consisting of the chemical potential $\mu \equiv q r_{\mathrm{h}}$ (3.19), the charge density ϱ (3.20), the temperature T (3.21) and the entropy density s (3.22), by the energy density ε and the pressure p

$$\varepsilon = (d-1)p = \frac{M(d-1)}{2\kappa^2}\,, \tag{A.12}$$

in terms of the black hole mass M given by

$$M = 1 + \frac{\mu^2}{r_{\mathrm{h}}^2\gamma^2}\,. \tag{A.13}$$

The charge diffusion constant D obtained via the fluid/gravity duality is given in equation (1.4) f. in [173]. Converted to our conventions and notation it is

$$D_R = \frac{2+(d-2)M}{(d-2)dMr_{\mathrm{h}}}\,. \tag{A.14}$$

The last step is to find a way to compute the thermodynamic derivatives in equation (A.11). The naive approach, which is to find explicit expressions for $\varrho(\mu,T)$ and $\varepsilon(\mu,T)$, fails because it is not possible to analytically solve for $r_{\mathrm{h}}(\mu,T)$ in arbitrary dimensions. One way to avoid this is to find the condition on δr_h such that $\delta T = 0$, i.e. $\delta T = \#_1\delta q + \#_2\delta r_{\mathrm{h}} = 0$, use it to calculate $\delta\mu = \#_3\delta q$ and conclusively find $\delta\varepsilon\big|_T = \#_4\delta\mu$ and $\delta\rho\big|_T = \#_5\delta\mu$. This leads to the following charge susceptibility

$$\chi_{CFT} = \left(\frac{sT}{\varepsilon+p}\right)^2 r_{\mathrm{h}}^{d-3}D^{-1}\,, \tag{A.15}$$

in terms of the diffusion constant D. Thus the prediction of the Einstein relation

(A.1) for the DC conductivity σ is

$$\sigma = \frac{(sT)^2}{(\varepsilon + p)^2} r_{\mathrm{h}}^{d-3} \,. \tag{A.16}$$

It remains to compare this prediction with results obtained from a holographic linear response calculation as explained in section 3.3 We are not aware of any such calculation in arbitrary dimensions $d > 2$. However, for $d = 3$ the prediction (A.16) agrees with the result derived in [174] in equation (8) in the limit of zero magnetic field and zero frequency. For $d = 4$ we computed σ in an expansion in small κ, which as we argued in the context of (3.41) parametrises the backreaction of the Maxwell field onto the geometry.

$$\sigma_{d=4} = r_{\mathrm{h}} \left(1 - \frac{2\mu^2\kappa^2}{r_{\mathrm{h}}^2} + \mathcal{O}\left(\kappa^4\right) \right) \,, \tag{A.17}$$

which to this order also agrees with the prediction of the Einstein relation (A.16).

Appendix B

Fermionic operators in holography

B.1 Boundary terms for fermions

When including fermionic fields to holographic models one is almost immediately confronted with a puzzle. In the first two chapters of this thesis we built up the intuition of the correspondence of quantum field theory operators and fields of the dual gravity theory. Bulk scalar fields remain boundary scalar operators (2.30), and bulk vector fields remain boundary vector operators (2.32), where the radial component of the vector is usually taken care off by the choosing the radial gauge. Moreover, the boundary conditions of those bulk fields determine the source of the dual field theory operator. As mentioned in 3.5, in contrast to those bosonic fields, the number of components of a spinor doubles upon increasing the dimension it lives in by one. In particular, it seems that imposing boundary conditions for all components of the bulk spinor somehow is dual to imposing twice as many boundary conditions on the boundary spinor compared to its number of components. It is therefore clear, that the field operator map for fermionic fields has to be carefully adjusted. To resolve this puzzle it is instructive to split up the bulk fermion field ψ into

$$\psi = \psi_+ + \psi_- \,, \quad \psi_\pm = \Gamma_\pm \psi \,, \quad \Gamma_\pm = \frac{1}{2}\left(1 \pm \Gamma^r\right) \,, \tag{B.1}$$

which implies

$$\Gamma^r = \Gamma_+ - \Gamma_- \,, \quad \Gamma_r \psi_\pm = \pm \psi_\pm \,. \tag{B.2}$$

Similarly to (2.25) we would like to find an expression for the on-shell action to explicitly see the relation between the fermion operators of the boundary theory and the fermionic fields in the bulk. The variation of the on-shell action is given by

$$\delta S_{\text{bulk}} = -\int \mathrm{d}^d x \sqrt{-g}\sqrt{g^{rr}}\,\bar{\psi}\Gamma^r \delta\psi \,+\, \text{DE for } \bar{\psi} \,+\, \text{DE for } \psi\,, \tag{B.3}$$

where 'DE' stands for Dirac equation. The terms proportional to the Dirac equation of course vanish when the action is evaluated on-shell. Expressing (B.3) in terms of $\psi_\pm$ the variation reduces to

$$S^{\text{os}}_{\text{bulk}} = -\int \mathrm{d}^d x \sqrt{-g}\sqrt{g^{rr}}\,\left[\bar{\psi}_-\delta\psi_+ - \bar{\psi}_+\delta\psi_-\right]\,. \tag{B.4}$$

This suggests that one can choose boundary conditions for both $\psi_\pm$ at the boundary. But just like in the case of bosonic fields, fermionic fields have to obey ingoing boundary conditions. As the Dirac equation is only a first order differential equation, imposing a condition at the horizon and the AdS boundary would completely fix the solution. This problem can be cured by adding a suitable boundary term

$$S_{\text{bdy}} = -\int \mathrm{d}^d x \sqrt{-g}\sqrt{g^{rr}}\,\bar{\psi}_+\psi_-\,, \tag{B.5}$$

which gives rise to the following total variation of the fermionic on-shell action

$$S^{\text{os}} = S^{\text{os}}_{\text{bulk}} + S_{\text{bdy}} = -\int \mathrm{d}^d x \sqrt{-g}\sqrt{g^{rr}}\,\left(\bar{\psi}_-\delta\psi_+ + \delta\bar{\psi}_+\psi_-\right)\,. \tag{B.6}$$

We now see that we really can only impose boundary conditions on just half of the components of the bulk spinor ψ. This is also intuitively compatible with the fact that the boundary spinor operator $\mathcal{O}$ only has half as many components as ψ. The conjugate momentum of ψ_+ is given by

$$\Pi_+ = \frac{\delta S^{\text{os}}}{\delta\psi_+} = -\sqrt{g}\sqrt{g^{rr}}\bar{\chi}_-\,, \quad \bar{\Pi}_+ = \frac{\delta S^{\text{os}}}{\delta\bar{\psi}_+} = -\sqrt{g}\sqrt{g^{rr}}\chi_-\,. \tag{B.7}$$

We can thus identify χ_+ with the source and χ_- with the fermionic operator $\mathcal{O}$ of the dual field theory.

B.2 Horizon expansion of $\mathcal{G}$

We now give more details about the horizon expansion of the Green's function matrix $\mathcal{G}$, governed by the equations of motion (4.23) in chapter 4. $\mathcal{G}$ obeys the equations of motion (4.23) and thus close to the horizon behaves as follows

$$\mathcal{G} = \mathcal{G}_0^{\mathrm{h}} + \begin{pmatrix} \left(\mathcal{G}_1^{\mathrm{h}}\right)_{1,1} & \left(\mathcal{G}_1^{\mathrm{h}}\right)_{1,2} \\ \left(\mathcal{G}_1^{\mathrm{h}}\right)_{2,1} & \left(\mathcal{G}_1^{\mathrm{h}}\right)_{2,2} \end{pmatrix} (r - r_{\mathrm{h}})^{1/2} + \mathcal{O}\left((r - r_{\mathrm{h}})^{3/2}\right) . \tag{B.8}$$

The leading term $\mathcal{G}_0$ is given in (4.31), satisfying the ingoing boundary conditions. The coefficients for the next to leading order are given by

$$\left(\mathcal{G}_1^{\mathrm{h}}\right)_{1,1} = \frac{4\sqrt{c_{h,1}^{\mathrm{h}}}\left(k - i\sqrt{c_{g,0}^{\mathrm{h}}} L m_f r_{\mathrm{h}}\right)}{\sqrt{c_{g,0}^{\mathrm{h}}}\left(c_{h,1}^{\mathrm{h}} - 4i\omega\right)} , \tag{B.9}$$

$$\left(\mathcal{G}_1^{\mathrm{h}}\right)_{1,2} = \frac{8iL\eta_5 r_{\mathrm{h}}\sqrt{c_{h,1}^{\mathrm{h}}}c_{\chi,0}^{\mathrm{h}}}{c_{h,1}^{\mathrm{h}} - 4i\omega} , \tag{B.10}$$

$$\left(\mathcal{G}_1^{\mathrm{h}}\right)_{2,1} = -\frac{8iL\eta_5^* r_{\mathrm{h}}\sqrt{c_{h,1}^{\mathrm{h}}}c_{\chi,0}^{\mathrm{h}}}{c_{h,1}^{\mathrm{h}} - 4i\omega} , \tag{B.11}$$

$$\left(\mathcal{G}_1^{\mathrm{h}}\right)_{2,2} = -\frac{4\sqrt{c_{h,1}^{\mathrm{h}}}\left(k + i\sqrt{c_{g,0}^{\mathrm{h}}} L m_f r_{\mathrm{h}}\right)}{\sqrt{c_{g,0}^{\mathrm{h}}}\left(c_{h,1}^{\mathrm{h}} - 4i\omega\right)} . \tag{B.12}$$

To this order the analogous horizon expansion of the Green's function matrix $\mathcal{G}$ in the Einstein-Maxwell-dilaton background of chapter 5 is the same.

Appendix C

Gauge invariant fluctuations

C.1 Gauge invariant transport coefficients

C.1.1 Gauge transformations acting on fluctuations

In AdS/CFT the background solution represents the field theory ground state. Perturbing this ground state gives access to its transport properties. As presented in section 3.3, one adds a spacetime dependent fluctuating contribution to each of the background fields. This also includes components of the background fields that are zero in the ground state. As these perturbations are understood to be small, the resulting correction of the action is only taken into account to second order in fluctuations and hence to first order in the equations of motion. In order to obtain information about the physical properties, the analysis of the fluctuations has to be done in terms of gauge invariant modes by which we mean gauge invariant combinations of the introduced perturbations. The prescription of how to obtain these gauge invariant modes can be outlined in full generality. In this review of the methodology we focus on the types of background fields which appear in this thesis: the metric g, a Maxwell field A and both a charged χ and and non-charged scalar ϕ. They all experience a non-zero change under a transformation of at least one of the two gauge symmetries, diffeomorphism invariance and the $U(1)$ gauge symmetry.

Let us start by writing down the effect of infinitesimal gauge transformation on those fields. The effect of a diffeomorphism symmetry transformation $x_\mu \to x_\mu - \Sigma_\mu$

on the fields can be expressed as Lie derivatives along Σ

$$\delta_\Sigma g_{\mu\nu} = \mathcal{L}_\Sigma g_{\mu\nu} = \nabla_\mu \Sigma_\nu + \nabla_\nu \Sigma_\mu \,, \tag{C.1}$$

$$\delta_\Sigma A_\mu = \mathcal{L}_\Sigma A_\mu = \Sigma^\nu \nabla_\nu A_\mu + A_\mu \nabla_\nu \Sigma^\nu \,, \tag{C.2}$$

$$\delta_\Sigma \chi = \mathcal{L}_\Sigma \chi = \Sigma^\nu \nabla_\nu \chi \,, \quad \delta_\Sigma \phi = \mathcal{L}_\Sigma \phi = \Sigma^\nu \nabla_\nu \phi \,. \tag{C.3}$$

The gauge transformation of the $U(1)$ Maxwell symmetry only affects the Maxwell field itself and the charged scalar fields. The infinitesimal version is given by

$$\delta_\Lambda A_\mu = \nabla_\mu \Lambda \,, \quad \delta\chi_e = -ie\Lambda \,, \tag{C.4}$$

where $\delta\chi_e$ represents any scalar field with charge e under the $U(1)$ gauge symmetry.

The background parts of the fields g, A, χ and ϕ representing the ground state of the field theory are fixed. The gauge transformations are thus understood to affect the perturbations of the ground state only while leaving the ground state itself unchanged. For each component of the fluctuations, we can now compute the individual effect of the transformations on them. Let us arrange each individual component of all perturbations δg, δA, $\delta\chi_e$ and $\delta\phi$ in a vector φ schematically transforming as

$$\varphi \;\to\; \varphi + (\delta_\Sigma + \delta_\Lambda)\,\varphi \,, \tag{C.5}$$

It is important to stress, that since we assume both the perturbations and the gauge transformations to be small, we consider the transformed φ only up to first order in perturbations or gauge transformations Σ and Λ, i.e. δ_Σ and δ_Λ are computed from the background fields only.

C.1.2 Construction of gauge invariant combinations

We are then interested in constructing linear combinations of the elements of φ that are invariant under the gauge transformations. The number of gauge invariant combinations is the number of the dynamical degrees of freedom of the problem. We start with a general ansatz

$$\Phi = \sum_i c_i \varphi_i \,, \tag{C.6}$$

and apply the gauge transformations on it

$$\Phi \;\rightarrow\; \Phi + \left(\delta_\Sigma + \delta_\Lambda\right)\Phi\,. \tag{C.7}$$

The equation we have to solve is thus given by

$$\left(\delta_\Sigma + \delta_\Lambda\right)\Phi = 0\,. \tag{C.8}$$

Φ is the weighted sum of all fluctuations. The transformations $\delta_{\Sigma,\Lambda}$ are different for each of those, depending on what component of which field they are. Eventually we want to know what linear combination, i.e. what values for the c_i yield the gauge invariant modes, and thus spell out (C.8) and set the prefactors of all appearances of $\delta_{\Sigma,\Lambda}$ to zero. Solving these equations allows us to express one part of the constants c_i in terms of the other part of constants. We call the latter the independent coefficients $\tilde{c}_i$. The choice of the set $\tilde{c}_i$ is not unique, their total number N_{indep} however is equal to the number of propagating degrees of freedom. The final step in constructing the gauge invariant modes is then to build N_{indep} linear combinations with the coefficients $\tilde{c}_i$ and plug them into the ansatz (C.6).

Let us work through an explicit example, the Einstein-Maxwell dilaton model 5.6 we discussed in chapter 5. As argued in section 5.4 therein, only individual groups among all fluctuations couple and hence the gauge invariant modes, the propagating degrees of freedom can only be formed within those groups. Being interested in the eletrical conductivity along the x-direction we focus on the group which contains δA_x. The ansatz for the gauge invariant combination in this group is

$$\Phi = c_1 \delta g_{tx} + c_2 \delta g_{xr} + c_3 \delta A_x + c_4 \delta \xi_x\,. \tag{C.9}$$

We work in Fourier space and expand the fluctuations and the gauge transformation functions Σ and Λ in Fourier modes as

$$\varphi_i = \int \mathrm{d}\omega e^{-i\omega t}\varphi_{i,\omega}\,,\;\; \Sigma = \int \mathrm{d}\omega e^{-i\omega t}\Sigma_\omega\,,\;\; \Lambda = \int \mathrm{d}\omega e^{-i\omega t}\Lambda_\omega\,, \tag{C.10}$$

for $\underline{k} = 0$. Applying an infinitesimal gauge transformation on Φ, we get a correction of the following form

$$\begin{aligned}\Phi \to \Phi + \delta\Phi =& c_1\left(\delta g_{tx} - i\omega\Sigma_x\right) + c_2\left(\delta g_{xr} - \Sigma_x\left(\frac{2}{r} + \frac{g'}{g}\right) + \Sigma_x'\right) + c_3\delta A_x \\ &+ c_4\left(\delta\xi_x + \frac{L^2 m\Sigma_x}{r^2 g}\right) .\end{aligned} \tag{C.11}$$

We see that δA_x does not transform under a gauge transformation and hence already is a gauge invariant mode.

In order to solve the equation (C.8), we note that the infinitesimal gauge transformations are arbitrary and hence we treat their derivatives as independent. Had we included all the fluctuations we would have found that the dependent part of the constants c_i expressed in terms of the independent ones $\tilde{c}_i$ do not mix those groups. We find

$$c_1 = \tilde{c}_1\,, \quad c_2 = 0\,, \quad c_3 = \tilde{c}_3\,, \quad c_4 = \frac{i\omega r^2 g}{m\,L^2}\tilde{c}_1\,. \tag{C.12}$$

It is straightforward to construct two linear independent gauge invariant combinations. We choose

$$I \quad \tilde{c}_1 = \frac{L^2}{r^2 g} \quad \text{and} \quad \tilde{c}_3 = 0\,, \tag{C.13}$$

$$II \quad \tilde{c}_1 = 0 \quad \text{and} \quad \tilde{c}_3 = 1\,, \tag{C.14}$$

where we essentially rescaled the first invariant combination with the x-component of the background metric's inverse. The resulting gauge invariant modes are

$$\Phi_1(\omega, r) = \delta g_t^x(\omega, r) + \frac{i\omega}{\alpha}\delta\xi_x(\omega, r)\,, \quad \Phi_2(\omega, r) = \delta A_x(\omega, r)\,. \tag{C.15}$$

C.1.3 Radial gauge

In many papers the authors choose the radial gauge. This means that the gauge symmetry is partially fixed in a way, that the radial components of the metric perturbations and the vector field perturbations are and remain zero. In this case the above procedure is modified such that the combinations are invariant under the remaining symmetry transformations. Even though this choice highlights the holographic dictionary, it is not necessary to explore the dynamical degrees of freedom.

For the sake of completeness let us explicitly compute the remaining gauge freedom after choosing the radial gauge. The first step is to write down the effect of (C.1)-(C.4) on the relevant fluctuations

$$\delta g_{tr} \to \delta g_{tr} - i\omega\Sigma_r + \Sigma_t' - \left(\frac{2}{r} - \frac{h'}{h}\right)\Sigma_t\,, \tag{C.16}$$

$$\delta g_{xr} \to \delta g_{xr} + \Sigma_x' - \left(\frac{2}{r} - \frac{h'}{h}\right)\Sigma_x\,, \tag{C.17}$$

$$\delta g_{yr} \to \delta g_{yr} + \Sigma_y' - \left(\frac{2}{r} - \frac{h'}{h}\right)\Sigma_y\,, \tag{C.18}$$

$$\delta g_{rr} \to \delta g_{rr} + 2\Sigma_r' + \left(\frac{2}{r} + \frac{h'}{h}\right)\Sigma_r\,, \tag{C.19}$$

$$\delta A_r \to \delta A_r + \Lambda' - \frac{L^2 A_t}{r^2 h}\Sigma_t' + \left(\frac{2}{r} + \frac{h'}{h}\right)\frac{L^2 A_t}{r^2 h}\Sigma_t\,. \tag{C.20}$$

Note that we again work at zero spatial momentum $\underline{k} = 0$. We then imagine to perform a gauge transformation which results in $\delta g_{tr} = \delta g_{xr} = \delta g_{yr} = \delta g_{rr} = \delta A_r = 0$ and subsequently only allow gauge transformations which preserve this choice. This partially fixes the gauge symmetries. This results in first order differential equations, solved by

$$\Sigma_t(\omega, r) = \sigma_t r^2 h(r) + i\omega r^2 h(r)\sigma_r \int_{r_\mathrm{h}}^{r} \mathrm{d}\tilde{r} h(\tilde{r})^{-3/2}\tilde{r}^{-3}\,, \tag{C.21}$$

$$\Sigma_{x,y}(\omega, r) = \sigma_{x,y} r^2 g(r)\,, \quad \Sigma_r(\omega, r) = \frac{\sigma_r}{r\sqrt{h(r)}}\,, \tag{C.22}$$

$$\Lambda(\omega, r) = \lambda 0 + iL^2\omega\sigma_r \int_{r_\mathrm{h}}^{r} \mathrm{d}\tilde{r}\frac{A_t(\tilde{r})}{h(\tilde{r})^{3/2}\tilde{r}^3}\,, \tag{C.23}$$

where σ_μ and λ are unspecified integration constants which parametrise the remaining gauge freedom.

C.2 Electrical conductivity

C.2.1 Equations of motion

Now that we have identified the gauge invariant combinations for the sector of fluctuations that we are interested in, the next step is to calculate the electrical conductivity σ in the logic outlined in 3.3. We start by looking at the equations of motion for the sector of interest, which contains the fluctuations appearing in

(C.9). They are

$$0 = \delta g_{tx}'' + \left(-\frac{2}{r^2} - \frac{L^4\alpha^2}{r^4 gh} + \frac{e^2 L^4 A_t^2 \chi^2}{r^4 h^2} - \frac{2g'}{rg} - \frac{g'^2}{2g^2} + \frac{3\phi'^2}{2} + \chi'^2\right)\delta g_{tx} \qquad \text{(C.24)}$$

$$+ i\omega\delta g_{xr}' + \left(\frac{2i\omega}{r} + \frac{i\omega g'}{g}\right)\delta g_{xr} + e^{\phi} A_t' \delta A_x' + \frac{2e^2 L^2 A_t \chi^2 \delta A_x}{r^2 h} - \frac{iL^2 \alpha\omega\delta\xi_x}{r^2 h}\,,$$

$$0 = \delta A_x'' + \left(\frac{2}{r} + \frac{h'}{h} + \phi'\right)\delta A_x' + \left(\frac{L^4\omega^2}{r^4 h^2} - \frac{2e^2 L^2 e^{-\phi}\chi^2}{r^2 h}\right)\delta A_x \qquad \text{(C.25)}$$

$$- \left(\frac{2L^2 A_t'}{r^3 h} + \frac{L^2 A_t' g'}{r^2 gh}\right)\delta g_{tx} + \frac{iL^2\omega A_t' \delta g_{xr}}{r^2 h}\,,$$

$$0 = \delta\xi_x'' + \left(\frac{4}{r} + \frac{g'}{g} + \frac{h'}{h}\right)\delta\xi_x' + \frac{L^4\omega^2\delta\xi_x}{r^4 h^2}\,, \qquad \text{(C.26)}$$

$$0 = \delta g_{tx}' - \left(\frac{2}{r} + \frac{g'}{g}\right)\delta g_{tx} + \left(i\omega - \frac{iq^2 h}{\omega g}\right)\delta g_{xr} + \mathrm{e}^{\phi} A_t' \delta A_x + \frac{iqr^2 h\delta\alpha_x}{L^2\omega}\,. \qquad \text{(C.27)}$$

Note that they are obtained by first expanding the action to quadratic order in fluctuations and then calculating the equations via the variational principle with respect to the fluctuations.

We now replace the original fluctuations δg_{tx} and δA_x by the gauge invariant combinations (C.15). The other two perturbations $\delta\xi_x$ and δg_{xr} are unaffected. It is then possible to rewrite the four equations such that two of them only depend on Φ_1 and Φ_2. They are given in the main text in equation (5.56). The remaining two equations mix all four perturbations.

$$0 = \delta\xi_x'' + \left(\frac{4}{r} + \frac{g'}{g} + \frac{h'}{h}\right)\delta\xi_x' - \frac{iL^4\alpha\omega\Phi_1}{r^4 h^2} - \frac{L^2\alpha\delta g_{xr}'}{r^2 g} - \left(\frac{2L^2\alpha}{r^3 g} + \frac{L^2 q h'}{r^2 gh}\right)\delta g_{xr}\,,$$

$$0 = \left(-\frac{i\omega r^2 g}{L^2\alpha} + \frac{iqr^2 h}{L^2\omega}\right)\delta\xi_x' + \frac{r^2 g\Phi_1'}{L^2} + e^{\phi} A_t' \Phi_2 + \left(i\omega - \frac{i\alpha^2 h}{\omega g}\right)\delta g_{xr}\,. \qquad \text{(C.28)}$$

This in particular implies, that in order to compute the optical conductivity, related to the mode Φ_2 we only have to solve a set of two coupled equations.

C.2.2 On-shell action

The electrical conductivity is directly proportional to the retarded Green's function of $\Phi_2 = \delta A_x$, see equations (3.29) and (3.30). After the discussion in subsection 3.3.2 the only thing that remains to be computed is the coefficient c in relation (3.38). To do so, we need the on-shell action on the level of the fluctuations.

First, we perform the radial integral of the action (5.6) by making use of the equations of motion (C.24)-(C.27). Using the definition of the gauge invariant modes (C.15) and expanding them in Fourier modes we obtain for the on-shell action

$$
\begin{aligned}
S^{\mathrm{os}}/V_2 = \int \mathrm{d}\omega \Bigg[&- \frac{e^{\phi} r^2 g\left(2\omega^2 g - \alpha^2 h\right) A_t' \Phi_1(\omega, r)\Phi_2(-\omega, r)}{2L^2\left(\omega^2 g - \alpha^2 h\right)} \\
&- \frac{i e^{\phi} r^2 \omega g A_t' \delta\alpha_x(-\omega, r)\Phi_2(\omega, r)}{L^2 \alpha} + \frac{\alpha^2 r^4 g^2 h \Phi_1(\omega, r)\partial_r \Phi_1(-\omega, r)}{2L^4\left(-\omega^2 g + \alpha^2 h\right)} \\
&- \frac{e^{\phi} r^2 h \Phi_2(\omega, r)\partial_r \Phi_2(-\omega, r)}{2L^2} \\
&\pm \left(\frac{2r^3 g^2}{L^4} - \frac{2r^3 g^2}{L^4\sqrt{h}} - \frac{3r^3 g^2 \phi^2}{4L^4\sqrt{h}} + \frac{r^4 g g'}{L^4}\right)\Bigg(\Phi_1(-\omega, r)\Phi_1(\omega, r) \\
&+ \frac{2i\omega}{\alpha}\delta\xi_x(-\omega, r)\phi 1(\omega, r) + \frac{\omega^2}{\alpha^2}\delta\xi_x(-\omega, r)\delta\xi_x(\omega, r)\Bigg) \\
&\frac{\alpha^2 r g}{2\sqrt{h}}\left(\frac{2i\omega}{\alpha}\delta\xi_x(-\omega, r)\Phi_1(\omega, r) + \frac{\omega^2}{\alpha^2}\delta\xi_x(-\omega, r)\delta\alpha_x(\omega, r)\right)\Bigg|_{r_{\mathrm{h}}}^{\infty}\Bigg] ,
\end{aligned}
\tag{C.29}
$$

divided by the spatial volume $V_2 = \int \mathrm{d}^2 x$. According to the general approach of section 3.3, the next step is to express the on-shell action in terms of boundary coefficients and match the resulting expression with equation (3.37).

The ansatz for the boundary coefficients of the background fields and the perturbations are given in equations (5.11) and (5.58), respectively. Expanding the corresponding set of equations at the boundary, we can solve for the coefficients c in terms of the independent ones $\tilde{c}$. The relations between the coefficients for the background fields that are required to rewrite the above on-shell action (C.29) are given by

$$
\begin{aligned}
c^{\mathrm{b}}_{h,1} &= -2\frac{3c^{\mathrm{b}}_{g,3} + c^{\mathrm{b}}_{g,0}\left(3c^{\mathrm{b}}_{\phi,1}c^{\mathrm{b}}_{\phi,2} + 2c^{\mathrm{b}}_{\chi,1}c^{\mathrm{b}}_{\chi,2}\right)}{c^{\mathrm{b}}_{g,0}\left(3\left(c^{\mathrm{b}}_{\phi,1}\right)^2\right) + 2\left(c^{\mathrm{b}}_{\chi,1}\right)^2} , \\
c^{\mathrm{b}}_{h,2} &= \frac{1}{4}\left(\left(c^{\mathrm{b}}_{h,1}\right)^2 - 3\left(c^{\mathrm{b}}_{\phi,1}\right)^2 - 2\left(c^{\mathrm{b}}_{\chi,1}\right)^2\right) - \frac{L^4\alpha^2}{2c^{\mathrm{b}}_{g,0}} , \\
c^{\mathrm{b}}_{g,1} &= c^{\mathrm{b}}_{g,0}c^{\mathrm{b}}_{h,1} , \\
c^{\mathrm{b}}_{g,2} &= \frac{c^{\mathrm{b}}_{g,0}}{8}\left(\left(c^{\mathrm{b}}_{h,1}\right)^2 + 4c^{\mathrm{b}}_{h,2} - 3\left(c^{\mathrm{b}}_{\phi,1}\right)^2 - 2\left(c^{\mathrm{b}}_{\psi,1}\right)^2\right) + \frac{L^4\alpha^2}{4} .
\end{aligned}
\tag{C.30}
$$

After choosing the radial gauge, which is required by the fact that we evaluate the expression action on a slice of fixed radial coordinate, we obtain the on-shell action given in equation (5.59).

Bibliography

[1] J. Erdmenger, D. Fernandez, M. Flory, E. Megias, A.-K. Straub and P. Witkowski, *Time evolution of entanglement for holographic steady state formation*, *JHEP* **10** (2017) 034, [1705.04696].

[2] N. Poovuttikul, K. Schalm, A.-K. Straub and J. Zaanen, *Fermionic excitations of a holographic superconductor*, *to appear* .

[3] J. M. Maldacena, *The Large N limit of superconformal field theories and supergravity*, *Int. J. Theor. Phys.* **38** (1999) 1113–1133, [hep-th/9711200].

[4] S. S. Gubser, I. R. Klebanov and A. M. Polyakov, *Gauge theory correlators from noncritical string theory*, *Phys. Lett.* **B428** (1998) 105–114, [hep-th/9802109].

[5] E. Witten, *Anti-de Sitter space and holography*, *Adv. Theor. Math. Phys.* **2** (1998) 253–291, [hep-th/9802150].

[6] J. D. Bekenstein, *Do we understand black hole entropy?*, gr-qc/9409015.

[7] G. 't Hooft, *Dimensional reduction in quantum gravity*, gr-qc/9310026.

[8] L. Susskind, *The World as a hologram*, *J. Math. Phys.* **36** (1995) 6377–6396, [hep-th/9409089].

[9] P. Kovtun, D. T. Son and A. O. Starinets, *Viscosity in strongly interacting quantum field theories from black hole physics*, *Phys. Rev. Lett.* **94** (2005) 111601, [hep-th/0405231].

[10] D. T. Son and A. O. Starinets, *Viscosity, Black Holes, and Quantum Field Theory*, *Ann. Rev. Nucl. Part. Sci.* **57** (2007) 95–118, [0704.0240].

[11] N. Iqbal and H. Liu, *Universality of the hydrodynamic limit in AdS/CFT and the membrane paradigm*, *Phys. Rev.* **D79** (2009) 025023, [0809.3808].

[12] A. O. Starinets, *Quasinormal spectrum and the black hole membrane paradigm*, *Phys. Lett.* **B670** (2009) 442–445, [0806.3797].

[13] U. Heinz, C. Shen and H. Song, *The viscosity of quark-gluon plasma at RHIC and the LHC*, *AIP Conf. Proc.* **1441** (2012) 766–770, [1108.5323].

[14] J. Zaanen, Y. Liu, Y. Sun and K. Schalm, *Holographic Duality in Condensed Matter Physics.* Cambridge University Press, 2015.

[15] S. S. Gubser, *Breaking an Abelian gauge symmetry near a black hole horizon*, *Phys. Rev.* **D78** (2008) 065034, [0801.2977].

[16] S. A. Hartnoll, C. P. Herzog and G. T. Horowitz, *Building a Holographic Superconductor*, *Phys. Rev. Lett.* **101** (2008) 031601, [0803.3295].

[17] S. A. Hartnoll, C. P. Herzog and G. T. Horowitz, *Holographic Superconductors*, *JHEP* **12** (2008) 015, [0810.1563].

[18] N. Iqbal, H. Liu and M. Mezei, *Semi-local quantum liquids*, *JHEP* **04** (2012) 086, [1105.4621].

[19] T. Faulkner, H. Liu, J. McGreevy and D. Vegh, *Emergent quantum criticality, Fermi surfaces, and AdS(2)*, *Phys. Rev.* **D83** (2011) 125002, [0907.2694].

[20] J. Bardeen, L. N. Cooper and J. R. Schrieffer, *Theory of superconductivity*, *Phys. Rev.* **108** (Dec, 1957) 1175–1204.

[21] U. H. Danielsson, E. Keski-Vakkuri and M. Kruczenski, *Black hole formation in AdS and thermalization on the boundary*, *JHEP* **02** (2000) 039, [hep-th/9912209].

[22] D. Grumiller and P. Romatschke, *On the collision of two shock waves in AdS(5)*, *JHEP* **08** (2008) 027, [0803.3226].

[23] S. Bhattacharyya, V. E. Hubeny, R. Loganayagam, G. Mandal, S. Minwalla, T. Morita et al., *Local Fluid Dynamical Entropy from Gravity*, *JHEP* **06** (2008) 055, [0803.2526].

[24] P. M. Chesler and L. G. Yaffe, *Horizon formation and far-from-equilibrium isotropization in supersymmetric Yang-Mills plasma*, *Phys. Rev. Lett.* **102** (2009) 211601, [0812.2053].

[25] P. M. Chesler and L. G. Yaffe, *Holography and colliding gravitational shock waves in asymptotically AdS_5 spacetime*, *Phys. Rev. Lett.* **106** (2011) 021601, [1011.3562].

[26] M. P. Heller, R. A. Janik and P. Witaszczyk, *The characteristics of thermalization of boost-invariant plasma from holography*, *Phys. Rev. Lett.* **108** (2012) 201602, [1103.3452].

[27] M. P. Heller, D. Mateos, W. van der Schee and D. Trancanelli, *Strong Coupling Isotropization of Non-Abelian Plasmas Simplified*, *Phys. Rev. Lett.* **108** (2012) 191601, [1202.0981].

[28] D. Fernández, *Towards Collisions of Inhomogeneous Shockwaves in AdS*, *JHEP* **07** (2015) 126, [1407.5628].

[29] S. Ryu and T. Takayanagi, *Holographic derivation of entanglement entropy from AdS/CFT*, *Phys. Rev. Lett.* **96** (2006) 181602, [hep-th/0603001].

[30] S. Ryu and T. Takayanagi, *Aspects of Holographic Entanglement Entropy*, *JHEP* **08** (2006) 045, [hep-th/0605073].

[31] A. Lewkowycz and J. Maldacena, *Generalized gravitational entropy*, *JHEP* **08** (2013) 090, [1304.4926].

[32] T. J. Reber, S. Parham, N. C. Plumb, Y. Cao, H. Li, Z. Sun et al., *Pairing, pair-breaking, and their roles in setting the Tc of cuprate high temperature superconductors*, *ArXiv e-prints* (Aug., 2015) , [1508.06252].

[33] T. Faulkner, G. T. Horowitz, J. McGreevy, M. M. Roberts and D. Vegh, *Photoemission 'experiments' on holographic superconductors*, *JHEP* **03** (2010) 121, [0911.3402].

[34] R. A. Davison, K. Schalm and J. Zaanen, *Holographic duality and the resistivity of strange metals*, *Phys. Rev.* **B89** (2014) 245116, [1311.2451].

[35] T. Andrade and S. A. Gentle, *Relaxed superconductors*, *JHEP* **06** (2015) 140, [1412.6521].

[36] K.-Y. Kim, K. K. Kim and M. Park, *A Simple Holographic Superconductor with Momentum Relaxation*, *JHEP* **04** (2015) 152, [1501.00446].

[37] M. J. Bhaseen, B. Doyon, A. Lucas and K. Schalm, *Far from equilibrium energy flow in quantum critical systems*, 1311.3655.

[38] D. Bernard and B. Doyon, *Energy flow in non-equilibrium conformal field theory*, *J. Phys.* **A45** (2012) 362001, [1202.0239].

[39] D. Bernard and B. Doyon, *Non-Equilibrium Steady States in Conformal Field Theory*, *Annales Henri Poincare* **16** (2015) 113–161.

[40] D. Bernard and B. Doyon, *Time-reversal symmetry and fluctuation relations in non-equilibrium quantum steady states*, *J. Phys.* **A46** (2013) 372001, [1306.3900].

[41] M. B. Green, J. H. Schwarz and E. Witten, *Superstring theory: volume 2, Loop amplitudes, anomalies and phenomenology*, vol. 2. Cambridge University Press, 1988.

[42] J. Polchinski, *String theory. Vol. 1: An introduction to the bosonic string.* Cambridge University Press, 2007.

[43] J. Polchinski, *String theory. Vol. 2: Superstring theory and beyond.* Cambridge University Press, 2007.

[44] D. Tong, *String Theory*, 0908.0333.

[45] C. Johnson, *D-Branes.* Cambridge Monographs on Mathematical Physics. Cambridge University Press, 2006.

[46] L. Thorlacius, *Introduction to D-branes*, *Nucl. Phys. Proc. Suppl.* **61A** (1998) 86–98, [hep-th/9708078].

[47] J. Polchinski, *Dirichlet Branes and Ramond-Ramond charges*, *Phys. Rev. Lett.* **75** (1995) 4724–4727, [hep-th/9510017].

[48] O. Aharony, S. S. Gubser, J. M. Maldacena, H. Ooguri and Y. Oz, *Large N field theories, string theory and gravity*, *Phys. Rept.* **323** (2000) 183–386, [hep-th/9905111].

[49] M. Ammon and J. Erdmenger, *Gauge/gravity duality.* Cambridge University Press, 2015.

[50] J. Erdmenger, *Introduction to gauge/gravity duality*, *Lect. Notes Phys.* **851** (2012) 99–145.

[51] G. 't Hooft, *A Planar Diagram Theory for Strong Interactions*, *Nucl. Phys.* **B72** (1974) 461.

[52] D. Z. Freedman, S. S. Gubser, K. Pilch and N. P. Warner, *Renormalization group flows from holography supersymmetry and a c theorem*, *Adv. Theor. Math. Phys.* **3** (1999) 363–417, [hep-th/9904017].

[53] L. Girardello, M. Petrini, M. Porrati and A. Zaffaroni, *The Supergravity dual of N=1 superYang-Mills theory*, *Nucl. Phys.* **B569** (2000) 451–469, [hep-th/9909047].

[54] S. A. Hartnoll, A. Lucas and S. Sachdev, *Holographic quantum matter*, 1612.07324.

[55] K. Skenderis, *Lecture notes on holographic renormalization*, *Class. Quant. Grav.* **19** (2002) 5849–5876, [hep-th/0209067].

[56] V. Balasubramanian, P. Kraus and A. E. Lawrence, *Bulk versus boundary dynamics in anti-de Sitter space-time*, *Phys. Rev.* **D59** (1999) 046003, [hep-th/9805171].

[57] P. Breitenlohner and D. Z. Freedman, *Positive Energy in anti-De Sitter Backgrounds and Gauged Extended Supergravity*, *Phys. Lett.* **115B** (1982) 197–201.

[58] P. Breitenlohner and D. Z. Freedman, *Stability in Gauged Extended Supergravity*, *Annals Phys.* **144** (1982) 249.

[59] V. Balasubramanian and P. Kraus, *A Stress tensor for Anti-de Sitter gravity*, *Commun. Math. Phys.* **208** (1999) 413–428, [hep-th/9902121].

[60] O. Aharony, O. Bergman, D. L. Jafferis and J. Maldacena, *N=6 superconformal Chern-Simons-matter theories, M2-branes and their gravity duals*, *JHEP* **10** (2008) 091, [0806.1218].

[61] E. Witten, *Anti-de Sitter space, thermal phase transition, and confinement in gauge theories*, *Adv. Theor. Math. Phys.* **2** (1998) 505–532, [hep-th/9803131].

[62] A. Karch and E. Katz, *Adding flavor to AdS / CFT*, *JHEP* **06** (2002) 043, [hep-th/0205236].

[63] V. E. Hubeny, M. Rangamani and T. Takayanagi, *A Covariant holographic entanglement entropy proposal*, *JHEP* **07** (2007) 062, [0705.0016].

[64] S. A. Hartnoll, *Lectures on holographic methods for condensed matter physics*, *Class. Quant. Grav.* **26** (2009) 224002, [0903.3246].

[65] S. Sachdev, *What can gauge-gravity duality teach us about condensed matter physics?*, *Ann. Rev. Condensed Matter Phys.* **3** (2012) 9–33, [1108.1197].

[66] N. Iqbal, H. Liu and M. Mezei, *Lectures on holographic non-Fermi liquids and quantum phase transitions*, in *Proceedings, Theoretical Advanced Study Institute in Elementary Particle Physics (TASI 2010). String Theory and Its Applications: From meV to the Planck Scale: Boulder, Colorado, USA, June 1-25, 2010*, pp. 707–816, 2011, 1110.3814, DOI.

[67] J. Schrieffer, *Theory of Superconductivity.* Advanced Book Program Series. Advanced Book Program, Perseus Books, 1983.

[68] R. Gross and A. Marx, *Festkörperphysik.* De Gruyter, 2012.

[69] C. M. Varma, P. B. Littlewood, S. Schmitt-Rink, E. Abrahams and A. E. Ruckenstein, *Phenomenology of the normal state of cu-o high-temperature superconductors*, *Phys. Rev. Lett.* **63** (Oct, 1989) 1996–1999.

[70] A. Chamblin, R. Emparan, C. V. Johnson and R. C. Myers, *Charged AdS black holes and catastrophic holography*, *Phys. Rev.* **D60** (1999) 064018, [hep-th/9902170].

[71] G. T. Horowitz, J. E. Santos and D. Tong, *Further Evidence for Lattice-Induced Scaling*, *JHEP* **11** (2012) 102, [1209.1098].

[72] S. S. Gubser and F. D. Rocha, *Peculiar properties of a charged dilatonic black hole in* AdS_5, *Phys. Rev.* **D81** (2010) 046001, [0911.2898].

[73] K. Goldstein, S. Kachru, S. Prakash and S. P. Trivedi, *Holography of Charged Dilaton Black Holes*, *JHEP* **08** (2010) 078, [0911.3586].

[74] C. Charmousis, B. Gouteraux, B. S. Kim, E. Kiritsis and R. Meyer, *Effective Holographic Theories for low-temperature condensed matter systems*, *JHEP* **11** (2010) 151, [1005.4690].

[75] B. Gouteraux and E. Kiritsis, *Generalized Holographic Quantum Criticality at Finite Density*, *JHEP* **12** (2011) 036, [1107.2116].

[76] R. Kubo, *The fluctuation-dissipation theorem*, *Reports on Progress in Physics* **29** (1966) 255.

[77] C. P. Herzog and D. T. Son, *Schwinger-Keldysh propagators from AdS/CFT correspondence*, *JHEP* **03** (2003) 046, [hep-th/0212072].

[78] M. Kaminski, K. Landsteiner, J. Mas, J. P. Shock and J. Tarrio, *Holographic Operator Mixing and Quasinormal Modes on the Brane*, *JHEP* **02** (2010) 021, [0911.3610].

[79] G. T. Horowitz, *Introduction to Holographic Superconductors*, *Lect. Notes Phys.* **828** (2011) 313–347, [1002.1722].

[80] C. P. Herzog, *Lectures on Holographic Superfluidity and Superconductivity*, *J. Phys.* **A42** (2009) 343001, [0904.1975].

[81] S. A. Hartnoll and P. Petrov, *Electron star birth: A continuous phase transition at nonzero density*, *Phys. Rev. Lett.* **106** (2011) 121601, [1011.6469].

[82] A. Allais, J. McGreevy and S. J. Suh, *A quantum electron star*, *Phys. Rev. Lett.* **108** (2012) 231602, [1202.5308].

[83] A. Allais and J. McGreevy, *How to construct a gravitating quantum electron star*, *Phys. Rev.* **D88** (2013) 066006, [1306.6075].

[84] N. Iqbal and H. Liu, *Real-time response in AdS/CFT with application to spinors*, *Fortsch. Phys.* **57** (2009) 367–384, [0903.2596].

[85] H. Liu, J. McGreevy and D. Vegh, *Non-Fermi liquids from holography*, *Phys. Rev.* **D83** (2011) 065029, [0903.2477].

[86] M. Cubrovic, J. Zaanen and K. Schalm, *String Theory, Quantum Phase Transitions and the Emergent Fermi-Liquid*, *Science* **325** (2009) 439–444, [0904.1993].

[87] J. Polchinski, *Effective field theory and the Fermi surface*, in *Theoretical Advanced Study Institute (TASI 92): From Black Holes and Strings to Particles Boulder, Colorado, June 3-28, 1992*, pp. 0235–276, 1992, hep-th/9210046.

[88] R. Shankar, *Renormalization-group approach to interacting fermions*, *Rev. Mod. Phys.* **66** (Jan, 1994) 129–192.

[89] S. Sachdev and B. Keimer, *Quantum Criticality*, *Phys. Today* **64N2** (2011) 29, [1102.4628].

[90] T. J. Reber, N. C. Plumb, Y. Cao, Z. Sun, Q. Wang, K. McElroy et al., *Prepairing and the “filling” gap in the cuprates from the tomographic density of states*, *Physical Review B* **87** (Feb., 2013) 060506, [1408.6084].

[91] T. J. Reber, S. Parham, N. C. Plumb, Y. Cao, H. Li, Z. Sun et al., *Coordination of the energy and temperature scales of pairing across the doping phase diagram of $Bi\_2Sr\_2CaCu\_2O\_8+\delta$*, *ArXiv e-prints* (Sept., 2015) , [1509.01556].

[92] S.-S. Lee, *A Non-Fermi Liquid from a Charged Black Hole: A Critical Fermi Ball*, *Phys. Rev.* **D79** (2009) 086006, [0809.3402].

[93] T. Faulkner and J. Polchinski, *Semi-Holographic Fermi Liquids*, *JHEP* **06** (2011) 012, [1001.5049].

[94] A. Mukhopadhyay and G. Policastro, *Phenomenological Characterization of Semiholographic Non-Fermi Liquids*, *Phys. Rev. Lett.* **111** (2013) 221602, [1306.3941].

[95] C. P. Herzog and J. Ren, *The Spin of Holographic Electrons at Nonzero Density and Temperature*, *JHEP* **06** (2012) 078, [1204.0518].

[96] A. Bagrov, B. Meszena and K. Schalm, *Pairing induced superconductivity in holography*, *JHEP* **09** (2014) 106, [1403.3699].

[97] T. Hartman and S. A. Hartnoll, *Cooper pairing near charged black holes*, *JHEP* **06** (2010) 005, [1003.1918].

[98] M. Edalati, R. G. Leigh and P. W. Phillips, *Dynamically Generated Mott Gap from Holography*, *Phys. Rev. Lett.* **106** (2011) 091602, [1010.3238].

[99] Y. Liu, K. Schalm, Y.-W. Sun and J. Zaanen, *Lattice Potentials and Fermions in Holographic non Fermi-Liquids: Hybridizing Local Quantum Criticality*, *JHEP* **10** (2012) 036, [1205.5227].

[100] Y. Ling, P. Liu, C. Niu, J.-P. Wu and Z.-Y. Xian, *Holographic fermionic system with dipole coupling on Q-lattice*, *JHEP* **12** (2014) 149, [1410.7323].

[101] Y. Ling, P. Liu, C. Niu and J.-P. Wu, *Pseudo-gap phase and duality in a holographic fermionic system with dipole coupling on Q-lattice*, *Chin. Phys.* **C40** (2016) 043102, [1602.06062].

[102] M. Ammon, J. Erdmenger, M. Kaminski and P. Kerner, *Superconductivity from gauge/gravity duality with flavor*, *Phys. Lett.* **B680** (2009) 516–520, [0810.2316].

[103] G. T. Horowitz, J. E. Santos and D. Tong, *Optical Conductivity with Holographic Lattices*, *JHEP* **07** (2012) 168, [1204.0519].

[104] G. T. Horowitz and J. E. Santos, *General Relativity and the Cuprates*, *JHEP* **06** (2013) 087, [1302.6586].

[105] Y. Ling, C. Niu, J.-P. Wu and Z.-Y. Xian, *Holographic Lattice in Einstein-Maxwell-Dilaton Gravity*, *JHEP* **11** (2013) 006, [1309.4580].

[106] P. Chesler, A. Lucas and S. Sachdev, *Conformal field theories in a periodic potential: results from holography and field theory*, *Phys. Rev.* **D89** (2014) 026005, [1308.0329].

[107] A. Ishibashi and K. Maeda, *Thermalization of boosted charged AdS black holes by an ionic Lattice*, *Phys. Rev.* **D88** (2013) 066009, [1308.5740].

[108] D. Vegh, *Holography without translational symmetry*, 1301.0537.

[109] M. Blake, D. Tong and D. Vegh, *Holographic Lattices Give the Graviton an Effective Mass*, *Phys. Rev. Lett.* **112** (2014) 071602, [1310.3832].

[110] R. A. Davison, *Momentum relaxation in holographic massive gravity*, *Phys. Rev.* **D88** (2013) 086003, [1306.5792].

[111] A. Donos and J. P. Gauntlett, *Novel metals and insulators from holography*, *JHEP* **06** (2014) 007, [1401.5077].

[112] R. Mahajan, M. Barkeshli and S. A. Hartnoll, *Non-Fermi liquids and the Wiedemann-Franz law*, *Phys. Rev.* **B88** (2013) 125107, [1304.4249].

[113] M. Blake and A. Donos, *Quantum Critical Transport and the Hall Angle*, *Phys. Rev. Lett.* **114** (2015) 021601, [1406.1659].

[114] X.-H. Ge, Y. Tian, S.-Y. Wu and S.-F. Wu, *Linear and quadratic in temperature resistivity from holography*, 1606.07905.

[115] A. Amoretti, M. Baggioli, N. Magnoli and D. Musso, *Chasing the cuprates with dilatonic dyons*, *JHEP* **06** (2016) 113, [1603.03029].

[116] M. Cvetic, M. J. Duff, P. Hoxha, J. T. Liu, H. Lu, J. X. Lu et al., *Embedding AdS black holes in ten-dimensions and eleven-dimensions*, *Nucl. Phys.* **B558** (1999) 96–126, [hep-th/9903214].

[117] M. Blake and D. Tong, *Universal Resistivity from Holographic Massive Gravity*, *Phys. Rev.* **D88** (2013) 106004, [1308.4970].

[118] S. F. Hassan, R. A. Rosen and A. Schmidt-May, *Ghost-free Massive Gravity with a General Reference Metric*, *JHEP* **02** (2012) 026, [1109.3230].

[119] Y. Ling and X. Zheng, *Holographic superconductor with momentum relaxation and Weyl correction*, *Nucl. Phys.* **B917** (2017) 1–18, [1609.09717].

[120] T. Andrade and B. Withers, *A simple holographic model of momentum relaxation*, *JHEP* **05** (2014) 101, [1311.5157].

[121] M. Bianchi, D. Z. Freedman and K. Skenderis, *How to go with an RG flow*, *JHEP* **08** (2001) 041, [hep-th/0105276].

[122] M. Bianchi, D. Z. Freedman and K. Skenderis, *Holographic renormalization*, *Nucl. Phys.* **B631** (2002) 159–194, [hep-th/0112119].

[123] J. Erdmenger, B. Herwerth, S. Klug, R. Meyer and K. Schalm, *S-Wave Superconductivity in Anisotropic Holographic Insulators*, *JHEP* **05** (2015) 094, [1501.07615].

[124] E. Berti, V. Cardoso, L. C. B. Crispino, L. Gualtieri, C. Herdeiro and U. Sperhake, *Numerical Relativity and High Energy Physics: Recent Developments*, *Int. J. Mod. Phys.* **D25** (2016) 1641022, [1603.06146].

[125] M. Guo, C. Niu, Y. Tian and H. Zhang, *Applied AdS/CFT with Numerics*, *PoS* **Modave2015** (2016) 003, [1601.00257].

[126] V. Cardoso et al., *NR/HEP: roadmap for the future*, *Class. Quant. Grav.* **29** (2012) 244001, [1201.5118].

[127] J. Abajo-Arrastia, J. Aparicio and E. Lopez, *Holographic Evolution of Entanglement Entropy*, *JHEP* **11** (2010) 149, [1006.4090].

[128] V. Balasubramanian, A. Bernamonti, J. de Boer, N. Copland, B. Craps, E. Keski-Vakkuri et al., *Thermalization of Strongly Coupled Field Theories*, *Phys. Rev. Lett.* **106** (2011) 191601, [1012.4753].

[129] V. Balasubramanian, A. Bernamonti, J. de Boer, N. Copland, B. Craps, E. Keski-Vakkuri et al., *Holographic Thermalization*, *Phys. Rev.* **D84** (2011) 026010, [1103.2683].

[130] V. Balasubramanian, A. Bernamonti, N. Copland, B. Craps and F. Galli, *Thermalization of mutual and tripartite information in strongly coupled two dimensional conformal field theories*, *Phys. Rev.* **D84** (2011) 105017, [1110.0488].

[131] H. Liu and S. J. Suh, *Entanglement Tsunami: Universal Scaling in Holographic Thermalization*, *Phys. Rev. Lett.* **112** (2014) 011601, [1305.7244].

[132] Y.-Z. Li, S.-F. Wu, Y.-Q. Wang and G.-H. Yang, *Linear growth of entanglement entropy in holographic thermalization captured by horizon interiors and mutual information*, *JHEP* **09** (2013) 057, [1306.0210].

[133] H. Liu and S. J. Suh, *Entanglement growth during thermalization in holographic systems*, *Phys. Rev.* **D89** (2014) 066012, [1311.1200].

[134] M. Alishahiha, A. Faraji Astaneh and M. R. Mohammadi Mozaffar, *Thermalization in backgrounds with hyperscaling violating factor*, *Phys. Rev.* **D90** (2014) 046004, [1401.2807].

[135] S. Kundu and J. F. Pedraza, *Spread of entanglement for small subsystems in holographic CFTs*, *Phys. Rev.* **D95** (2017) 086008, [1602.05934].

[136] P. Caputa, M. Nozaki and T. Takayanagi, *Entanglement of local operators in large-N conformal field theories*, *PTEP* **2014** (2014) 093B06, [1405.5946].

[137] P. Caputa, J. Simón, A. Štikonas and T. Takayanagi, *Quantum Entanglement of Localized Excited States at Finite Temperature*, *JHEP* **01** (2015) 102, [1410.2287].

[138] P. Caputa, J. Simón, A. Štikonas, T. Takayanagi and K. Watanabe, *Scrambling time from local perturbations of the eternal BTZ black hole*, *JHEP* **08** (2015) 011, [1503.08161].

[139] M. Rangamani, M. Rozali and A. Vincart-Emard, *Dynamics of Holographic Entanglement Entropy Following a Local Quench*, *JHEP* **04** (2016) 069, [1512.03478].

[140] J. R. David, S. Khetrapal and S. P. Kumar, *Universal corrections to entanglement entropy of local quantum quenches*, *JHEP* **08** (2016) 127, [1605.05987].

[141] M. Rozali and A. Vincart-Emard, *Comments on Entanglement Propagation*, *JHEP* **06** (2017) 044, [1702.05869].

[142] M. Nozaki, T. Numasawa and T. Takayanagi, *Holographic Local Quenches and Entanglement Density*, *JHEP* **05** (2013) 080, [1302.5703].

[143] A. Jahn and T. Takayanagi, *Holographic Entanglement Entropy of Local Quenches in AdS_4/CFT_3: A Finite-Element Approach*, 1705.04705.

[144] A. F. Astaneh and A. E. Mosaffa, *Quantum Local Quench, AdS/BCFT and Yo-Yo String*, *JHEP* **05** (2015) 107, [1405.5469].

[145] J. Erdmenger, M. Flory, M.-N. Newrzella, M. Strydom and J. M. S. Wu, *Quantum Quenches in a Holographic Kondo Model*, *JHEP* **04** (2017) 045, [1612.06860].

[146] T. Nishioka, S. Ryu and T. Takayanagi, *Holographic Entanglement Entropy: An Overview*, *J. Phys.* **A42** (2009) 504008, [0905.0932].

[147] V. E. Hubeny and M. Rangamani, *Causal Holographic Information*, *JHEP* **06** (2012) 114, [1204.1698].

[148] M. Headrick and T. Takayanagi, *A Holographic proof of the strong subadditivity of entanglement entropy*, *Phys. Rev.* **D76** (2007) 106013, [0704.3719].

[149] M. Headrick, *Entanglement Renyi entropies in holographic theories*, *Phys. Rev.* **D82** (2010) 126010, [1006.0047].

[150] A. Allais and E. Tonni, *Holographic evolution of the mutual information*, *JHEP* **01** (2012) 102, [1110.1607].

[151] H. Araki and E. H. Lieb, *Entropy inequalities*, *Commun. Math. Phys.* **18** (1970) 160–170.

[152] M. Banados, M. Henneaux, C. Teitelboim and J. Zanelli, *Geometry of the (2+1) black hole*, *Phys. Rev.* **D48** (1993) 1506–1525, [gr-qc/9302012].

[153] M. Banados, C. Teitelboim and J. Zanelli, *The Black hole in three-dimensional space-time*, *Phys. Rev. Lett.* **69** (1992) 1849–1851, [hep-th/9204099].

[154] M. Banados, *Three-dimensional quantum geometry and black holes*, in *Trends in theoretical physics II. Proceedings, 2nd La Plata Meeting, Buenos Aires, Argentina, November 29-December 4, 1998*, pp. 147–169, 1998, hep-th/9901148, DOI.

[155] W. Israel, *Singular hypersurfaces and thin shells in general relativity*, *Il Nuovo Cimento B (1965-1970)* **44** (1966) 1–14.

[156] M. Hoogeveen and B. Doyon, *Entanglement negativity and entropy in non-equilibrium conformal field theory*, *Nucl. Phys.* **B898** (2015) 78–112, [1412.7568].

[157] S. H. Shenker and D. Stanford, *Black holes and the butterfly effect*, *JHEP* **03** (2014) 067, [1306.0622].

[158] T. Hartman and J. Maldacena, *Time Evolution of Entanglement Entropy from Black Hole Interiors*, *JHEP* **05** (2013) 014, [1303.1080].

[159] C. Ecker, D. Grumiller and S. A. Stricker, *Evolution of holographic entanglement entropy in an anisotropic system*, *JHEP* **07** (2015) 146, [1506.02658].

[160] A. C. Wall, *Maximin Surfaces, and the Strong Subadditivity of the Covariant Holographic Entanglement Entropy*, *Class. Quant. Grav.* **31** (2014) 225007, [1211.3494].

[161] A. Prudenziati, *Strong subadditivity and holography*, *Phys. Rev.* **D93** (2016) 106003, [1509.07885].

[162] M. Alishahiha, M. R. M. Mozaffar and M. R. Tanhayi, *On the Time Evolution of Holographic n-partite Information*, *JHEP* **09** (2015) 165, [1406.7677].

[163] S. Mirabi, M. R. Tanhayi and R. Vazirian, *On the Monogamy of Holographic n-partite Information*, *Phys. Rev.* **D93** (2016) 104049, [1603.00184].

[164] N. Bao, S. Nezami, H. Ooguri, B. Stoica, J. Sully and M. Walter, *The Holographic Entropy Cone*, *JHEP* **09** (2015) 130, [1505.07839].

[165] H.-C. Chang, A. Karch and A. Yarom, *An ansatz for one dimensional steady state configurations*, *J. Stat. Mech.* **1406** (2014) P06018, [1311.2590].

[166] I. Amado and A. Yarom, *Black brane steady states*, *JHEP* **10** (2015) 015, [1501.01627].

[167] M. Spillane and C. P. Herzog, *Relativistic Hydrodynamics and Non-Equilibrium Steady States*, *J. Stat. Mech.* **1610** (2016) 103208, [1512.09071].

[168] A. Lucas, K. Schalm, B. Doyon and M. J. Bhaseen, *Shock waves, rarefaction waves, and nonequilibrium steady states in quantum critical systems*, *Phys. Rev.* **D94** (2016) 025004, [1512.09037].

[169] D. T. Son and A. O. Starinets, *Hydrodynamics of r-charged black holes*, *JHEP* **03** (2006) 052, [hep-th/0601157].

[170] P. Kovtun, *Lectures on hydrodynamic fluctuations in relativistic theories*, *J. Phys.* **A45** (2012) 473001, [1205.5040].

[171] M. Rangamani, *Gravity and Hydrodynamics: Lectures on the fluid-gravity correspondence*, *Class. Quant. Grav.* **26** (2009) 224003, [0905.4352].

[172] N. Banerjee, J. Bhattacharya, S. Bhattacharyya, S. Dutta, R. Loganayagam and P. Surowka, *Hydrodynamics from charged black branes*, *JHEP* **01** (2011) 094, [0809.2596].

[173] M. Torabian and H.-U. Yee, *Holographic nonlinear hydrodynamics from AdS/CFT with multiple/non-Abelian symmetries*, *JHEP* **08** (2009) 020, [0903.4894].

[174] S. A. Hartnoll and C. P. Herzog, *Ohm's Law at strong coupling: S duality and the cyclotron resonance*, *Phys. Rev.* **D76** (2007) 106012, [0706.3228].